INAUGURAL - DISSERTATION

submitted to the
Combined Faculties of the Natural Sciences and Mathematics
of the Ruperto-Carola Heidelberg University, Germany
for the degree of
Doctor of Natural Sciences

Presented by:
M.Sc. Zhuang Lin
Born in: Fuzhou, China

Oral examination: _____

Fluorescence Lifetime Imaging Camera: Image Analysis, Optimization and Enhancement

Advisor : Prof. Dr. Bernd Jähne

Abstract

Fluorescence lifetime imaging microscopy (FLIM) is an imaging technique for producing an image based on differences in fluorescence lifetimes. The present thesis is devoted to analyzing a novel Fluorescence Lifetime Imaging Camera (FLI-Cam) system. The principle of the applied camera system is based on the Time-of-Flight (ToF) technique, which was originally designed for 3D depth scene imaging. Such a camera provides a high frame rate and realizes direct nanosecond-range fluorescence lifetime sensing. The main scope of this thesis is to deliver an optimized solution and rapid sophisticated algorithm for the FLI-Cam system with high accuracy. New time-gated schemes and heterodyne modulation scheme for FLIM using the pulse-based and continuous-wave-based (phase-based) ToF camera, respectively, are presented. In order to optimize the performance of the FLI-Cam system, a thorough statistical analysis is implemented and the photon economy of our FLIM techniques is investigated. Various operation modes and experimental parameters for the measurement have been studied and optimized. The presented theoretical result is validated by numerical simulations using the Monte Carlo method and real experiments. For the enhancement of the FLIM images from our system, the vector-valued total variation technique is applied to improve the quality of FLIM images for the first time. It shows better performance than other existing approaches.

Zusammenfassung

Die Fluoreszenzlebensdauer-Mikroskopie (FLIM) ist eine Bildgebungstechnik, welche auf den Unterschieden in der Fluoreszenzlebensdauer eines Farbstoffes basiert. Die vorliegende Arbeit beschäftigt sich mit der Analyse eines neuartigen Kamerasystems “Fluorescence Lifetime Imaging Camera” (FLI-Cam), dessen Funktionsprinzip auf der so genannten Time-of-Flight (ToF) Technik basiert. Diese Technik wird bereits bei der 3D Bildgebung eingesetzt. FLI-Cam soll eine Bestimmung der Fluoreszenzlebensdauer im Nanosekundenbereich ermöglichen. Das Ziel dieser Arbeit ist die Entwicklung eines geeigneten, für das FLI-Cam-Kamerasystem optimierten und schnellen Auswerte-algorithmus mit hoher Genauigkeit. Es werden sowohl ein neues Schema zum zeitlichen Abtasten des Lichtsignals bei pulsbasierten ToF-Kamerasystemen als auch ein heterodynes Modulationsschema für phasenbasierte ToF-Messtechnik präsentiert. Zur Optimierung des Messverfahrens wurden eine statistische Analyse durchgeführt und die Photoneneffizienz der FLI-Cam-Messtechnik untersucht. Unterschiedliche Operationsmodi und experimentelle Parameter wurden studiert und konnten so optimiert werden. Die präsentierten theoretischen Ergebnisse wurden anhand von Monte-Carlo-Simulationen und realen Experimenten validiert. Zur Verbesserung der FLIM-Messdaten-qualität wurde ein vektorbasiertes Variationsverfahren, welche deutlich bessere Ergebnisse als bereits existierende Methoden lieferte, eingesetzt.

Acknowledgements

I would like to express my gratitude to all those who gave me the possibility to complete this thesis.

First of all, I would like to thank Prof. Dr. Bernd Jähne for his great supervision, invaluable support, stimulating suggestions and constant encouragement during the whole work. I also thank Prof. Dr. Karl-Heinz Brenner for kindly accepting to become the co-supervisor of this thesis.

I thank the staff in Heidelberg Collaboratory for Image Processing (HCI), Ms. Barbara Werner and Ms. Karin Kruljac for their excellent job of simplifying bureaucracy things.

I am grateful to Dr. Michael Erz for good cooperation, experimental support for the theories in this thesis and extensive proofreading of this thesis. I thank Robert Frank and Prof. Fred Wouters for providing me the FLIM data for validating the image analysis algorithm of this thesis.

I thank Dr. Martin Schmidt for the nice introduction of Time-of-Flight camera and various helps with software issues.

I thank Dr. Florian Becker and Dr. Frank Lenzen for the discussions and suggestions in the areas of the image denoising and variational methods. I am grateful to Dr. Frank Lenzen for the proofreading and feedback of this dissertation.

I thank Dr. Marco Roelcke for the friendship and his continuous support and encouragement during my PhD period.

I also thank my family for their sympathy. Without their support and I would not be able to have the chance to study abroad.

A special thanks goes to my girlfriend Yan Yu for her enormous affection and great understanding. She did all she could to support me during my dissertation writing, which I am really appreciated.

Heidelberg November 2011

Zhuang Lin

Contents

List of Figures

List of Tables

Nomenclature

Roman Symbols

$\mathcal{H}(x)$	Heaviside step function.
h	hth harmonic.
m	Modulation depth.
$\mathbb{E}$	Mathematical expectation.
$\mathbf{u}$	Phasor vector.
f_i	Fluorescence fraction intensity.
$\tilde{t}$	Dimensionless time variable, where $\tilde{t} = \omega t$
c_k	kth frame cross-correlation function.
C_{AC}	Amplitude of Fourier spectral content, AD component
C_{DC}	Offset of Fourier spectral content, DC component.
D	Duty cycle.
E	Irradiance, power incident on a surface, also called radiant flux density.
f_s	Sampling frequency.
h_p	The Plank's constant.
j	Imaginary number.
K	Overall system gain.
N_d	Total number of dark electrons.
N_e	Total number of electrons.
N_h	Total number of harmonics.

n_h Index of DFT output of hth harmonic.

N_p Total number of photons.

N_s Total number of sampling points.

N_τ Total number of fluorescence components.

PA Peak amplitude.

T Period of a periodic signal.

t_{exp} Exposure time.

y Camera digital output.

F F-value, photon economy.

Greek Symbols

$\tilde{\omega}$ Dimensionless quantity of modulation frequency, where $\tilde{\omega} = \omega\tau$.

α Fraction amplitude.

$\bar{\tau}$ Average fluorescence lifetime.

Δt Unit length of exposure time of time-gated camera.

η The quantum efficiency.

Γ_{nr} Rate constant for non-radiative deactivation.

Γ_{r} Rate constant for radiative deactivation, photon emission.

λ_c Wavelength of the light.

Ω Image domain.

ω Angular modulation frequency of excitation light.

$\Phi(x)$ Moment generating function.

ϕ Phase angle.

σ_τ Standard deviation of the fluorescence lifetime τ under repeated measurements.

τ Fluorescence lifetime.

θ Phase shift of the camera modulation.

ξ Relative length of lifetime τ to the unit length of exposure time Δt of time-gated camera, where $\xi = \tau / \Delta t$.

Subscripts

$_{\text{cam}}$ Camera sampling function.

$_{\text{ex}}$ Fluorescence excitation signal.

$_{\delta}$ Dirac pulse.

$_{\text{em}}$ Fluorescence emission signal.

$_{\text{Re,Im}}$ Real and imaginary coordinate of phasor plane.

Acronyms

CCD Charge-coupled device

CMOS Complementary metalCoxideCsemiconductor

DFT Discrete Fourier Transform

DSNU Dark Signal Non-Uniformity

EMVA European Machine Vision Association

FD Frequency Domain

FFT Fast Fourier Transform

FLIM Fluorescence Lifetime Imaging Microscopy

FRET Förster Resonance Energy Transfer

HtM-FLIM Heterodyne Modulation method for FD-FLIM

MSE Mean Squared Error

PMD Photonic Mixing Device

PRNU Photo Response Non-Uniformity

PSNR Peak Signal-to-Noise Ratio

RLD Rapid Lifetime Determination method

RMS Root Mean Square

SIP Semi-infinite programming

SNR Signal-to-noise ratio

TCSPC Time-Correlated Single-Photon Counting

TD Time Domain

ToF Time-of-Flight

TV Total Variation

Chapter 1

Introduction

1.1 Motivation

In recent years *fluorescence lifetime imaging microscopy (FLIM)* [Lak06] has been developed into an important technique to image the lifetimes of fluorophores in cells. One of the important properties of fluorescence lifetime is that it does not depend on the local concentration of the fluorophore, but it can be influenced by the environmental conditions such as oxygen concentration [LW73, GSD$^+$97], ionic strength and pH value [CLAB00] and excited-state reactions such as *Förster Resonance Energy Transfer (FRET)* [Cle95, WP05, GZM$^+$08, CC09] - properties that can be exploited to resolve physiological parameters on its local molecular microenvironment. For this reason the fluorescence lifetime is often used as an indicator of these physical parameters and for the detection of intracellular events. For instance, in a combined FRET-FLIM approach, the occurrence of FRET is measured by monitoring the change in donor's lifetime, since the fluorescence lifetime is effected by FRET, which shortens or changes the excited state lifetime of the donors. FRET-FLIM analysis has recently been used in several applications such as the analysis of protein interactions with high spatial-temporal specificity, the study of conformational changes and high-throughput screening.

The current available FLIM systems can be categorized into two large groups: *frequency-domain* and *time-domain*. In frequency-domain FLIM (FD-FLIM) the excitation light is generally intensity modulated, the lifetime can be determined by measuring the phase delay and demodulation of the response signal caused by the short time lag between the absorbtion and emission. In the time-domain FLIM (TD-FLIM) method, a train of short pulses of light is used as the excitation source and the fluorescence intensity decay versus time is recorded. The decay time can be retrieved by means of fitting the recorded data to the exponential model. However, the current TD-FLIM systems usually use image intensifier or scanning microscopes, which are expensive for practical use.

A *Time-of-Flight (ToF)* camera is a range imaging camera that resolves distance based on the known speed of light, measuring the time-of-flight of a light signal between the camera and the subject. ToF cameras are relatively recent devices for normal product, as the semiconductor processes have only recently become fast enough for such devices. The ToF cameras generally consist of two types: pulsed-based and continuous-wave-based (phase-based), depending on the types of the light sources.

Recent work [EOG+05] demonstrated the possibility of using ToF camera for FLIM. This technique provides a non-expensive alternative FLIM solution. However, such cameras are optimized for measuring the 3D depth scene and do not provide the optimized operation mode for FLIM measurement. For this reason, several companies and universities collaborate together in the BMBF project "Fluorescence Lifetime Imaging Camera" (FLI-Cam). This project focuses on developing of a new innovative camera system, which is able to measure the fluorescence lifetime directly by phase-based ToF technique with high accuracy.

However, the modulation frequency of the current available 3D ToF image sensor is generally not higher enough to perform the synchronous demodulation of above 80 MHz excitation frequency required by short range lifetimes measurements. Therefore, an asynchronous demodulation scheme (heterodyne modulation) especially tailored for FLIM system is required.

In order to avoid the photonbleaching, unexpected cell responses and sample damages, the excitation intensities used for FLIM are usually much lower than the excitation intensities applied for depth scene measurement by ToF camera. Additionally, high frame-rate ToF camera leads to short exposure time. Both factors result in very few available photons in the FLIM measurement, i.e., the FLIM data are generally very noisy. Therefore, the task of obtaining a reasonable lifetime accuracy from such poor signal-to-noise ratio FLIM data is challenging. It requires a careful statistical analysis for the noise behavior and a optimization procedure to obtain the most appropriate experimental parameters and operation modes in order to achieve the best performance.

Noise often reduces the SNR of FLIM images so that small changes in lifetimes are difficult to distinguish. It always leads to a uncorrect data interpretation for the quantitative analysis such as study of FRET efficiency. To tackle this problem, it requires a robust image analysis algorithm to improve the quality of the FLIM images.

1.2 States of the Art

For many applications of FLIM, it is desirable to acquire fluorescence lifetime images as fast as possible. This suggests that wide-field FLIM with parallel image pixel acquisition is an appropriate approach. The wide-field FLIM images always consists of hundreds of thousands pixels so that the lifetime calculation techniques are required to be performed rapidly and accurately. Traditionally, the iterative numerical technique such as global analysis [KBB83, LLC+84, Bee92, VSB00] are applied. However, if they are implemented in so many pixels, enormous amount of time are

consumed. To solve this problem, there are recent works devoting to the noniterative lifetime calculation approaches. Malachowski and Ashcroft [MCR07] proposed a noniterative data regression approaches using Chebyshev and Laguerre polynomials for data fitting. Weber's method [Web81] and LiMA method [EOG+05] provide analytical lifetime calculation method for FD-FLIM data. Both of them are extremely faster than the iterative approaches, but are relatively vulnerable to noise compare to the iterative approaches.

Phasor plot approach is nowadays extensively applied in FLIM data analysis. This technique was originally proposed by Jameson et al. [JGH84], and subsequently expanded by Clayton el al. [CHV04] and Redford et al. [RC05]. Instead of exact lifetime values calculation, the phasor approach tends to group the species with similar lifetime in the same position of the phasor plane. By means of phasor approach, different species with distinct lifetimes are possible to be segmented by classification technique even the noisy FLIM data is present.

For the imaging devices of FLIM, the pioneering work of Mitchell et al. [MWMM02a, MWMM02b] presented the possibility of direct fluorescence lifetime sensing with a modified commercial CCD. However, in their work, a maximum modulation frequency of 10MHz was realized and only 500KHz could be used for FLIM experiment. This is far too low for measuring typical fluorophores in biological applications. The work of Esposito et al. [EOG+05] suggested wide-field FLIM can be realized by CMOS/CCD hybrid lock-in image sensor, which is originally developed for 3D ToF imaging. Such a technique provides the possibility of direct nanosecond range fluorescence lifetime sensing without reducing the frequency of the fluorescence signal such as homodyne and heterodyne detection techniques.

A detailed error analysis to the ToF camera were implemented by [RFHJ08, FPR+09] in order to improve the performance for 3D depth map. However, compare to broadness of the FLIM applications, much few attentions have been paid to the performance analysis and optimization of the FLIM system based on the statistical analysis. The current work are only restricted to few TD-FLIM methods and homodyne detection methods in FD-FLIM. For the TD-FLIM, Leray et al. [LST+11] provided an theoretical investigation on the performance of the phasor approach in terms of phase lifetime and modulation lifetime acquired by the Fourier analysis of the TD-FLIM data. For FD-FLIM, the first attempt towards this area was done by Philip and Carlsson. In their excellent work [PC03], the first analytical forms of F-value with the FD-FLIM has been derived. Elder et al. [ESK08] extended their work to the case of least square data fitting of fluorescence signal using multiple harmonics excitation. Lin and Gmitro [LG10] presented a general approach to compute the probability density of the estimated lifetime for FD-FLIM using homodyne lock-in detection.

There are only a few works concerning about the improvement of the quality of the FLIM images using image analysis techniques. For TD-FLIM, the enhancement of the FLIM data by total variation (TV) methods has been proposed by Chang and Mycek [Cha09, CM10], two schemes including the intensity data denoising and lifetime data denoising have been proposed and compared. For FD-FLIM data denoising, Buranachai et al. [BKC+08] showed that wavelets are useful for distinguish fluorescence lifetime components based on spatial morphology. The researches Spring and

Clegg [SC09b] extended their work and proposed an image analysis technique, which is based on wavelet TI-Haar denoising [WN04], specifically designed to remove signal-dependent noise from FLIM data by FD homodyne detection technique.

1.3 Scope of the Work

This work is dedicated to deliver a fast solution and new sophisticated algorithm of the FLIM system using ToF camera with a relatively high accuracy and to provide a theoretical analysis, Monte-Carlo simulation and optimization of the imaging scheme in order to guide the direction of the design for the high performance ToF based FLIM camera.

The following is a list of major contributions of this thesis

- Analysis and optimization of the time-gated TD-FLIM scheme using a pulse-based ToF camera: TriDiCam, suggestion of best time-gated schemes for measuring of different fluorophore samples with different lifetime ranges.
- Proposing a general formula for the multiple harmonics FLIM using heterogeneous modulation of phase-based ToF camera, which enables the possibility of exploration of the optimum FLIM measurement parameter and facilitates the designing of new imaging sensors for high performance multi-frequency FD-FLIM.
- Development of a simulation software focused on the multi-frequency multi-sampling fluorescence lifetime camera, which is able to reproduce the sensor behavior and generate realistic data, thus facilitating the validation of the theoretical model proposed in this thesis.
- Thorough statistical analysis of the generalized FLIM system using heterodyne modulation, Quantification of the performance of different FLIM schemes which realizes the optimization of the FLIM system.
- Optimization of the excitation waveform using semi-infinity programming technique so that best FLIM measurement performance can be achieved under the constrain of peak amplitude of the excitation.
- Improvement of the quality of poor SNR FLIM images based on modern image analysis technique. Proposing for the first time of the vector-valued total variational denoising of the FD-FLIM images, which shows better performance than other existing approaches.

1.4 Overview of the Work

The remainder of the thesis is organized as follows.

Chapter 2 This chapter gives the theoretical basis of the fluorescence lifetime measurement principle. The model-free analysis of FLIM-data, so called phasor plot approach, is then described. Two types of FLIM data from TD and FD are both analyzed and visually represented on the phasor plane. In the end of this chapter, three most common used lifetime calculation algorithms are presented and compared.

Chapter 3 The most common used techniques for TD-FLIM and FD-FLIM are introduced in this chapter. Then we concentrate on the theoretical solutions of using two type of ToF cameras, which are pulse-based and continuous-wave (phase-based) system, for the TD- and FD-FLIM, respectively. For the commercially available TriDiCam camera system (pulse-based), several time-gated schemes are proposed. For the phase-based cameras, instead of using common used homodyne camera modulation scheme, a general formula describing the heterodyne camera modulation is derived and discussed. Then a discrete Fourier transform based demodulation method is given for reconstruct the fluorescence signal from discrete samples of multiple harmonics excitation.

Chapter 4 In this chapter, the physical model of the camera used in FLIM is presented within the framework of EMVA 1288 [EMV10]. Combining with the fluorescence lifetime measurement techniques presented in Chapter 3, a simulation software is developed to reproduce the imaging procedure and generate the realistic data.

Chapter 4 This chapter presents a detailed error analysis to the FLIM solutions given in Chapter 3 based on statistical analysis. We evaluate the performance of the measurements using different types of ToF camera, and same camera measurement using different experimental parameters by the photon economy quantification. In the end of this chapter, the optimization procedure based on this statistical quantification is performed and the suggestions of the optimal measurement parameter for the real experiment in different circumstances are given.

Chapter 5 In this chapter, a novel image denoising algorithm used for the improvement of SNR of the FD-FLIM images is proposed. This algorithm is based on total variational regularization of vector-valued data. Both simulated and realistic noisy FLIM images are used to test the performance of the proposed denoising algorithm. The comparison to other FLIM image denoising schemes are also presented.

Chapter 6 Finally, this chapter summarizes the main results and the contributions of this thesis. Meanwhile, some remarks and outlooks for further research are concluded.

Appendix A Several detail mathematical derivations supporting the theories of this thesis are given in this chapter.

Chapter 2

Fluorescence Lifetime Measurement and Data Analysis

2.1 Overview

The fluorescence lifetime measurements can be generally categorized into two types: time-resolved and steady-state [Lak06]. The time-resolved method is one of the types of fluorescence measurements usually used for measuring intensity decays. The sample is exposed to a δ-pulse, which is typically shorted than the decay time of the sample. The intensity decay of fluorescence is normally recorded by a high-speed detection system that permits the intensity measurements in very short time scale. The other type is called steady-state, which is performed with constant illumination and observations. The sample is illuminated with a continuous beam of light, and the intensity or emission spectrum is recorded.

In this chapter we first introduce the physical background of the fluorescence lifetimes in Sect. 2.2. And then we describe the time-resolved techniques which consists of TD- and FD-domain lifetime measurement depending on different excitation sources in Sect. 2.3. Subsequently, we propose the transfer function idea to describe the relation between the excitation input and fluorescence emission output in Sect. 2.4. In the same section, the theory of graphical representation of the FLIM data acquired from both TD and FD in the phasor plane is explained and discussed. In Sect. 2.5, we will introduce the most common calculation schemes for resolving multiple lifetime components system and evaluate the performance between them.

2.2 Rate Constants and Fluorescence Lifetimes

A molecule can exist in various energy states defined by the distribution of electrons in orbitals of different energies. When a molecule is exited by light, a photon boosts an electron from an orbital

of lower energy to its orbital with a higher energy level. In the new orbital, the electron is said to be in an excited state. However, the excited state is so unstable that an electron can only persist for a very short time period. During this process, the average amount of time of a population of molecules stay in the excited state before returning to the ground state by emitting a photon is fluorescence lifetime.

Release from the excited state to the ground state may go through several pathways. If an excited electron drops back to the ground state with the emission of a photon, the pathway is said to be radiative, the release of light energy is called fluorescence. Otherwise, if no light energy is released, it is said to be non-radiative. In chemical kinetics, the rate of the deactivation of the excited molecules with time following optical excitation with a very short light pulse (δ-pulse) can be expressed by the following differential equation

$$-\frac{dM^*}{dt} = (\Gamma_{\mathrm{r}} + \Gamma_{\mathrm{nr}})M^* \tag{2.1}$$

where M^* is the number of molecules having been reached the exited state. Γ_{nr} is the rate constant which includes all non-radiative deactivation pathways, Γ_{r} is the rate constant for radiative deactivation with emission of fluorescence. Integration of Eq. 2.1, we may obtain the solution of the differential equation.

$$M(t) = M_0 \exp\big(-t(\Gamma_{\mathrm{r}} + \Gamma_{\mathrm{nr}})\big) \tag{2.2}$$

where $M(t)$ is the number of excited state molecules at time t, M_0 is the initial number of molecules. The sum of Γ_{r} and Γ_{nr} determines the exponential decay rate of fluorescence intensity. The fluorescence lifetime τ is the reciprocal of the sum of the rate constants.

$$\tau = \frac{1}{\Gamma_{\mathrm{r}} + \Gamma_{\mathrm{nr}}} \tag{2.3}$$

The mathematical expression of fluorescence lifetime (see Eq. 2.3) reveals that both radiative and non-radiative processes coexist during the fluorophore deactivation. The fluorescence lifetime is the sum of rate which depopulate the excited state. As the number of excited state molecules $M(t)$ is proportional to the fluorescence intensity of the δ pulse response $I_\delta\,(t)$, integration between $t = 0$ and t yields a exponential function similar to a radioactive decay.

$$I_\delta\,(t) = I_0 \exp\left(-\frac{t}{\tau}\right) \tag{2.4}$$

where I_0 is the initial total intensity at time 0. The fluorescence lifetime can be determined by measuring the time it takes the fluorescence intensity to reach $1/e$ of its original value I_0 at $t = 0$ upon optical excitation with a δ-pulse.

In many applications, the sample composes of a mixture of fluorophore components, each displaying its individual decay time. We may use the multi-exponential model to describe the intensity decay as the sum of individual exponential decays.

$$I_\delta(t) = \sum_{i=1}^{N_\tau} \alpha_i \exp\left(-\frac{t}{\tau_i}\right) \tag{2.5}$$

Eq. 2.5 contains multiple fluorophore components, where N_τ denotes the total number of different fluorophore components, each has a lifetime τ_i and an *intensity amplitude* or *pre-exponential amplitude* α_i. Eq. 2.5 describes a model of time-resolved fundamental fluorescence response to a delta function excitation pulse, which is also referred to the fluorescence decay model.

It is different from the intensity amplitude α_i, the contribution of each individual fluorescence component to the total steady-state intensity is described as the *fraction intensity* or *fraction contribution* f_i. The f_i for the ith fluorophore in a mixture is given by

$$\mathrm{f}_i = \frac{\int_0^\infty I_{\delta,i}(t)\,dt}{\int_0^\infty I_\delta(t)\,dt} = \frac{\alpha_i\tau_i}{\sum_{i=1}^{N_\tau}\alpha_i\tau_i} \tag{2.6}$$

In the above expression, $I_{\delta,i}$ is the fluorescence intensity calculated for the ith fluorophore at a particular wavelength and α_i is the corresponding fraction amplitude of its exponential decay. We have

$$I_{\delta,i}(t) = \alpha_i \exp\left(-t/\tau_i\right) \tag{2.7}$$

In a multi-exponential decay model, we skip the initial total intensity I_0. Instead, the amplitudes α_i or fractions f_i are used. This is because in most intensity analysis the total intensity is not measured, as the sum of amplitudes $\sum \alpha_i$ or fractions $\sum \mathrm{f}_i$ is normalized to unity. So we have

$$\sum_{i=1}^{N_\tau} \alpha_i = \sum_{i=1}^{N_\tau} \mathrm{f}_i = 1 \tag{2.8}$$

Since the sum of f_i or α_i is known, in a multi-exponential decay analysis there are N_τ lifetimes and N_τ or $N_\tau - 1$ amplitudes or fractions. The means, in a three decay-time fit, there are only five independent variable parameters, three lifetimes and two amplitudes or fractions.

In multi-exponential decay, it is often useful to determine the *average lifetime* $\bar{\tau}$. The average lifetime is the average amount of time a fluorophore spends in the excited state. It can be calculated

by averaging the time over the intensity decay of each individual fluorophore component.

$$\bar{\tau} = \frac{\int_0^\infty t I_\delta(t)\, dt}{\int_0^\infty I_\delta(t)\, dt} = \frac{\int_0^\infty t \sum_{i=1}^{N_\tau} \alpha_i \exp\left(-\frac{t}{\tau_i}\right) dt}{\int_0^\infty \sum_{i=1}^{N_\tau} \alpha_i \exp\left(-\frac{t}{\tau_i}\right) dt} \tag{2.9}$$

After integration we obtain

$$\bar{\tau} = \frac{\sum_{i=1}^{N_\tau} \alpha_i \tau_i^2}{\sum_{i=1}^{N_\tau} \alpha_i \tau_i} = \sum_{i=1}^{N_\tau} \mathrm{f}_i \tau_i \tag{2.10}$$

2.3 Time-Resolved Fluorescence Techniques

There are a number of experimental techniques carried out by resolving the fluorescence lifetime. Generally, these time-resolved fluorescence approaches can be categorized as operating in either *time-domain* (TD) or *frequency domain* (FD).

2.3.1 Time Domain Lifetime Measurement

Fig. 2.1 shows the principle of TD-measurement.

Measuring lifetime via TD approaches is intuitive. It exploits the fact that the fluorescence emission is theoretically proportional to the number of molecules in the first excited state, and hence it decays exponentially. In the TD measurement, the examined quantity is the decay of the fluorescence intensity which is produced in response to a train of δ-pulses, commonly known as a "dirac comb" function.

$$\Delta_T(t) = \Delta_0 \sum_{k=0}^{N_\Delta} \delta(t - kT). \quad k \in \mathbb{N} \tag{2.11}$$

where T is the period of the repeated pulses, N_Δ is the number of δ-pulse periods, Δ_0 is the intensity of the pulse. The fluorescence response caused by the δ-pulse at time $t = 0$ can be described by Eq. 2.4. With the illumination $\Delta_T(t)$, the intensity of the fluorescence light is the

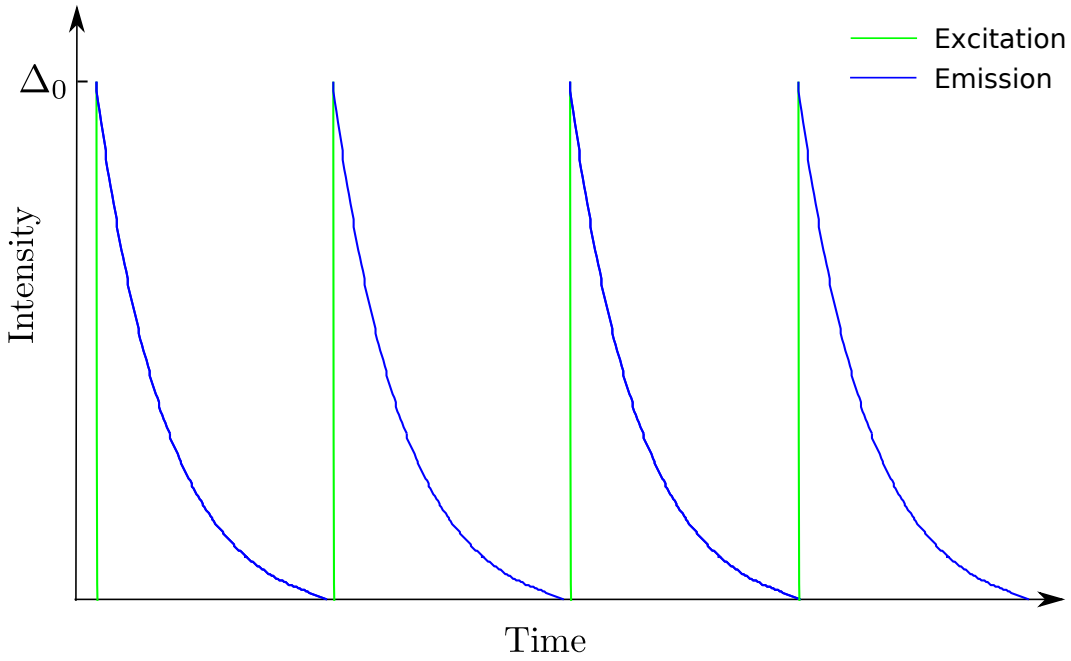

Figure 2.1: The principles of TD- measurement approaches. A Dirac comb excitation and the exponential decays of the fluorescence signal. Δ_0 is the initial intensity.

convolution

$$I_{\text{em}}(t) = \big(\Delta_T \star I_\delta\big)(t) = \int_0^\infty \Delta_T(t') \cdot I_\delta(t - t')dt' \tag{2.12}$$

After derivation we get the result

$$I_{\text{em}}(t) = \Delta_0 \cdot \frac{\exp\left(-\dfrac{t - kT}{\tau}\right)}{1 - \exp\left(-\dfrac{T}{\tau}\right)}, \quad kT \leqslant t < (k+1)T, \quad k \in \mathbb{N} \tag{2.13}$$

which is a periodic function. The measurement is made in each period of pulse train

2.3.2 Frequency Domain Lifetime Measurement

Rather than acquiring the data in TD, it is equally feasible to acquire the data in the frequency-domain. The FD-measurement technique is very well established in the field of fluorescence lifetime measurement. FD-measurement approaches have many attractive features and are widely used over the past decade, especially in the biological application [Gol09, GJJC93]. FD-measurement

depends on the delay in the emission following photo-excitation, resulting from the finite fluorescence lifetime of the intervening excited singlet state. The excitation light source is normally a sinusoidal function modulated at a certain frequency and the fluorescence emitted light will also be modulated at the same frequency only with some phase delay and some loss in the depth of the modulation relative to the scattered excitation light, as depicted in Fig. 2.2.

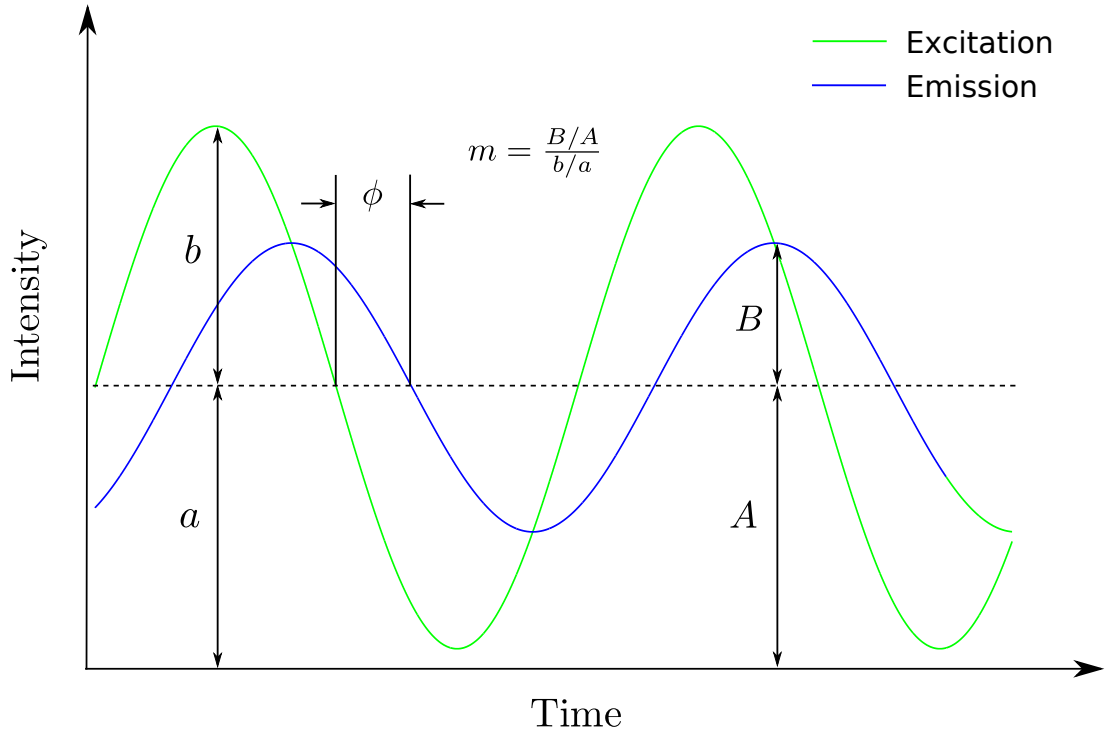

Figure 2.2: The principles of FD-measurement approaches. A sinusoidal wave excitation with the offset a, amplitude b and the resulting fluorescence emission which has the offset A, amplitude B and a phase delay ϕ, a decreased modulation depth m.

We assume a generalized excitation signal, which contains multiple harmonics. Let $I_{\text{ex}}(t)$ indicate an arbitrary fluorescence excitation signal modulated at a fundamental frequency ω. It can be described by a Fourier expansion with different modulation depths and phase angles at each harmonic frequency.

$$I_{\text{ex}}(t) = 1 + \sum_{h=1}^{N_h} m_{\text{ex},h} \sin(h\omega t + \phi_{\text{ex},h}) \tag{2.14}$$

where h represents the hth harmonic, ω is the angular excitation frequency of oscillations, $m_{\text{ex},h}$ and $\phi_{\text{ex},h}$ indicate initial the modulation depth and phase angle of the excitation at hth harmonic. $I_{\text{ex}}(t)$ is normalized so that its integral of complete periods over time greater than zero is equal to unity.

The fluorescence emission $I_{\text{em}}(t)$ can be derived by the convolution between the excitation function and the fluorescence response of a dirac pulse function.

$$I_{\text{em}}(t) = (I_{\text{ex}} \star I_{\delta})(t) = \int_0^{\infty} I_{\text{ex}}(t') \cdot I_{\delta}(t - t')dt' \tag{2.15}$$

The convolution product yields

$$I_{\text{em}}(t) = 1 + \sum_{h=1}^{N_h} m_{\text{em},h} \sin(h\omega t + \phi_{\text{em},h}) \tag{2.16}$$

which contains the same frequencies at each harmonic but has a different modulation depth $m_{\text{em},h}$ and phase angle $\phi_{\text{em},h}$ in the hth harmonic of fluorescence emission. The phase shift ϕ_h of the excitation and emission signal can calculated as

$$\phi_h = \phi_{\text{em},h} - \phi_{\text{ex},h} = \arctan(h\omega\tau_{\phi,h}) \tag{2.17}$$

The modulation depth m_h, defined as the amplitude of the modulation divided by the average intensity, is given by

$$m_h = \frac{m_{\text{em},h}}{m_{\text{ex},h}} = \frac{1}{\sqrt{1 + h^2\omega^2\tau_{m,h}^2}} \tag{2.18}$$

where $\tau_{\phi,h}$ and $\tau_{m,h}$ are apparent lifetimes by phase shift and modulation depth of the h-th harmonic. They can be directly determined from the ϕ_h and m_h.

$$\tau_{\phi,h} = \frac{1}{h\omega}\tan(\phi_h) \tag{2.19}$$

$$\tau_{m,h} = \frac{1}{h\omega}\sqrt{\frac{1}{h^2 m_h^2} - 1} \tag{2.20}$$

As the excitation frequency ω is increased from 0 to ∞, the phase shift ϕ_h also increases from 0° to $\pi/2$, and the modulation depth m_h decreases from 1 to 0. As can be seen, the fluorescence response is getting weaker and weaker as the frequency increases. The fluorescence lifetime works like an effective low-pass filter and removes the effect of high frequency or high harmonic components in the fluorescence emission.

It is worth to notice that apparent lifetimes should not be confused with real lifetimes. The values of apparent lifetimes depend on the method of measurements and are not true molecular parameters. In the case of mono-exponential decay, there is only a single lifetime, both of the apparent lifetime estimations yields the same value, $\tau_\phi = \tau_m = \tau$. This is normally the case when only a single fluorescent species of fluorophore is present. For a single species, the apparent

lifetimes are wavelength-constant. However, for a mixture of fluorophores, the apparent lifetimes exhibit wavelength-dependent behavior. As the wavelength decreases, the apparent lifetimes also decrease, and the apparent lifetimes of phase are always shorter than the apparent lifetimes of modulation, $\tau_\phi < \tau_m$.

2.4 Interpretation of the Fluorescence Lifetime Measurement Data in Polar Plane

2.4.1 Transfer Function of Fluorescence Response Signal

So far, we have shown the representation of the dynamic behavior of the TD- and FD-measurement systems by the constructed mathematical models. The FLIM measurement system usually uses a excitation signal as the input and investigates the response signal to that input signal. We may use the *transfer function*, which is well known in analyzing the system behavior in control engineering, to describe the connection between the input and output signal of the FLIM system.

In order to derive the transfer function of FLIM model, we introduce the Fourier analysis to investigate a FLIM system consisting of N_τ non-interacting fluorophores. For using sinusoidal excitation, contains only a fundamental frequency ω, we define $\hat{I}_\delta(t)$ as the result after taking the Fourier transform of the δ-pulse fluorescence response, the transfer function $\mathcal{G}(j\omega)$ is the result been normalized by the total intensity of the fluorescence sample.

$$\mathcal{G}(j\omega) = \frac{\hat{I}_\delta(t)}{\int_0^\infty I_\delta(t)dt} = \frac{\int_0^\infty I_\delta(t)\exp(-j\omega t)dt}{\int_0^\infty I_\delta(t)dt} \tag{2.21}$$

If $\hat{I}_\delta(t)$ is a single exponential decay function, we obtain

$$\mathcal{G}(j\omega) = \frac{\mathrm{f}}{1+j\omega\tau}, \ \ \mathrm{f} = 1 \tag{2.22}$$

Mathematically it is equivalent to the transfer function of the 1st-order RC circuit system as shown in Fig. 2.3 with the excitation as the system input and the fluorescence emission as the system output.

The transfer function $\mathcal{G}(j\omega)$ of a multiple fluorescence lifetimes system is the linear combination of the transfer function of each single fluorescence component $\mathcal{G}_i(j\omega)$ because of the linearity

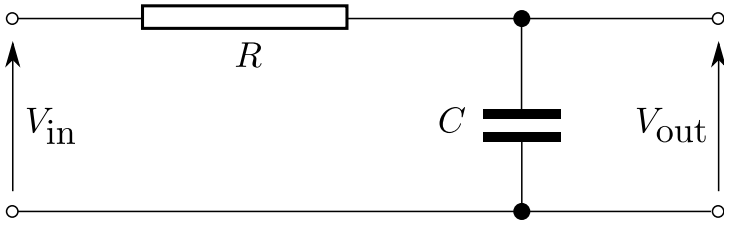

Figure 2.3: A series RC circuit which its transfer function is equivalent to the one of mono-exponential decay.

property of the Fourier transform.

$$\mathcal{G}(j\omega) = \sum_{i=1}^{N_\tau} \mathcal{G}_i(j\omega) = \sum_{i=1}^{N_\tau} \frac{\mathrm{f}_i}{1 + j\omega\tau_i}, \sum_{i=1}^{N_\tau} \mathrm{f}_i = 1 \tag{2.23}$$

The combined transfer function $\mathcal{G}(j\omega)$ can be separated into real part $\mathrm{Re}(\omega)$ and imaginary part $\mathrm{Im}(\omega)$.

$$\mathcal{G}(j\omega) = \underbrace{\sum_{i=1}^{N_\tau} \mathrm{f}_i \frac{1}{1 + \omega^2\tau_i^2}}_{\mathrm{Re}(\omega)} - j \underbrace{\sum_{i=1}^{N_\tau} \mathrm{f}_i \frac{\omega\tau_i}{1 + \omega^2\tau_i^2}}_{\mathrm{Im}(\omega)} \tag{2.24}$$

The multiple fluorescence lifetimes system is equivalent to the parallel connection of multiple RC circuits. The phase angle and modulation can be expressed as

$$\phi = \angle\mathcal{G}(j\omega) = \arctan \frac{\displaystyle\sum_{i=1}^{N_\tau} \mathrm{f}_i \frac{\omega\tau_i}{1 + \omega^2\tau_i^2}}{\displaystyle\sum_{i=1}^{N_\tau} \mathrm{f}_i \frac{1}{1 + \omega^2\tau_i^2}} \tag{2.25}$$

$$m = |\mathcal{G}(j\omega)| = \sqrt{\left(\sum_{i=1}^{N_\tau} \mathrm{f}_i \frac{\omega\tau_i}{1 + \omega^2\tau_i^2}\right)^2 + \left(\sum_{i=1}^{N_\tau} \mathrm{f}_i \frac{1}{1 + \omega^2\tau_i^2}\right)^2} \tag{2.26}$$

Each fluorophore component can be represented as a vector in the complex plane, and the length of each is the modulation depth. It can be calculated as

$$m_i = |\mathcal{G}_i(j\omega)| = \mathrm{f}_i \frac{1}{\sqrt{1 + \omega^2\tau_i^2}} \tag{2.27}$$

For a single fluorescence component with a given frequency ω, we have the maximum length

$|\mathcal{G}_i(j\omega)| = \mathrm{f}_i$, when $\tau_i = 0$; and minimum length $|\mathcal{G}_i(j\omega)| = 0$, when $\tau_i = \infty$. As the lifetime τ_i increases, the vector rotates counterclockwise with the angle

$$\phi_i = \angle\mathcal{G}_i(j\omega) = \arctan(\omega\tau_i) \tag{2.28}$$

Two Components System

Two lifetime components system is commonly used in many biological applications. This system contains two fluorophores having different fluorescence lifetimes.

$$\mathcal{G}(j\omega) = \left(\mathrm{f}_1\frac{1}{1+\omega^2\tau_1^2} + \mathrm{f}_2\frac{1}{1+\omega^2\tau_2^2}\right) - j\left(\mathrm{f}_1\frac{\omega\tau_1}{1+\omega^2\tau_1^2} + \mathrm{f}_2\frac{\omega\tau_2}{1+\omega^2\tau_2^2}\right) \tag{2.29}$$

For a two components system, we have $\mathrm{f}_1 + \mathrm{f}_2 = 1$. By combining this relation into Eq. 2.25 and 2.26, we may come up with the formula of the modulation depth and phase shift for two components system.

$$m = |\mathcal{G}(j\omega)| = \sqrt{\frac{1+\omega^2(\tau_1 - \mathrm{f}_1\tau_1 - \mathrm{f}_2\tau_2)^2}{(1+\omega^2\tau_1^2)(1+\omega^2\tau_2^2)}} \tag{2.30}$$

$$\phi = \angle\mathcal{G}(j\omega) = \arctan\frac{\omega(\mathrm{f}_1\tau_2 + \omega^2\mathrm{f}_1\tau_1^2\tau_2 - \omega^2\mathrm{f}_1\tau_1\tau_2^2 - \omega^2\tau_1^2\tau_2 - \mathrm{f}_1\tau_1 - \tau_2)}{\omega^2\mathrm{f}_1\tau_1^2 - \omega^2\mathrm{f}_1\tau_2^2 - \omega^2\tau_1^2 - 1} \tag{2.31}$$

2.4.2 Phasor Plot Representation of Fluorescence Lifetime Measurement Data

A Nyquist plot is a parametric plot of a transfer function used in automatic control and signal processing. It provides a graphical representation to assess the system behaviors. Similar to the Nyquist plot in the control engineering, we can use the polar plot to represent the signal of fluorescence response graphically. This graphical representation is known as the *phasor plot* [DCZG08], or *polar plot* [RC05] or *A-B plot* [HC05] in FLIM system analysis.

On the phasor plane, an arbitrary fluorescence signal $\mathbf{u}$, its phase angle and amplitude is given by Eqs. 2.25 and 2.26, its real coordinate "Re" and imaginary coordinate "Im" can be written as

$$\begin{aligned} u_{\mathrm{Re}} &= m\cos\phi \\ u_{\mathrm{Im}} &= m\sin\phi \end{aligned} \tag{2.32}$$

Fig. 2.4 illustrates a phasor plot $\mathbf{u}$ on the phasor plane. It can be derived that a phasor plot of one component system always appears in the unit semicircle of the phasor plane [Red05]. The

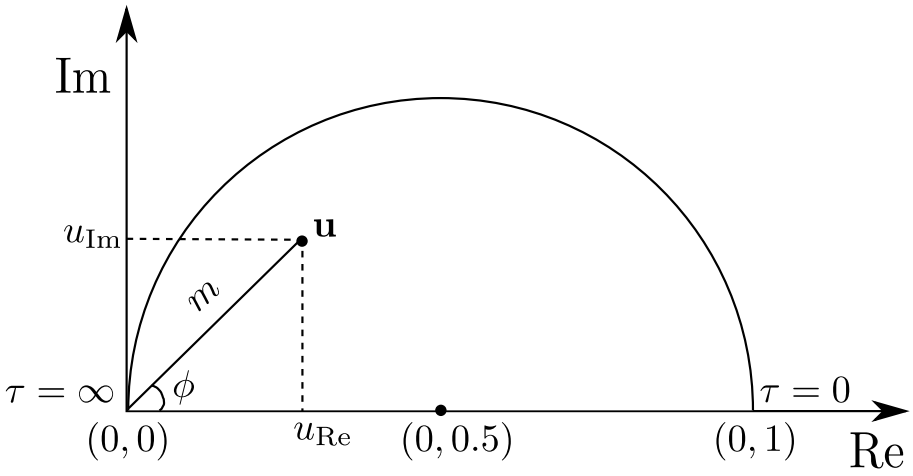

Figure 2.4: A fluorescence signal plot on the phasor plane.

phasor plot of multiple components system does not lie on the semicircle but appears inside the region of the semi-circle. The phasor plot of one component system moves along the semicircle from (0, 1) to (0, 0) as the lifetime increases from zero to infinity. The relation of the position in the semicircle and the lifetime value is nonlinear, it follows the relation of tangent function. The proof is given in the appendix A.1 of this thesis.

The position of the phasor plot on the phasor plane depends not only on the lifetime but also on excitation frequency applied in FD measurement. To identify the lifetimes on the phasor plane, there are frequency sensitive and less frequency sensitive regions. The phasor plot approaches to the origin point as the excitation frequency increases to infinity, because the modulation depth decreases to zero. It is hard to resolve lifetimes closed to origin since slightly small position difference in such area corresponds to very big change in lifetime value.

It is rather sensitive to use relatively low frequency for the lifetime measurement because the linear approximation of tangent value of phase shift and lifetime value can be applied when low excitation frequency is used. When the phase shift ϕ approaches zero, the tangent value can be even approximated by the small-angle approximation $\tau_\phi \approx \phi$. It is the truncation of the Taylor series of tangent function to a second-order approximation. In this case, the phase lifetime τ_ϕ can be approximated by

$$\tau_\phi \approx \frac{\phi}{\omega}; \quad \text{for small } \phi \tag{2.33}$$

The error of this approximation is smaller than 1% when $\phi < 0.176$ [rad], or 31°.

One of the important applications of phasor plot approach is the analysis of multiple components system. Instead of resolving each individual lifetime from the mixture, the phasor approach represents a mixture of fluorophores graphically on the phasor plane as a phasor plot. The phasor

plot of two components system lies on the line segments connecting the phasor plots of two single component. The phasor plot of N_τ components system lies on the polygon area that its N_τ vertices are the phasor plots of components from the mixture.

For a lifetime image composed of a mixture of two component with different fraction intensities. The phasor plots are distributed along a line segment which provides the clue to simplify the calculation of the lifetimes by a simple linear estimation, for which an equation has previously been derived by Clayton [CHV04]. The expressions for the offset a_L and slope b_L of straight line $u_{\text{Im}} = a_L + b_L u_{\text{Im}}$ ca be described as

$$a_L = \frac{1}{\omega(\tau_1 + \tau_2)}; \qquad b_L = \frac{\omega\tau_1\tau_2 - 1}{\omega(\tau_1 + \tau_2)} \tag{2.34}$$

The two lifetimes can be directly calculated with a known a_L and b_L.

$$\tau_{1,2} = \frac{1 \pm \sqrt{1 - 4a_L(a_L + b_L)}}{2\omega a_L} \tag{2.35}$$

Therefore, in order to find the component lifetime in a mixture of two with a set of $(u_{\text{Re}}, u_{\text{Im}})$ pairs, the linear regression can be applied to fit a straight line of a plot of u_{Re} vs. u_{Im} and one can calculate the lifetime using Eq. 2.35.

2.4.3 Representing the Time Domain Lifetime Data on Phasor Plane

The TD data reveals the equivalent information as the FD data. The connection between them are related by a Fourier transform. To represent the data from TD-measurement on the phasor plane, one should perform the Fourier transform on the decay data $I_\delta(t)$ obtained in discredited time variable t_l, $l = 0, 1, 2, \cdots, N_s - 1$, where N_s is the number of discrete time samples. Using the Eq. 2.21, we may find spectrum of the transfer function $\mathcal{G}(\omega_k)$ of $I_\delta(t)$ in discrete form with N_s number.

$$\mathcal{G}(\omega_k) = \frac{\sum_{l=0}^{N_s-1} I_\delta(t_l) \exp(-j\omega_k t_l) dt}{\sum_{l=0}^{N_s-1} I_\delta(t_l) dt} \tag{2.36}$$

The discrete $\mathcal{G}(\omega_k)$ values are distributed at discrete angular frequencies with

$$\omega_k = k\frac{2\pi}{N_s T} \ \text{[rad/sec]}, \quad k = 0, 1, 2, \cdots, N_s - 1 \tag{2.37}$$

where T is the time length of sampling interval. The phase angle ϕ_k and the modulation m_k of the each frequency step k can be calculated by Eq. 2.25 and 2.26.

Fig. 2.5 shows an example of phasor plots histogram representation of the TD lifetime data. The data were obtained from LaVision BioTec GmbH, Bielefeld, which is one of the cooperation member in the FLI-Cam project. The original FLIM image shown in Fig. 2.5(a) contains fluorescence intensity decay in 618×568 pixels. The record time lasts for $10\,\text{ns}$ consisting of $N_s = 50$ sampling points. Fig. 2.5(b) shows the histogram of phasor plots of the TD-FLIM data. Three frequency steps are shown. According to Eq. 2.37, the minimum available frequency is $f_1 = \omega_1/2\pi = 1/T = 1/(10 \times 10^{-9}) = 100\,\text{MHz}$. As can be seen, The frequency span depends on the recording time. In order to achieve the finer frequency resolutions of the spectrum, the longer recording time with more data samples in TD must be taken.

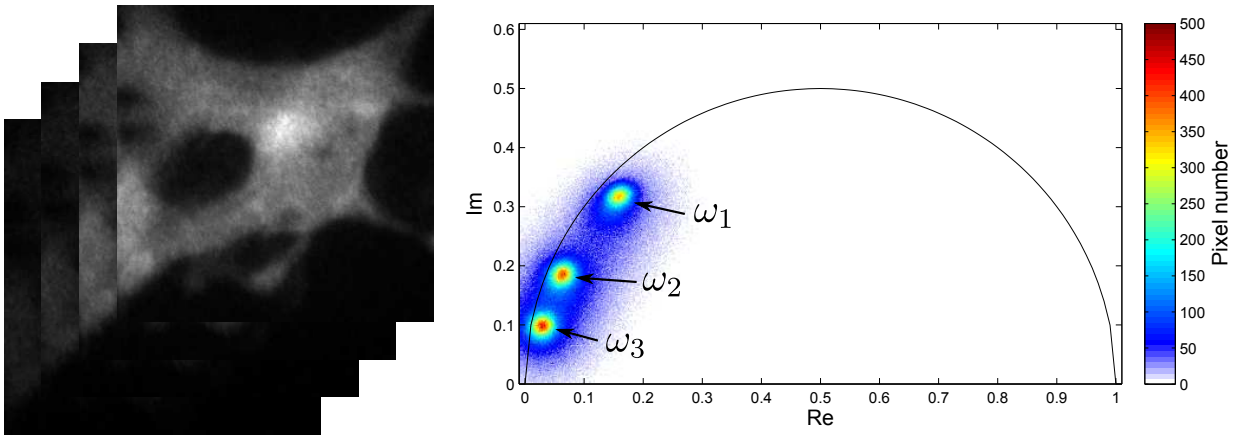

(a) (b)

Figure 2.5: (a) Fluorescence intensity decay images in time series. (Data from LaVison BioTec GmbH) (b) The calculated phasor plots in three frequencies.

The three clusters in Fig. 2.5(b) correspond to three frequencies $f_1 = 100\text{MHz}$, $f_2 = 200\text{MHz}$ and $f_3 = 300\text{MHz}$. As the frequency increases, the cluster is slowly moving towards the origin. The pixels within the cluster show similar lifetime value although their gray value intensities vary in the fluorescence decay image.

2.5 Lifetime Calculation Methods

From the previous section, we know that for one component system both modulation lifetime and phase lifetime equal to the actual mono-exponential lifetime. However, it is not the case for multiple components system. There are several approaches to resolve the lifetimes and their corresponding fraction amplitude or fraction intensity by measuring phase shift and modulation depth, including iterative ones and non-iterative (analytical) ones.

2.5.1 Global Analysis

Global analysis [KBB83, LLC+84, Bee92, VSB00] is an approach to improve the accuracy of a data fit by the analysis of data sets from FD-FLIM that are acquired under multiple experimental conditions to a common model . The global analysis assumes some of the parameters are identical for each experiment.

In multiple fluorescence lifetimes system, the unknowns f_i and τ_i can be find by least-square approach, the best fit between the calculated values and measured data under multiple frequencies. The function to be minimized is defined as

$$\chi_R^2 = \frac{1}{v}\sum_{\omega}\left(\frac{\phi_\omega - \phi_{c\omega}}{\delta\phi}\right)^2 + \frac{1}{v}\sum_{\omega}\left(\frac{m_\omega - m_{c\omega}}{\delta m}\right)^2 \tag{2.38}$$

where ϕ_ω and m_ω are the measured values of phase angle and modulation at frequency ω, $\delta\phi$ and δm are the experimental uncertainties in the measurements. $\phi_{c\omega}$ and $m_{c\omega}$ indicate the calculated values of phase and modulation, respectively. v defines the degrees of freedom. The value of v is given by the number of measurement.

In some cases when the initial values are not well chosen, the iterative result might not converge to the true lifetimes because multiple fluorescence lifetimes component system has the problem of parameters correlation.

2.5.2 LiMA Algorithm

The LiMA algorithm proposed by A. Esposito et al. [EGW05] provides a robust way of lifetime calculation in FD measurement. The LiMA algorithm was motivated from the quantitative and precise data analysis of FRET data on biological samples. From FD measurement, two lifetime estimations (demodulation lifetime τ_m and phase lifetime τ_ϕ) can be achieved. The LiMA algorithm analyzes the relationship between the τ_m and τ_ϕ and provides an analytical estimates of the decay time variance and average lifetime, which enables fast pixel-wise computation of the lifetime image.

In LiMA approach, the following quantity substitutions are used

$$\tilde{\omega}_i = \omega\tau_i; \quad \rho_i = \frac{\mathrm{f}_i}{1+\tilde{\omega}_i^2} \tag{2.39}$$

with which the formulas 2.25 and 2.26 are replaced as

$$\phi = \arctan\frac{\sum_{i=1}^{N_\tau}\rho_i\tilde{\omega}_i}{\sum_{i=1}^{N_\tau}\rho_i}; \quad m = \sqrt{\left(\sum_{i=1}^{N_\tau}\rho_i\tilde{\omega}_i\right)^2 + \left(\sum_{i=1}^{N_\tau}\rho_i\right)^2} \tag{2.40}$$

then we have $\rho = [\tilde{\omega}_i, \rho_i(\tilde{\omega}_i)]$ which represents the distribution of weighted and normalized lifetime components. The moment of the distribution is defined as

$$q_k = \sum_{i=1}\rho_i\tilde{\omega}_i^k \tag{2.41}$$

The apparent lifetimes can be then expressed in terms of the moments of the distribution

$$\tilde{\omega}_\phi = \frac{q_1}{q_0} = \tau_\phi\omega; \quad \tilde{\omega}_m = \sqrt{\frac{1}{q_0^2+q_1^2} - 1} = \tau_m\omega \tag{2.42}$$

Here a new distribution $[\tilde{\omega}_i, \rho_i(\tilde{\omega}_i)/q_0]$ is defined. the apparent lifetimes can be rewritten as

$$\tilde{\omega}_\phi = Q_1; \quad \tilde{\omega}_m = \sqrt{\frac{Q_2(2+Q_2) - Q_1^2}{1+Q_1^2}} \tag{2.43}$$

Note that the first moment of the new distribution Q_1 is equal to the mean μ_{LiMA} of distribution ρ, the variance σ_{LiMA} is the second moment Q_2 centered on the mean

$$\sigma_{\text{LiMA}}^2 = Q_2 - \mu_{\text{LiMA}}^2 \tag{2.44}$$

And therefore

$$\tilde{\omega}_\phi = \mu_{\text{LiMA}}; \quad \tilde{\omega}_m = \sqrt{\mu_{\text{LiMA}}^2 + \sigma_{\text{LiMA}}^2\left(\frac{\sigma_{\text{LiMA}}^2}{1+\mu_{\text{LiMA}}^2} + 2\right)} \tag{2.45}$$

the expression for $\tilde{\omega}_m$ is rather complicated. A coefficient of variation of the distribution $CV =$

$\sigma_{\text{LiMA}}/\mu_{\text{LiMA}}$ is defined. If $CV < 1$, we may further simplify the formulism of $\tilde{\omega}_m$

$$\tilde{\omega}_m \approx \sqrt{\mu_{\text{LiMA}} + 2\sigma^2_{\text{LiMA}}} \tag{2.46}$$

By the approximation the variance, CV and second moment Q_2 can be estimated by

$$\sigma_{\text{LiMA}} \approx \sqrt{\frac{1}{2}\left(\tilde{\omega}_m^2 - \tilde{\omega}_\phi^2\right)} \tag{2.47}$$

$$CV \approx \frac{1}{\tilde{\omega}_\phi}\sqrt{\frac{1}{2}\left(\tilde{\omega}_m^2 - \tilde{\omega}_\phi^2\right)} \tag{2.48}$$

$$Q_2 \approx \frac{1}{2}\left(\tilde{\omega}_m^2 + \tilde{\omega}_\phi^2\right) \tag{2.49}$$

After derivation the average lifetime can then be calculated by approximated moments parameter

$$\bar{\tau} = \tau_\phi \left(1 + \frac{2\sigma^2_{\text{LiMA}}}{1 + Q_2}\right) \tag{2.50}$$

It is worth to notice that the LiMA algorithm only provides the approximate average lifetime estimates. It does not give the lifetime and its amplitude or fraction of each individual component in a mixture of fluorophores.

2.5.3 Weber's Moment Algorithm

Weber [Web81] derived a closed-form analytical method to extract the multi-component lifetimes and the relative contributing intensities from multi-harmonic excitation frequency measurements. By this method moments of multi-component lifetime distribution can be analytically evaluated from the phase angles and modulation depths obtained at several harmonic frequencies. Since there is no iterative minimization required, the computation time is much faster compared to the global analysis approach. By Weber's moment algorithm the fluorescence lifetime can be directly calculated without performing the expensive least square fitting procedure.

For a system containing only two lifetime components and two excitation frequencies are used, the algorithm of the general case reduces to a very simple form. The moments of the distribution of lifetimes take the form:

$$M_0 = p_1^2 u_{\text{Re},1} - p_2^2 u_{\text{Re},2} \quad M_1 = p_1 u_{\text{Im},1} - p_2 u_{\text{Im},2} \tag{2.51}$$

$$M_2 = -u_{\text{Re},1} + u_{\text{Re},2} \quad M_3 = -u_{\text{Im},1}/p_1 + u_{\text{Im},2}/p_2 \tag{2.52}$$

where $u_{\text{Re},1}$, $u_{\text{Im},1}$ and $u_{\text{Re},2}$, $u_{\text{Im},2}$ are the phasor plot data from two frequency measurements. p_1 and p_2 are small dimensionless numbers given by

$$p_1 = \frac{\omega_1}{\omega_0}; \quad p_2 = \frac{\omega_2}{\omega_0} \tag{2.53}$$

with ω_0 chosen as a base frequency such as one megahertz.

$$\gamma_1 = \frac{M_3 M_0 - M_2 M_1}{M_2 M_0 - M_1} \quad \gamma_2 = \frac{M_3 M_1 - M_2}{M_2 M_0 - M_1} \tag{2.54}$$

$$\tau_1', \tau_2' = \frac{\frac{\gamma_1}{2} \pm \sqrt{\frac{\gamma_1^2}{4} - \gamma_2}}{\omega} \tag{2.55}$$

where the two roots of the quadratic expression are $\omega_0\tau_1$ and $\omega_0\tau_2$

$$\alpha = 1 - \frac{u_{\text{Re},1} - (1 + p_1^2\tau_1^2)^{-1}}{(1 + p_1^2\tau_2^2)^{-1} - (1 + p_1^2\tau_1^2)} \tag{2.56}$$

2.5.4 Evaluation of Lifetime Calculation Methods

According to the work made by Schlachter et al. [SEE+09] , the global analysis approach has only a slightly better performance than the other analytical lifetime calculation approaches but consumes much more computation power. In their work, a comparison was performed between the global analysis method and Weber's moment method. The test sample had 256×256 pixels. It took 4400 seconds for the global analysis and less than 1 second for the Weber's method. This is because the nonlinear minimization procedure in the global analysis is very expensive, especially in dealing with wide-field FLIM images. Therefore, the global analysis method is not suitable for a rapid FLIM acquisition system.

Average Lifetime Calculation by LiMA and Weber's method

A few tests were made to analyze the ability of the non-iterative lifetime calculation methods. The test pattern contains 128×128 pixels. There were two lifetime components on the test pattern, one had a lifetime $\tau_1 = 4$ ns, the other one had a lifetime $\tau_2 = 2$ ns. The fraction amplitude α varied

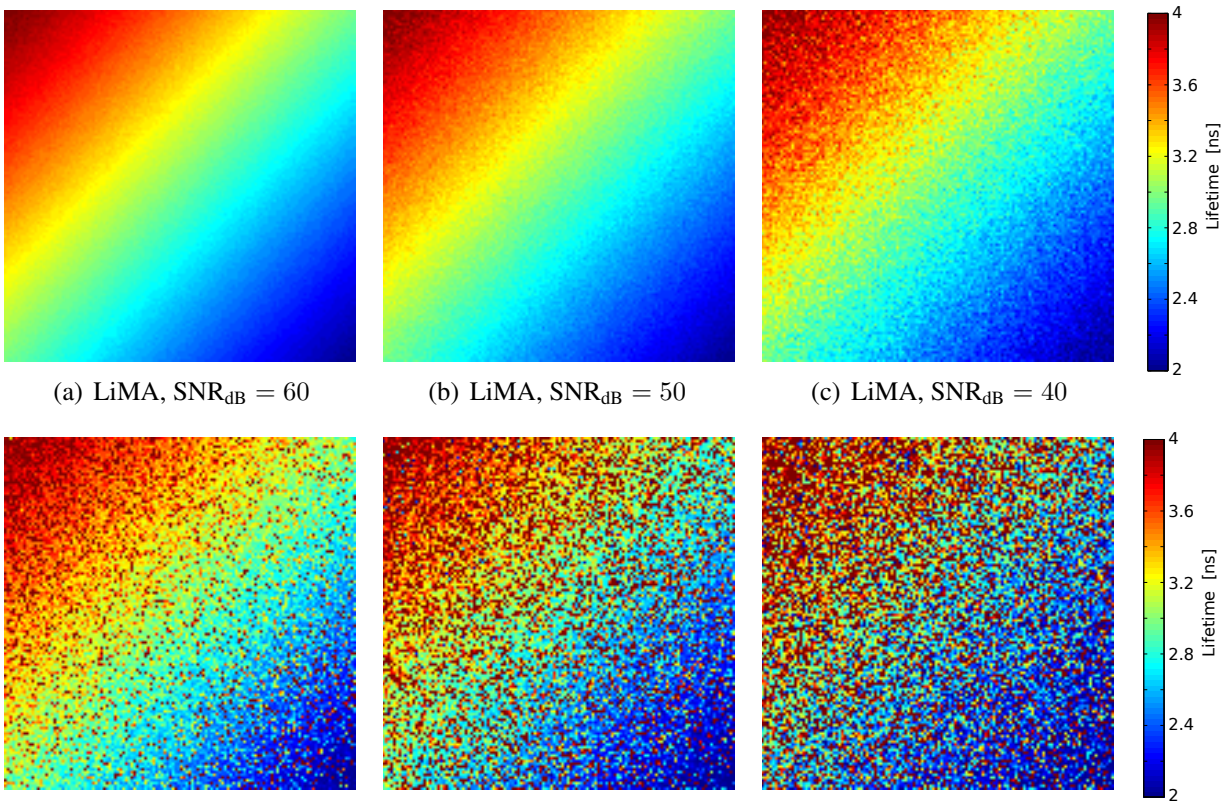

(a) LiMA, $\mathrm{SNR}_{\mathrm{dB}} = 60$ (b) LiMA, $\mathrm{SNR}_{\mathrm{dB}} = 50$ (c) LiMA, $\mathrm{SNR}_{\mathrm{dB}} = 40$

(d) Weber, $\mathrm{SNR}_{\mathrm{dB}} = 60$ (e) Weber, $\mathrm{SNR}_{\mathrm{dB}} = 50$ (f) Weber, $\mathrm{SNR}_{\mathrm{dB}} = 40$

Figure 2.6: Comparison of average lifetime calculation by LiMA's method and Weber's moment method with different noises level of 60dB, 50dB and 40dB in three different columns. The test pattern contains a two lifetime components system with $\tau_1 = 4$ ns, $\tau_2 = 2$ ns, α_1 increases from 0 to 1 along the diagonal from the upper left to bottom right.

along the direction of the diagonal from 0 to 1. Two excitation at frequencies 40 MHz and 60 MHz were applied to the test pattern to obtain the measurement results.

Fig. 2.6 compares the performance of the lifetime calculation by LiMA method and Weber's method. The computation times of both approaches are nearly the same. But it is obvious that average lifetime calculation using LiMA method shows much better performance than using the Weber's method, especially in very noisy images. However, the LiMA's method only provides the average lifetime estimation and does not calculates the lifetime values of each component in the mixture.

Average Lifetime Calculation

If the lifetimes of each mixing component are needed, the LiMA can not fulfill the requirements anymore, and the Weber's method has to be used. Fig. 2.7 shows a test to further explore the ability of the Weber's approach. Similar to the results shown in 2.6, Weber's method is very vulnerable to the noise. We found that more and more singularities appear in the result as the noise level raises. It almost failed in the calculation of mixing fraction intensity image by a SNR level of 35 dB. Since Weber's method calculates the lifetime from only two data samples (two frequencies data) analytically, it will produce large error deviation when outliers exist.

Furthermore, Weber's method confuses the two lifetimes a little when one of the component in the mixture dominates, i.e., fraction amplitude α_1 or α_2 approaches 1. In such cases, the two roots results calculated from Eq. 2.55 reverse from each other. When the fraction amplitudes of two components are equally distributed, the results of Weber's method are reasonable.

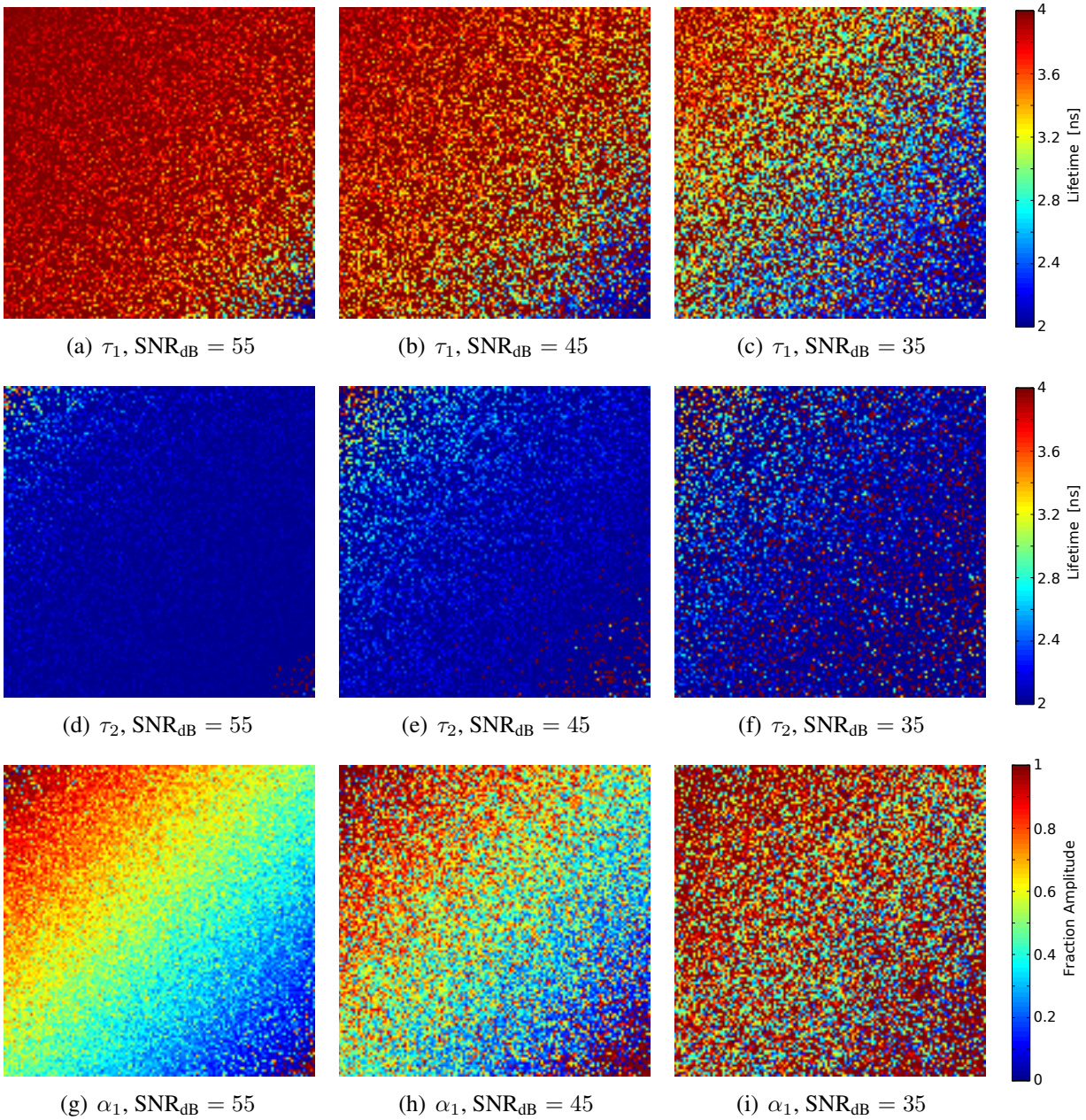

(a) τ_1, $\text{SNR}_{\text{dB}} = 55$ (b) τ_1, $\text{SNR}_{\text{dB}} = 45$ (c) τ_1, $\text{SNR}_{\text{dB}} = 35$

(d) τ_2, $\text{SNR}_{\text{dB}} = 55$ (e) τ_2, $\text{SNR}_{\text{dB}} = 45$ (f) τ_2, $\text{SNR}_{\text{dB}} = 35$

(g) α_1, $\text{SNR}_{\text{dB}} = 55$ (h) α_1, $\text{SNR}_{\text{dB}} = 45$ (i) α_1, $\text{SNR}_{\text{dB}} = 35$

Figure 2.7: Lifetime calculation by Weber's moment method with different noises level of 55dB, 45dB and 35dB in three different columns. The first two rows are the calculated lifetimes from each component of the mixture. The third row shows the calculated mixing fraction intensity α_1. The test pattern contains a two lifetime components system with $\tau_1 = 4$ ns, $\tau_2 = 2$ ns, α_1 increases from 0 to 1 along the diagonal from the upper left to bottom right.

2.5.5 Summary

In this chapter we analyze both TD- and FD-measurement data in a model-free fashion. Although the imaging techniques for TD- and FD-measurment are quite different, the theoretical frameworks are equivalent. The different fluorescence responses result from the convolution with different excitation signal inputs. TD- and FD-measurement data output can also be connected by a Fourier transform. Both of them can be graphically represented on the phasor plane, which provides a unique mapping between the fluorescence lifetime measurement data and phasor plots. On the phasor plane, the fluorophores having the similar lifetimes can be easily identified and classified.

In the end, we have reviewed three different lifetime calculation methods, including global analysis (iterative), LiMA method and Weber's method (non-iterative). For rapid lifetime calculation of wide-field FLIM, it is not wise to choose iterative approaches like global analysis using the contemporary computation power. In such case, non-iterative methods are much more effective and provide reasonable precision. According to the comparison results, LiMA method is more suitable for the applications in which only average lifetime is required. To resolve individual lifetimes from a mixture multiple components, it is highly recommended to perform a preprocessing step of image denoising before using Weber's method if too low intensity FLIM images are encountered. A novel denoising algorithm specially designed for the enhancement of FLIM images, which facilitates the FLIM post-processing approaches such as Weber's method, will be presented in Chapter 6 of this thesis.

Chapter 3

Fluorescence Lifetime Imaging Techniques

3.1 Overview

In last chapter, the theoretical background of the fluorescence lifetime measurement is described. And we focus on the imaging techniques of fluorescence lifetime measurements in this chapter. The FLIM images are based on the differences in the lifetimes of the fluorescence from fluorescent molecules. The FLIM can be used as an imaging technique in confocal microscopy, two-photon excitation microscopy and multiphoton tomography.

Creation of a lifetime image with reasonable spatial resolution requires measurement of 256×256 or more individual lifetime measurements, or even more lifetimes if higher spatial resolution is required. Usually, the FLIM images can be acquired either using scanning method or using wide-field method [Lak06]. About 20 years ago, due to the difficulty of single lifetime measurement, the FLIM technique was nearly unimaginable. As the development of the modern imaging technology, the FLIM techniques are becoming very practical and are able to be applied for studying of living cells.

FLIM can be performed using TD or FD methods depending on different excitation sources. In Sect. 3.2 we first review the most common used methods for TD-FLIM, and then focus on the theoretical realization of using a time-gated pulse-based ToF camera, TriDiCam for FLIM image acquisition. Several time-gated schemes including both overlapping gate and contiguous gates are presented for the single and double exponential lifetime. In Sect. 3.3, the commonly used homodyne and heterodyne detection methods, which aim at reducing the frequency of measured signal, are reviewed. And then we propose a multi-sampling heterodyne frequency modulation technique using the continuous-wave-based ToF camera. The demodulation algorithm based on DFT is given. In the end, some cautions of using DFT for demodulation are discussed.

3.2 TD-FLIM

3.2.1 General Approaches

3.2.1.1 Time-Correlated Single-Photon Counting

The most widely used TD-FLIM measurement technique is *Time-Correlated Single Photon Counting (TCSPC)* [OP86, BBH$^+$04], which is able to record very low excitation intensity with a lifetime range from sub-nanosecond to hundreds of nanoseconds. The TCSPC is based on the fact that the probability of detecting a single photon at time t after an exciting pulse is proportional to the fluorescence intensity at that time. Usually the light intensity of the repetitive pulse excitation is very low, the probability of a single photon detection in a signal period is much less than one. The detection of serval photons in a signal period is considered as a small probability event.

The principle of TSCPC is the detection of single photons and the measurement of their arrival times. TSCPC uses high repetitive light pulse as the excitation and accumulates a sufficient number of photon events in order to achieve the statistical data precision. From those data the decay curve can be reconstructed.

The TSCPC imaging can be accomplished by laser scanning microscopes combined with a multi-detector technique that allows to record time-resolved image in several wavelength channels simultaneously. This technique relies on a multi-dimensional histogramming process that records the photon density versus the time within the fluorescence decay function [BBB$^+$03].

3.2.1.2 Time-Gating

Time-gated [SVDGG98, GAAVS02, Gad08] schemes can be considered as a simplified version of TCSPC. In time-gated detection approaches, the fluorescence emission is usually detected in two or more different time channels, each delayed by a different time offset relative to the excitation pulse. The collection time of time-resolved image by TD-FLIM based time gating method is generally very short (within a few seconds), much less than the collection time required by TSCPC device, which takes several minutes. Furthermore, according to the work of Gerritsen et al. [GAAVS02], time-gated method shows its advantage of better signal-to-background ratio in the images by suppressing background signals correlated with the excitation pulse. Therefore, it is optimal for discriminating autofluorescence in biological specimens.

3.2.2 Lifetime Measurement Using TriDiCam Image Sensor

In the scope of this thesis we emphasize on the implementation based on the time-gated TD-FLIM methods. A theoretical solution of using TriDiCam [Tri] for the TD-FLIM is presented. It can be applied for resolving lifetimes in both mono-exponential and double-exponential decays by

using simultaneous recording of the time-gated images. This technique brings a higher frame rates than very common used sequential pixel data acquisition FLIM system like time-correlated single-photon counting (TCSPC) in TD or heterodyne detection scheme in FD. In the approaches based on sequential recording, a series of sub-images samples time-varying FLIM signal at different time-gated settings (TD) or phase angles (FD). They are therefore vulnerable to motion artifacts. The prospect of the FLIM system in high speed is attractive because the motion artifacts can be reduced and observation of samples in realtime can be realized.

3.2.2.1 Working Principle of TriDiCam

The TriDiCam is a fast and accurate 3D imaging system. It measures the distance by the ToF principle. The ToF, which provides the depth information of the scene, is measured and calculated by sending laser pulses to the object and analyzing the received reflected pulses in each pixel of the 3D sensor chip.

The principle of the TriDiCam is sketched in Fig. 3.1. The depth information can be calculated by two simultaneous measurements with two different shutter times T_A and T_B. Both measurements start at the same time as soon as the laser pulse begins. The first shutter integrates the reflected light for exact time interval of one laser pulse. The length of the second shutter is longer than the length of the first one so that the whole laser pulse can be integrated in the second measurement. The depth information can be calculated from the two different amounts of photons received from the two shutters after substraction of the background light.

The image sensor records the fluorescence decay signal by accumulating photons over a certain shutter time, i.e. exposure time. We define the minimum adjustable shutter time as Δt (unit shutter time). As shown in Fig. 3.2, the fluorescence decay curve is divided into serval contiguous areas with the same length Δt. The area of any interval with length Δt can be calculated by taking integration of the decay curve from a starting time point $k \cdot \Delta t$ to $(k+1) \cdot \Delta t$. After taking the normalization onto the integration result, then we have:

$$c'_k = \frac{1}{\Delta t} \int_{k \cdot \Delta t}^{(k+1) \cdot \Delta t} \alpha \exp\left(-\frac{t}{\tau}\right) dt \tag{3.1}$$

$$= \frac{\alpha\tau}{\Delta t} \left(\exp\left(-k \cdot \frac{\Delta t}{\tau}\right) - \exp\left(-(k+1) \cdot \frac{\Delta t}{\tau}\right) \right) \tag{3.2}$$

To simplify the derivation we use such replacements:

$$\upsilon = \frac{\tau}{\Delta t}; \;\; C_0 = \alpha\upsilon; \;\; \varrho = \exp\left(-\frac{1}{\upsilon}\right) \tag{3.3}$$

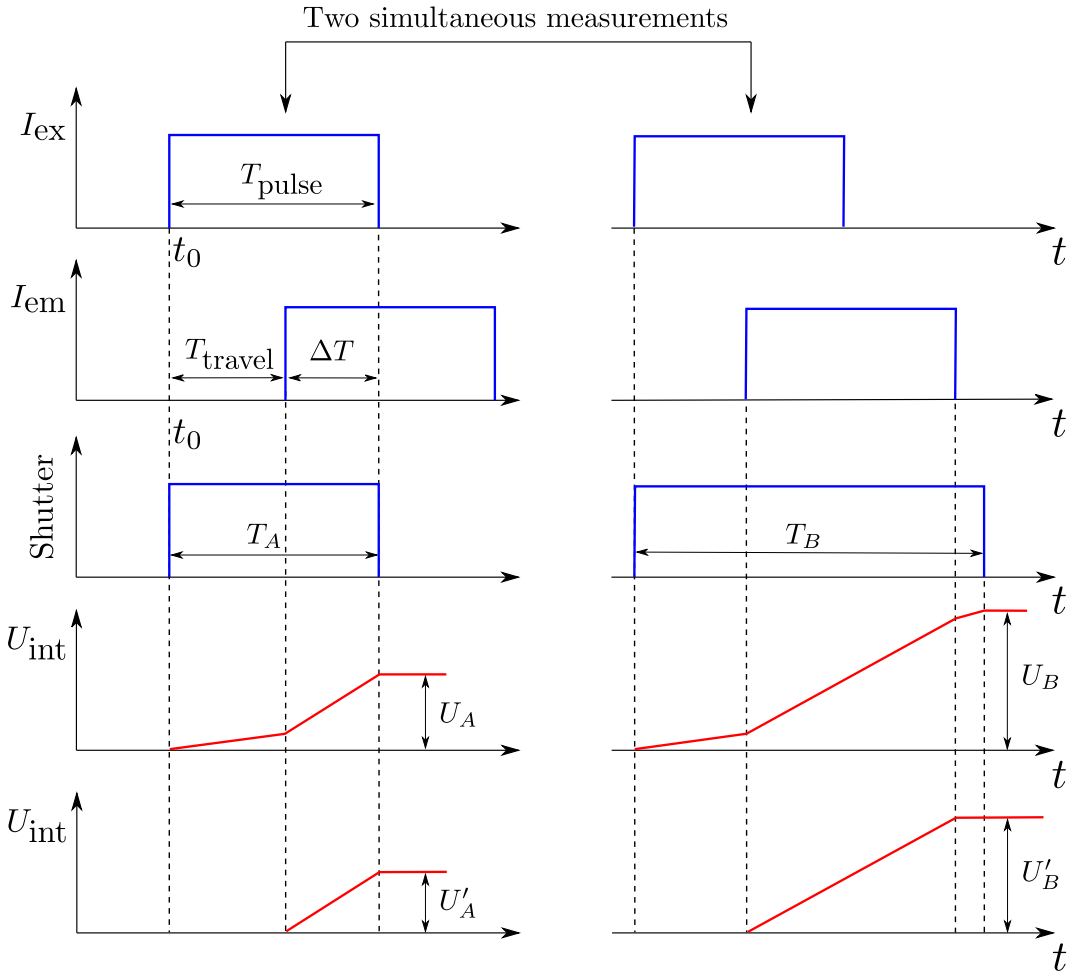

Figure 3.1: The Time-of-Flight measurement principle of the TriDiCam 3D sensor chip for distance measurement. Revised from [Tri09].

so that

$$c'_k = C_0(\varrho^k - \varrho^{k+1}) \tag{3.4}$$

In TriDiCam image sensor chip, two measurements c_0 and c_1 can be acquired simultaneously after a laser pulse. Both of them are the combination of one or more c'_ks at even, discrete intervals. In mono-exponential decays, two unknowns C_0 and ϱ in Eq. 3.24 can be analytically derived by two different measurements c_0 and c_1. The lifetime τ and initial intensity α may be calculated once ϱ and C_0 are determined.

$$\tau = -\frac{\Delta t}{\ln(\varrho)} \tag{3.5}$$

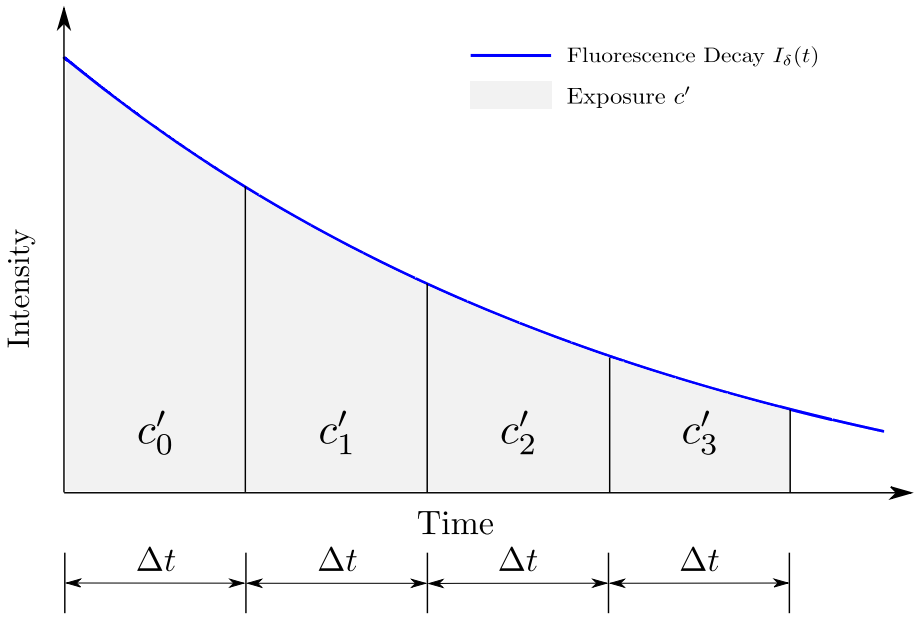

Figure 3.2: Graphical representation of sampling scheme of TriDiCam image sensor for fluorescence lifetime measurement.

$$\alpha = \frac{C_0}{\upsilon} = \frac{C_0 \Delta t}{\tau} \tag{3.6}$$

3.2.2.2 The Rapid Lifetime Determination (RLD) Method

Different from the standard approach which fits the data to the exponential intensity decay function $I(t)$ versus time t by a weighted non-linear least squares (WNLLS). The rapid lifetime determination method (RLD) [BD89, BD91], however, provides a significant faster way for lifetime acquisition and keeps the precision of calculation under optimum conditions. The RLD method calculates the fluorescence lifetime analytically by only two measurements [1] instead of performing the iterative curve fitting procedure.

The RLD method requires two measurements with their shutter time in the same length. After the pulse excitation, the first shutter integrates the decay from 0 to Δt. The second shutter starts from Δt ends at $2\Delta t$. The areas of the two measurements are:

$$c_0 = c'_0; \;\; c_1 = c'_1 \tag{3.7}$$

[1] In RLD method one more measurements is necessary if the exponential decay has unknown base line. In this thesis we assume the a zero base line since TriDiCam image sensor also does a background light measurement.

The two unknowns may be extracted easily by using

$$\varrho = \frac{c_1}{c_0};\;\; C_0 = \frac{c_0^2}{c_0 - c_1} \tag{3.8}$$

3.2.2.3 Overlapping Gates Schemes

Scheme RLDo1

The RLD method can be slightly modified to be adapted to the time-gated setting used in TriDiCam. Similar to the 3D ToF measurement, both shutters start at the same time after the excitation. The open time of the second shutter is twice as long as the one of the first shutter. Assuming the length of the first shutter is Δt, we have:

$$c_0 = c_0';\;\; c_1 = c_0' + c_1' \tag{3.9}$$

The two unknowns can be derived as:

$$\varrho = \frac{c_1}{c_0} - 1;\;\; C_0 = \frac{c_0^2}{2c_0 - c_1} \tag{3.10}$$

Scheme RLDo2

Unlike the scheme RLDo1 , which takes advantage of the RLD method, scheme RLDo2 extends the shutter length of the second measurement to three times of the length of the first shutter. The two measurements are:

$$c_0 = c_0';\;\; c_1 = c_0' + c_1' + c_2' \tag{3.11}$$

After the derivation the unknowns C_0 and ϱ can be found:

$$\varrho = \frac{-c_0 + \sqrt{-3c_0^2 + 4c_0c_1}}{2c_0} \tag{3.12}$$

$$C_0 = \frac{c_0\left(3c_0 + \sqrt{c_0\left(-3c_0 + 4c_1\right)}\right)}{6c_0 - 2c_1} \tag{3.13}$$

Scheme RLDo3

In this scheme, the length of the first shutter is extended. The second shutter is kept the same as scheme RLDo2. The two shutters in this scheme possess a larger common region. The two measurements are:

$$c_0 = c'_0 + c'_1; \;\; c_1 = c'_0 + c'_1 + c'_2 \tag{3.14}$$

After the derivation the unknowns C_0 and ϱ can be found:

$$\varrho = \frac{-c_0 + c_1 + \sqrt{-3c_0^2 + 2c_0c_1 + c_1^2}}{2c_0} \tag{3.15}$$

$$C_0 = \frac{3c_0^2 - c_1^2 + (c_1 - c_0)\sqrt{-3c_0^2 + 2c_0c_1 + c_1^2}}{6c_0 - 4c_1} \tag{3.16}$$

3.2.2.4 Contiguous Gates Schemes

Schemes RLDo1, RLDo2 and RLDo3 can be easily accomplished using current TriDiCam imaging system without too much changes of the time-gated settings used for depth measurements. Nevertheless, schemes using overlapping gates collect extra amount of photons than contiguous gates approaches like RLD method. Are they really necessary for the lifetime calculations? Do they improve the performance of the FLIM system? Before answering these questions, we present two other schemes without overlapping gates to make a more comprehensive comparison.

RLDc1

In this scheme two contiguous shutters cover a larger region than RLD method. The first shutter starts from 0 to Δt, the second shutter starts from Δt to $2\Delta t$. The two measurements are:

$$c_0 = c'_0; \;\; c_1 = c'_1 + c'_2 \tag{3.17}$$

Two unknowns can be derived:

$$\varrho = \frac{-c_0 + \sqrt{c_0^2 + 4c_0c_1}}{2c_0} \tag{3.18}$$

$$C_0 = \frac{2\sqrt{c_0^3}}{3\sqrt{c_0} - \sqrt{c_0 + 4c_1}} \tag{3.19}$$

Scheme RLDc2

In this scheme, two shutters have the same length as the RLD method. But there is a Δt length interval in between. The two measurements are:

$$c_0 = c_0'; \;\; c_1 = c_2' \tag{3.20}$$

Two unknowns can be derived:

$$\varrho = \sqrt{\frac{c_1}{c_0}} \tag{3.21}$$

$$C_0 = \frac{c_0^2 + \sqrt{c_0^3 c_1}}{c_0 - c_1} \tag{3.22}$$

3.2.2.5 Extended RLD Method in Double Exponential Lifetime

In a double exponential decay, two fluorescence lifetimes and their initial intensities are encountered. We have:

$$I_\delta(t) = \alpha_1 \exp\left(-\frac{t}{\tau_1}\right) + \alpha_2 \exp\left(-\frac{t}{\tau_2}\right) \tag{3.23}$$

and

$$c_k = C_1(\varrho_1^k - \varrho_1^{k+1}) + C_2(\varrho_2^k - \varrho_2^{k+1}) \tag{3.24}$$

Sharman et al. [SPA+99] have developed a modified RLD method for the case of double exponential lifetime. In their methods, four contiguous measurements with same shutter time are required.

$$c_0 = c_0'; \;\; c_1 = c_1'; \;\; c_2 = c_2'; \;\; c_3 = c_3' \tag{3.25}$$

To simplify the form of the lifetime results some intermediate calculations are used.

$$D_1 = c_1 c_1 - c_0 c_2 \tag{3.26}$$
$$D_2 = c_1 c_2 - c_0 c_3 \tag{3.27}$$
$$D_3 = c_2 c_2 - c_1 c_3 \tag{3.28}$$
$$R = D_2 D_2 - 4 D_1 D_3 \tag{3.29}$$

Four unknowns can be calculated as:

$$\varrho_1 = \frac{-D_2 + \sqrt{R}}{2D_1} \tag{3.30}$$

$$\varrho_2 = \frac{-D_2 - \sqrt{R}}{2D_1} \tag{3.31}$$

$$\alpha_1 = \frac{(\varrho_2 c_0 - c_1)^3 \ln(\varrho_1)}{\Delta t \, (\varrho_2 c_0 - \varrho_2 c_1 + c_2 - c_1) \, (\varrho_2^2 c_0 - 2\varrho_2 c_1 + c_2)} \tag{3.32}$$

$$\alpha_2 = \frac{-D_1 \left(\ln(\varrho_1 c_1 - c_2) - \ln(\varrho_1 c_0 - c_1)\right)}{\Delta t(\varrho_2 - 1)(\varrho_2^2 c_0 - 2\varrho_1 c_1 + c_2)} \tag{3.33}$$

The lifetimes τ_1 and τ_2 can be then calculated by Eq. 3.5.

However, in current TriDicam system it is not possible to obtain four measurements using a single laser pulse. In order to resolve the double exponential decays, two laser pulses must be used. The measurement c_0, c_1 and c_2, c_3 are recorded simultaneously after the first and second laser pulse, respectively.

3.3 FD-FLIM

An overview of FD-FLIM detection techniques can be found in [CCG+98]. FD-FLIM approaches always compare the phase degree and the modulation of the fluorescence signal with the modulated excitation. The modulation of the excitation light can be a continuous laser or even using pulsed laser modulated with very hight repetition rate. The phase shift and modulation depth can be then measured at the fundamental frequency of the repetitive pulsed laser.

If the continuous light wave is used as the excitation source, the amplitude is always modulated repetitively at high frequency. To detect the fluorescence lifetime within few nanoseconds range, the excitation light is always modulated at the range between 1 to 200 MHz so that the fluorescence response signal is sensitive enough for the nanosecond range lifetime measurement. The waveform of the excitation light is often sinusoidal, but it can be any periodical waves. Such a repetitive waveform can be decomposed into multiple harmonics by the Fourier analysis, and the fluorescence response signal of each single harmonics can be analyzed separately.

3.3.1 Homodyne and Heterodyne Detection Method

To measure the modulation depth and the phase shift of the fluorescence signal with lifetimes within few nanoseconds, the fluorescence decays are probed using megahertz frequencies. Because of

the simplicity and convenience of the instrumentation, the high frequency fluorescence response signal is not directly measured. Usually gain modulated detectors are used to covert the megahertz frequency signal to a low frequency 10 Hz - 10 KHz or constant (DC) signal, which can be easily measured. There are two approaches, which are implemented using high-speed image intensifier devices, to achieve the desired low frequency output from high frequency input.

The first one is called *homodyne detection* [CL97, CL98]. It is realized by mixing, which is carried out by multiplying, the detection signal with the modulation signal, The result is a DC signal that contains both the phase shift and modulation. An additional measurement at a different reference phase is required to make the result distinct. Homodyne approaches show very high acquisition speed since the gain-modulated image intensifier and CCD detector can be used which enables the possibility of full-field FLIM imaging.

The second one is called *heterodyne detection* [BW04, SC09a, SFY$^+$95]. It is different from the homodyne detection in the way that the heterodyne detection mixes the detection signal with a detector gain modulated at a frequency very close to the excitation modulation frequency. The difference of the frequency is usually chosen to be in the range of few hundreds or few thousands hertz. The result is that the phase angle and modulation depth are transferred to the different frequency signals. The detector output can be sampled at the lower cross-correlation frequency which makes the measurements much easier.

3.3.2 FLIM Measurement Using ToF Image Sensors

The ToF camera [FAT11] is a relatively new type of image sensor which provides 3D imaging at a high frame rate, and with ToF camera the intensity data and depth map can be achieved simultaneously. Esposito et al. [EOG$^+$05] demonstrated the FLIM can be realized by a phase-based ToF camera, MESA SwissRanger SR-2 [mes], at a modulation frequency of 20 MHz. The sensor was developed for high speed lock-in imaging. Therefore, further modification of the CCD were not required.

Similar to the working principle of SwissRanger camera, an innovation optoelectronic device so called *photonic mixing device* (PMD) [Lan00, Sch08, SSVH95, RMH07] realizes ToF-range measurement by continuous wave modulation using multiple detection units, also referred as taps, per pixel. This “smart” pixel is able to perform multiple measurement in parallel.

Fig 3.3 shows the working principle of PMD image sensor. It has two quantum wells (i.e. two taps), where the electrons generated by the incident photons can be accumulated in. The most essential part is the electronic switch, which decides the electrons to be go to the quantum well A or B. If the electronic switch is synchronized with the modulated light source, the accumulated chargers is proportional to a sample of the cross-correlation signal. Therefore, the sensor is able to acquire two samples $c(\theta)$ and $c(\theta + \pi)$ simultaneously.

The discrete switching can be approximated by a rectangular shaped reference signal with frequencies of 10 MHz, which enables the possibility of direct nanosecond range fluorescence lifetime

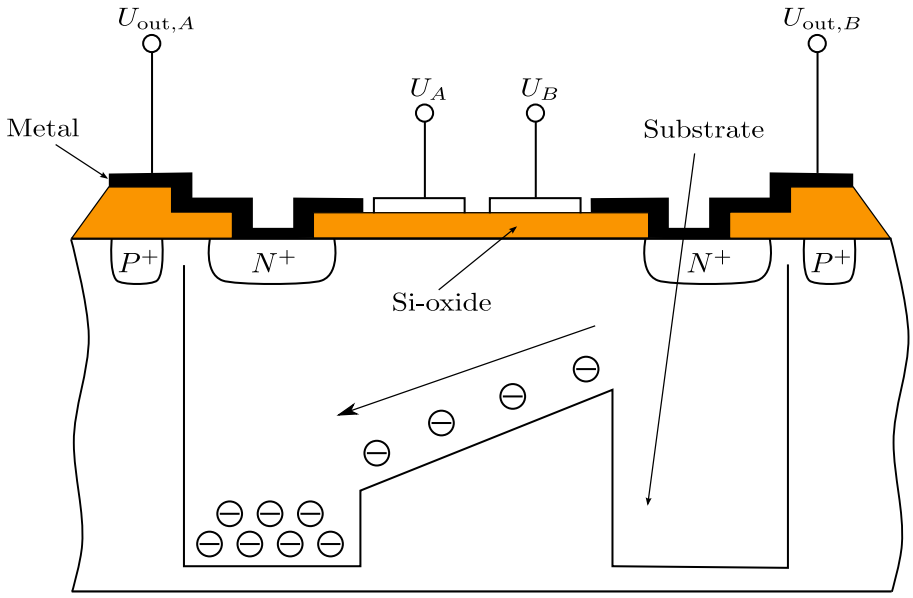

Figure 3.3: Schematic representation of the working principle of PMD (Photonic mixing device) image sensor. Revised from [Zim04].

sensing without reducing the frequency of the fluorescence signal such as homodyne and heterodyne detection techniques.

3.3.3 Heterodyne Modulation Method

Most current available ToF image sensors have a modulation frequency of 20 MHz or 40 MHz, and modulate the camera frequency the same as the excitation frequency, also referred as homodyne modulation technique. This would not have problems for the application of depth sensing. However, for the biological FLIM applications, species having short range lifetimes, which are smaller than 2 ns, are very common. In such cases an excitation frequency above 80 MHz is required to achieve the reasonable accuracy. However, such a frequency is too high for current available ToF image sensors to perform the synchronous demodulation.

To solve this problem, we present an asynchronous scheme – *heterodyne modulation FLIM (HtM-FLIM)* technique which allows different frequencies of light modulation and camera modulation. It can not only be used to demodulate the much higher frequency signals using low camera modulation frequency, but also used for achieving best performance by adjusting the camera modulation to a optimum frequency with a fluorescence signal with a certain known frequency.

Apart from the flexibility of camera modulation frequency, the number of sampling points can be also much more than the current available ToF image sensors, which usually have $N_s = 4$. Raising the number of sampling points in HtM-FLIM enables the detection of multi-harmonics

signal for the application of multiple frequency measurements required by lifetime resolving from multiple components fluorescence system.

Fig. 3.4 shows the sketch of the heterodyne modulation scheme.

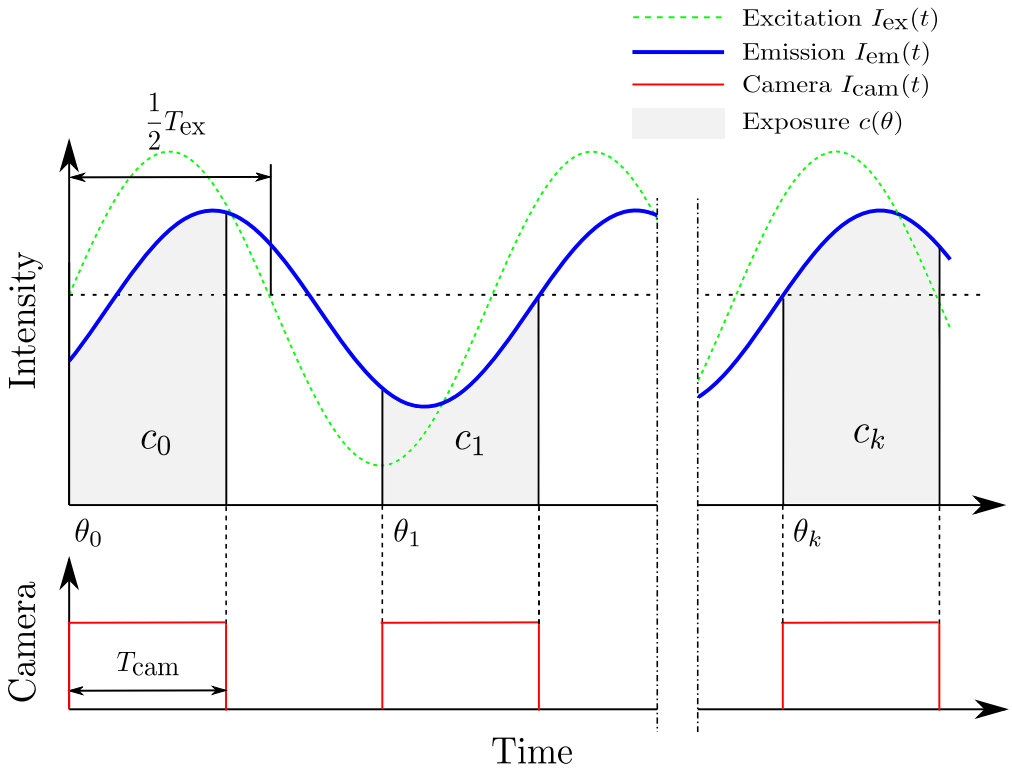

Figure 3.4: Sampling scheme of heterodyne modulation method. The fluorescence emission is acquired by integration of the camera exposure time.

In homodyne modulation scheme, the modulation frequency of the camera ω_{cam} is equal to the frequency of the excitation light source ω. However, in the case of heterodyne modulation, it is not necessary to be the same. We consider the reference signal as a heaviside step function

$$\mathcal{H}(x) = \begin{cases} 0 & x < 0 \\ 1 & x \geqslant 0 \end{cases} \tag{3.34}$$

The output signal can be considered as an correlation result between the fluorescence emission and the heaviside function $\mathcal{H}\big(\sin(\omega_{cam}t - \theta_k)\big)$. The camera modulation function can be therefore written as

$$I_{cam}(t) = \mathcal{H}\big(\sin(\omega_{cam}t - \theta_k)\big) \tag{3.35}$$

Where θ_k is the phase shift of the beginning of the kth exposure time of the camera, with $k \in \mathbb{N}$. θ_0 is the initial phase shift of the camera modulation. It can be adjust to different values to sample the signal at different phase steps.

The measured signal, c_k, is the real-time cross-correlation result of the fluorescence signal and the reference signal of the camera. For an arbitrary phase step θ_k, the corresponding value of the cross-correlation function can be calculated as

$$c_k = \frac{1}{t_{\text{exp}}} \int_0^{T_{\text{cam}}} I_{\text{cam}}(t) \cdot I_{\text{em}}(t) \tag{3.36}$$

$$= \frac{1}{t_{\text{exp}}} \int_0^{T_{\text{cam}}} \mathcal{H}\big(\sin(\omega_{\text{cam}} t - \theta_k)\big) \cdot \left(1 + \sum_{h=1}^{N_h} m_{\text{em},h} \sin(h\omega t + \phi_{\text{em},h})\right) dt \tag{3.37}$$

For simplicity, we use the reference signal as a square wave in the rest of this thesis. Therefore, the actual integration only spans over one half of the camera modulation period. We have $t_{\text{exp}} = T_{\text{cam}}/2$. The product of sampling function and fluorescence response signal can be considered as a multi harmonics sinusoidal wave with interval $[0,\ T_{\text{cam}}/2]$ and a phase shift $h\theta_k$ on each harmonic.

Therefore, we get the cross-correlation frame as

$$c_k = \frac{1}{t_{\text{exp}}} \int_0^{\frac{1}{2}T_{\text{cam}}} \left(1 + \sum_{h=1}^{N_h} m_{\text{em},h} \sin(h\omega t + \phi_{\text{em},h} + h \cdot \theta_k)\right) dt \tag{3.38}$$

$$= 1 - \frac{1}{t_{\text{exp}}} \sum_{h=1}^{N_h} \frac{m_{\text{em},h}}{h\omega} \cos(h\omega t + \phi_{\text{em},h} + h \cdot \theta_k)\Big|_0^{\frac{1}{2}T_{\text{cam}}} \tag{3.39}$$

$$= 1 - \frac{1}{t_{\text{exp}}} \sum_{h=1}^{N_h} \frac{m_{\text{em},h}}{h\omega} \cdot \left(\cos\left(\frac{1}{2} h\omega T_{\text{cam}} + \phi_{\text{em},h} + h \cdot \theta_k\right) - \cos(\phi_{\text{em},h} + h \cdot \theta_k)\right) \tag{3.40}$$

By using the trigonometric product-to-sum relationship

$$\cos x - \cos y = -2 \sin\left(\frac{x+y}{2}\right) \sin\left(\frac{x-y}{2}\right) \tag{3.41}$$

We get the kth camera output frame c_k as

$$\begin{aligned} c_k &= 1 - \Bigg(-2 \sum_{h=1}^{N_h} \frac{m_{\text{em},h}}{h\omega t_{\text{exp}}} \cdot \\ &\qquad \sin\left(\frac{1}{2} h\omega t_{\text{exp}}\right) \sin\left(\frac{1}{2} h\omega t_{\text{exp}} + \phi_{\text{em},h} + h \cdot \theta_k\right) \Bigg) \qquad (3.42) \\ &= 1 + \sum_{h=1}^{N_h} \frac{m_{\text{em},h}}{\frac{1}{2} h\omega t_{\text{exp}}} \sin\left(\frac{1}{2} h\omega t_{\text{exp}}\right) \sin\left(\frac{1}{2} h\omega t_{\text{exp}} + \phi_{\text{em},h} + h \cdot \theta_k\right) \qquad (3.43) \end{aligned}$$

By using the replacement

$$\psi_h = \frac{1}{2} h\omega t_{\text{exp}} \qquad (3.44)$$

the expression 3.42 can be further simplified as

$$c_k = 1 + \sum_{h=1}^{N_h} m_{\text{cam},h} \sin(\phi_{\text{cam},h}) \qquad (3.45)$$

with the following replacements

$$m_{\text{cam},h} = \operatorname{sinc}(\psi_h) \cdot m_{\text{em},h} \qquad (3.46)$$

$$\phi_{\text{cam},h} = \psi_h + \phi_{\text{em},h} + h \cdot \theta_k \qquad (3.47)$$

Where ψ_h represents the phase shift of the hth harmonic, which is caused by the integration. The modulation depth of the camera output signal $m_{\text{cam},h}$ yields a very interesting result that it is the product of the modulation depth of the fluorescence signal $m_{\text{em},h}$ and a sinc function of ψ_h. By taking the sampling method illustrated in Fig. 3.4, the camera exposure time equals to a half of the camera period. Therefore, we have

$$t_{\text{exp}} = \frac{T_{\text{cam}}}{2} = \frac{1}{2 f_{\text{cam}}} = \frac{\pi}{\omega_{\text{cam}}} \qquad (3.48)$$

So that we may obtain a more meaningful expression for ψ_h from Eq. 3.44.

$$\psi_h = \frac{h\pi}{2} \cdot \frac{\omega}{\omega_{\text{cam}}} = \frac{\pi}{2} h \cdot \nu \qquad (3.49)$$

with

$$\nu = \frac{\omega}{\omega_{\text{cam}}} = \frac{T_{\text{cam}}}{T_{\text{ex}}} \tag{3.50}$$

Where ν is defined as a dimensionless quantity which represents the relative frequency of the excitation light and camera modulation (or the relative length of the period of camera sampling period and the period of excitation function) . The parameter ν is also an indicator, which represents the degree of camera modulation. If the camera sampling signal is modulated at the same frequency as the one of the excitation light, it is the case of homodyne modulation, we have $\nu = 1$. If the frequency of camera sampling signal is either larger or smaller than the frequency of the excitation light, this case is said to be the heterodyne modulation, then we have $\nu \neq 1$.

The magnitude of modulation depth of the cross-correlation frame shows a sinc function behavior. As shown in Fig. 3.5, the magnitude of sinc curve can be expressed by a function of ν. Different m_{cam} relative to the m_{em} can be found for different sampling schemes. For the 4-tap image sensor, the exposure time of each measurement equals to one fourth of a modulation period, which we have $m_{\text{cam}} \approx 0.9\, m_{\text{em}}$. For 2-taps sampling system, i.e., exposure time equals to half of the modulation period, we have $m_{\text{cam}} \approx 0.63\, m_{\text{em}}$.

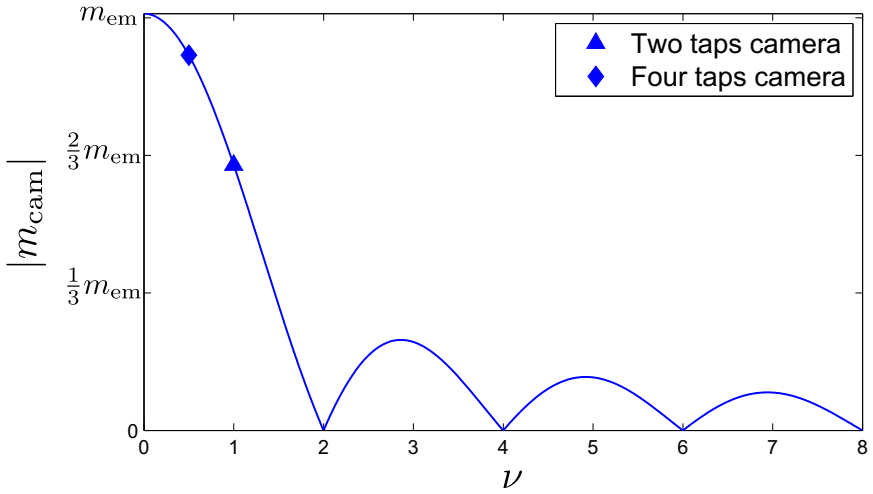

Figure 3.5: sinc function behavior of modulation depth of the camera output.

The larger m_{cam} can be obtained when the ν gets smaller. When $t_{\text{exp}} \to 0$, i.e., $\nu \to 0$, m_{cam} approaches its maximum with $m_{\text{cam}} = m_{\text{em}}$. It is the case of ideal sampling. Within a very short exposure time, one may obtain relatively larger modulation depth but as a cost of poor SNR since very less number of photons are collected. Attention should be paid that all zero crossings of m_{cam} are taking place when ν equals to an even integer number. It corresponds to the cases that the length of the exposure area equals to that a nonzero integer times the modulation period, where

$t_{\text{exp}} = kT_{\text{ex}} = 2k\pi/\omega, k \in \mathbb{N}$. In such circumstances, modulation depth m_{cam} disappears, and no fluorescence response information can be retrieved from the camera outputs. It is also not wise to use too long exposure time because the amplitude of sinc function is gradually decreasing as ν increases. Modulation depth m_{cam} is close related to the system performance. The corresponding theoretical study and a detailed discuss will be given in the later chapters.

3.3.4 Demodulation using Discrete Fourier Analysis

Eq. 3.45 shows that the sampled signal from the camera is also a periodic signal which can be expressed as a sum of sinusoidal functions with different harmonics. The *discrete Fourier transform (DFT)* [Lyo04, Sun01] can be applied to determine the spectral content of the signal numerically, i.e., both amplitude and phase angle of the base frequency and other harmonics contained in the signal.

Suppose we have a sequence of N_s number of time-domain input data samples $c_k,\ k \in \mathbb{N}$, the DFT defines the discrete frequency-domain sequence C_n, where

$$C_n = \frac{1}{N_s}\sum_{k=0}^{N_s-1} c_k \exp\left(-\frac{j2\pi kn}{N_s}\right) \tag{3.51}$$

$$= \frac{1}{N_s}\left(\sum_{k=0}^{N_s-1} c_k \cos\left(2\pi k\frac{n}{N_s}\right) + j\sum_{k=0}^{N_s-1} c_k \sin\left(-2\pi k\frac{n}{N_s}\right)\right) \tag{3.52}$$

where C_n is the nth DFT output component, which contains both real part and imaginary part. n indicates the index of DFT output in the frequency domain, k is the time domain index of the input samples. For the standard DFT notation, the indices of input data k and DFT output data n always range from 0 to $N_s - 1$. That means with N_s discrete time-domain data points the DFT generates spectral content at N_s equally spaced frequency points.

The resolution of the frequency-domain results can be determined by both the number of input samples N_s and the sampling frequency f_s, the fundamental frequency is f_s/N_s. And the other analysis frequencies (harmonics) are integer multiples of the fundamental frequency. The N_s separate DFT analysis frequencies are

$$f_a(n) = \frac{nf_s}{N_s} \tag{3.53}$$

For instance, if the signal is sampled at a rate of $40\,\text{MHz}$, and we perform a 8-point DFT on the sampled data, then the fundamental frequency of the sinusoids is $f_s/N_s = 40\,\text{MHz}/8 = 5\,\text{MHz}$, and other $f_a(n)$ analysis frequencies are

$$\begin{aligned} f_a(0) &= 0\,\text{MHz} \\ f_a(1) &= 5\,\text{MHz} \\ f_a(2) &= 10\,\text{MHz} \\ \dots &\quad \dots \end{aligned}$$

From Eq. 3.53, we know that the resolution of analysis frequency increases if the number of sampling points is raised and the sampling frequency is kept the same. However, it is not possible to just increase the sampling frequency without increasing the number of sampling points. This is because the Fourier analysis assumes that it is dealing with a periodic signal, which means the all data points representing the whole period of the signal should be presented, otherwise it causes the DFT leakage. The detail of the DFT leakage will be explained in later sections.

To deal with the multi-harmonic FD-FLIM data, we are interested in the index of each harmonic component in the DFT output vector in the frequency-domain. Let us look at the Eq. 3.53 in another perspective. Assuming the sampling rate f_s is the number of sampling points per cycle of the signal, then the analysis frequency $f_a(n)$ indicates integer multiplier of the fundamental frequency, with $f_a(1) = 1, f_a(2) = 2, \ldots$, i.e., the harmonic number. In this case we have $f_a(n) = h$. The index of DFT output of the hth harmonic n_h can be calculated as

$$n_h = \frac{hN_s}{f_s} \tag{3.54}$$

For instance, if we sample the signal at a rate of 8 points/cycle, then perform a 40-point DFT on the sampled data, then the index of the fundamental frequency component is $h \cdot N_s/f_s = 40 \cdot 1/8 = 5$, the index of the second harmonic component would be 10.

Once the index of the hth harmonic in the DFT output vector is determined, both phase angle and the magnitude contained in each C_n term can be calculated by the following equations.

The phase angle of the hth harmonic

$$\tan\phi_{\text{cam},h} = -\frac{\sum_{k=0}^{N_s-1} c_k \sin\left(2\pi k\frac{n_h}{N_s}\right)}{\sum_{k=0}^{N_s-1} c_k \cos\left(2\pi k\frac{n_h}{N_s}\right)} \tag{3.55}$$

By combing the Eq. 2.17 and 3.47, the phase shift of the hth harmonic can then be calculated as

$$\phi_h = \phi_{\text{cam},h} - (\psi_h + \phi_{\text{ex},h} + h \cdot \theta_k) \tag{3.56}$$

Amplitude of the hth harmonic, which is the "AC" part of the signal

$$C_{\text{AC},h} = \frac{2}{N_s}\sqrt{\left(\sum_{k=0}^{N_s-1} c_k \cos\left(2\pi k\frac{n_h}{N_s}\right)\right)^2 + \left(\sum_{k=0}^{N_s-1} c_k \sin\left(-2\pi k\frac{n_h}{N_s}\right)\right)^2} \tag{3.57}$$

The C_0 contains only the real part, which is the "DC " or mean value of the signal. It is also the magnitude or offset contained in the input signal. We have

$$C_{\text{DC},h} = C_0 = \frac{1}{N_s}\sum_{k=0}^{N_s-1} c_k \tag{3.58}$$

$C_{N_s/2}$ also contains only the real value. In between C_0 and $C_{N_s/2}$, there are $N_s/2 - 1$ unique complex values. The C values from $C_{N_s/2+1}$ to C_{N_s-1} are complex conjugate pairs of the values from $C_{N_s/2-1}$ down to C_1. Using N_s input data samples, we can calculate $N_s - 1$ harmonics of the fundamental frequency.

And the modulation depth as

$$m_{\text{em},h} = \frac{\pi}{2}\frac{C_{\text{AC},h}}{C_{\text{DC},h}} \tag{3.59}$$

By combing the Eq. 2.18 and 3.59, the modulation depth of the hth harmonic can then be calculated as

$$m_h = \frac{\pi}{2}\frac{C_{\text{AC},h}}{C_{\text{DC},h}} \cdot \frac{1}{m_{\text{ex},h}} \tag{3.60}$$

4 Samples Demodulation

Most available ToF systems use sinusoidal signal containing only one base frequency. They modulate the camera frequency the same as the excitation frequency, i.e., $\nu = 1$. And $N_s = 4$ samples are used in one period because of a relatively better performance and simpler reconstruction formulas can be achieved simultaneously.

The demodulation scheme follows

$$\tan \phi_{\text{cam}} = -\frac{c_3 - c_1}{c_2 - c_0} \tag{3.61}$$

$$C_{\text{AC}} = \frac{1}{2}\sqrt{(c_3 - c_1)^2 + (c_2 - c_0)^2} \tag{3.62}$$

$$C_{\text{DC}} = \frac{1}{4}(c_0 + c_1 + c_2 + c_3) \tag{3.63}$$

These results are also known from [FPR+09].

2 Samples Demodulation with a Known Background

For a special case when the background intensity (C_{DC}) is known and the signal contains only base frequency, the demodulation only needs two samples with

$$c_0 = c(\theta_0 = 0) = C_{\text{DC}}(1 + m_{\text{cam}} \sin(\phi_{\text{cam}})) \tag{3.64}$$

$$c_1 = c(\theta_1 = \frac{3}{2}\pi) = C_{\text{DC}}(1 - m_{\text{cam}} \cos(\phi_{\text{cam}})) \tag{3.65}$$

Since the C_{DC} is known, the demodulation scheme follows

$$\tan \phi_{\text{cam}} = -\frac{c_0 - C_{\text{DC}}}{c_1 - C_{\text{DC}}} \tag{3.66}$$

$$C_{\text{AC}} = \frac{1}{2}\sqrt{(c_0 - C_{\text{DC}})^2 + (c_1 - C_{\text{DC}})^2} \tag{3.67}$$

3.3.5 Cautions of Using DFT

The goal of using DFT is to approximate the Fourier transform of a continuous time signal. Due to the limitation of the discrete version of the Fourier transform, there are several phenomena that could result in errors between computed and desire transform. In this section, these problems and the ways of avoiding them are discussed.

3.3.5.1 Aliasing and Undersampling

The spectrum of the DFT is symmetric about the half of the sampling frequency f_s, and this folding frequency is known as the *Nyquist frequency*

$$f_N = \frac{1}{2} f_s \tag{3.68}$$

The Nyquist criterion suggests that the signal must be digitized at a sampling rate of at least twice the highest frequency of the signal so that the periodic signal can be uniquely represented (aliasing-free sampling) .

$$\min f_s \geqslant 2 \cdot f_a \tag{3.69}$$

The detection of short range lifetime requires relatively high frequency ($\geqslant 80$ MHz). To reach the Nyquist limit to get a aliasing-free sampling of fluorescence signal, there are two approaches. The first one is to raise the camera modulation frequency f_{cam} to very high. But it is hard to be realized due to technical difficulties. The other way is to adjust the initial phase shift of camera modulation θ_0 and perform the measurement many times to get the sampling points condensed enough to achieve the Nyquist criterion. The disadvantage of this approach is that more recording time is required. For instances, sampling a 80 MHz signal with a 20 MHz camera modulation, to reach the Nyquist limit (160 MHz), the measurement has to be carried out 8 times with 8 different initial phase shift θ_0. Therefore, both approaches are not practical.

But reaching the Nyquist limit is not the only way to reconstruct the signal without error. Since we know ahead of time the frequency of the fluorescence signal, which is in accordance with the excitation light, the position of the actual frequency of the aliased signal in the frequency domain is possible to be estimated. The fluorescence signal with frequencies above the Nyquist limit can still be reconstructed correctly. This technique is referred as *undersampling* in signal processing terms [McC04].

Fig. 3.6 shows an example of aliasing frequency. The excitation frequency f_{ex} is larger than the Nyquist limit f_N.

In the frequency domain, the aliased signal appears at $f_s - f_{\text{ex}} = f_a$. Since we know the signal is aliased, the actual frequency f_{ext} can be reversed by the following relationship:

$$f_a = |n_c f_s - f_{\text{ex}}| \tag{3.70}$$

where n_c indicates the closest integer multiple of the sampling rate f_s to the signal being aliased, i.e., f_{ex}. n_c can be even larger than 1. For example if a signal with the frequency 82 MHz is sampled with a camera modulation at 20 MHz, the $n_c = 4$ in this case, the aliased signal at frequency $|4 \times 20 - 82| = 2$ MHz is found. It contains the phase shift and modulation depth of correct fluorescence response.

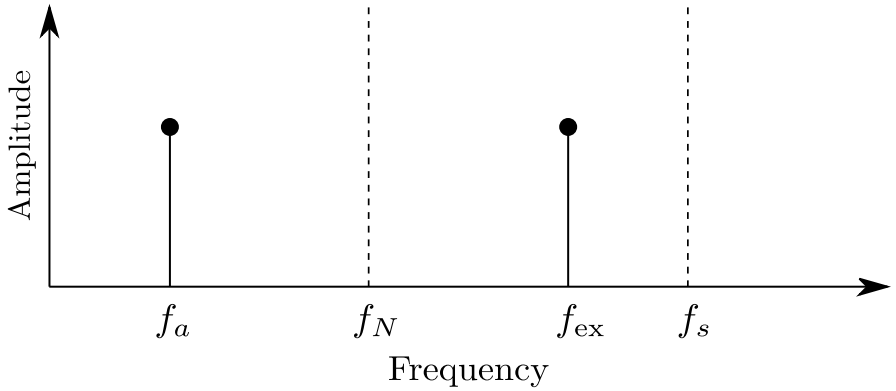

Figure 3.6: Amplitude versus frequency plot showing the aliased signal f_a occurs due to the signal been sampled f_{ex} beyond the Nyquist frequency f_N.

Since DFT samples signal with finite number of sampling points, the aliasing error occurs when a signal contains infinity number of harmonics even when we apply the undersampling. However, Previous studies have shown that the excitation with a Dirac delta function provides optimal SNR for FD-FLIM measurement [PC03, ESK08]. However, the combination of a Dirac delta function for fluorescence excitation contains many higher harmonics. These higher harmonic contents are also useful since they enables the analysis of multiple frequencies from a signal measurement. In this case, a low pass filter has to be applied to eliminate the effect caused by the higher harmonics and we only pay attention to the first few harmonics of interests.

3.3.5.2 Leakage

The DFT does not have infinite resolution. A consequence of this is that sometimes frequencies that are present in a signal are not sharply defined in the DFT. DFT only produces correct results when the input data sequence c_k contains energy precisely at the analysis frequencies given in Eq. 3.53, at integral multiples of the fundamental frequency f_s/N_s. If the endpoint of the sample appears as discontinuity, i.e., non-integral cycles of input signal is sampled, the frequency's magnitude response appears to be spread out over serval analysis frequencies, i.e., the actual information "leaks" into other DFT output bins. The is so called *DFT leakage*.

A window is a way of modifying the input signal so that there are no discontinuities in it. Such discontinuities represent as in the frequency response as the sinc function. Windowing reduces the sidelobes of the sinc function, which in turn decreases the effect of leakage.

However, leakage effects can be totally avoided if the measurement parameters are carefully chosen according to Eg. 3.53 to ensure that the analysis frequency is always the integral multiplies of the fundamental frequency f_s/N_s.

Fig. 3.7 shows an example of choosing the appropriate parameters to avoid leakage. The fluorescence signal has a base frequency at 82 MHz, and a 2nd harmonic. If we use camera modulation

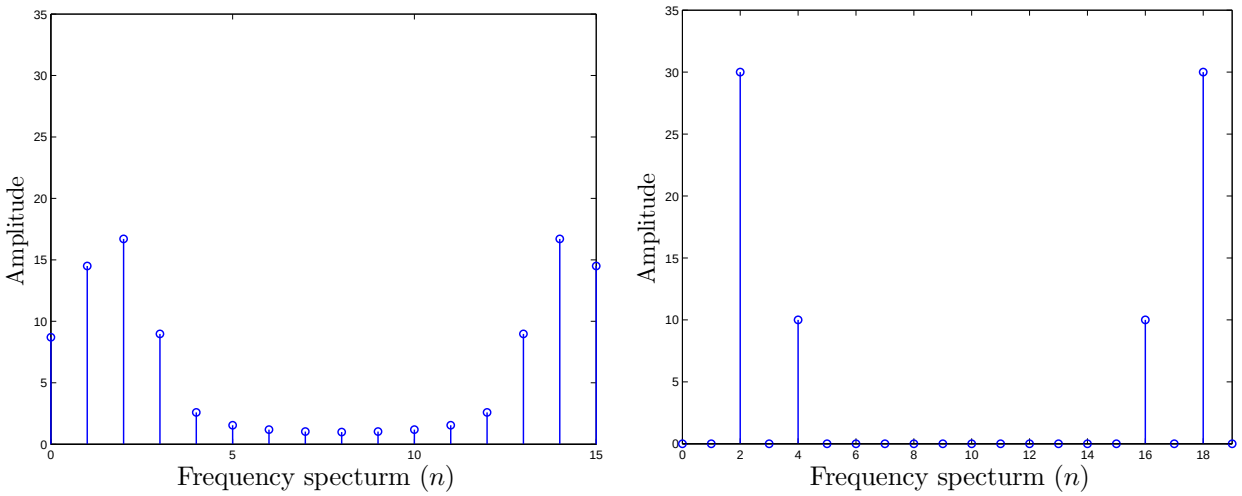

(a) $N_s = 16$, $f_s = 20$ MHz, $f_{\text{ex}} = 82$ MHz (b) $N_s = 20$, $f_s = 20$ MHz, $f_{\text{ex}} = 82$ MHz

Figure 3.7: (a) Frequency content appears spread out over analysis frequencies. (b) Frequency content appears at exact analysis frequencies.

at 20 MHz, the aliased signal with frequencies of the fluorescence are at 2 and 4 MHz for undersampling. Fig. 3.7(a) shows the scheme with $N_s = 16$ sampling points, the fundamental frequency is $20/16 = 1.25$ MHz. The analysis frequencies 2 and 4 MHz can not be divided by it. So the leakage appears. If we raises the number of sampling points to $N_s = 20$, leakage effect disappears since integral cycles of input signal is sampled.

3.4 Summary

In this chapter we demonstrated the theoretical solution of using both pulse-based (TD) and phase-based (FD) ToF camera for fluorescence lifetime imaging.

For the TD-FLIM, we use the time-gated TriDiCam camera. Besides the well known RLD method, several lifetime acquisition schemes based on simultaneous recording technique have been proposed in order to exploit the possibilities of the TriDiCam image sensor. By using such schemes, the frame rate can be drastically increased compared to sequential pixel data acquisition using fitting the data to the exponential model.

For the FD-FLIM, we have proposed a heterodyne modulation scheme which enables the camera modulation frequency to be different from that of the excitation source. Such a system provides the flexibility of the excitation signal type and sampling procedure. And it possess a large range of operation modes and measurement parameters to optimize the system performance. By the derivation of the general form of the HtM-FLIM, we discovered the sinc function relation between the modulation depth of fluorescence signal and camera output, which plays an important role in the

system performance. By undersampling technique, including frequency components with frequencies much hight than the Nyquist criterion, the measurement of fluorescence lifetimes much shorter than the sampling interval is possible.

Chapter 4

Simulation of the Fluorescence Lifetime Imaging System

4.1 Overview

This chapter deals with the simulation of a multi-frequency modulation multi-sampling fluorescence lifetime camera using the schemes proposed in Chapter 3. The simulation framework is in particular designed form the generation of synthetic data from the image sensor. The generated data can be severed as the input data for further validation of the theoretical results and algorithm development. The motivation of this simulation framework is to reproduce the behavior of imaging sensors and FLIM procedure in order to guide the design of best performance FLIM system. Therefore, the data-manipulation and sensor-simulation parts of this framework are very generic.

4.2 Linear Signal Model of the Imaging Device

Before the simulation, it is necessary to understand the working principle of imaging sensor. The hardware model of this simulation follows the *EMVA standard 1288* [EMV10].

One of an important characteristic of a photodetector system is its quantum efficiency η, which describes the ratio of electrons that are generated by an incident photons with wavelength λ_c. It is given by

$$\eta(\lambda_c) = \frac{N_e}{N_p} \tag{4.1}$$

Here N_e denotes the number of electrons produced, N_p denotes the number of photons absorbed. The number of photons that hit a area A during a certain exposure time t_{exp} can on calcu-

lated from the irradiance E with the unit W/m^2 [EMV10]

$$N_p = \frac{AEt_{\text{exp}}}{h_p c/\lambda_c} \tag{4.2}$$

where h_p indicates the Planck's constant, c is the speed of light.

Except for the electrons generated from incident photons, there will be spontaneous generation of electron/hole pairs that is unrelated to the light intensity. This process is exponentially dependent on temperature and contributes "dark" electrons N_d.

The camera converts the accumulated electrons $N_p + N_d$ into voltage, and amplified. And finally the analog digital converter (ADC) digitizes the current output into gray scale levels. This conversion is considered as linear, and the slope equals to the overall system gain K with the unit DN/e^-, i.e., digits per electrons. So that the digital output y can be calculated as

$$y = K(N_e + N_d) \quad \text{or} \quad y = y_d + KN_e \tag{4.3}$$

Combining the Eq. 4.1 and 4.3 we get

$$y = y_d + K\eta N_p \tag{4.4}$$

which defines a linear relation between the gray value output and the number of collected photons.

4.3 Simulation Modules and Flowchart

A FLIM system consists of a modulated excitation light source and a fluorescence sample as the input and a camera which generates the output images from the fluorescence emission. To guarantee the full flexibility, the whole simulation process is subdivided in to different modules. Fig. 4.1 shows the imaging pipeline of the FLIM simulation. Each parallelogram shape in the pipeline represents the input or output signal. Each box shape represents a processing unit.

At first excitation waveform is generated. It can be either pulse wave or any periodic wave. The fluorescence decay function is calculated according to the lifetime of the fluorescent sample to be measured. The fluorescence response signal is then computed by taking a numerical convolution of both input functions. Sampling process of the fluorescence response is implemented in the cross-correlation unit by combining with the camera modulation function. The sampling function of the camera is modulated as a square wave with a certain duty cycle of exposure time and a certain frequency, which is not necessary the same as the frequency of the excitation light (heterodyne modulation).

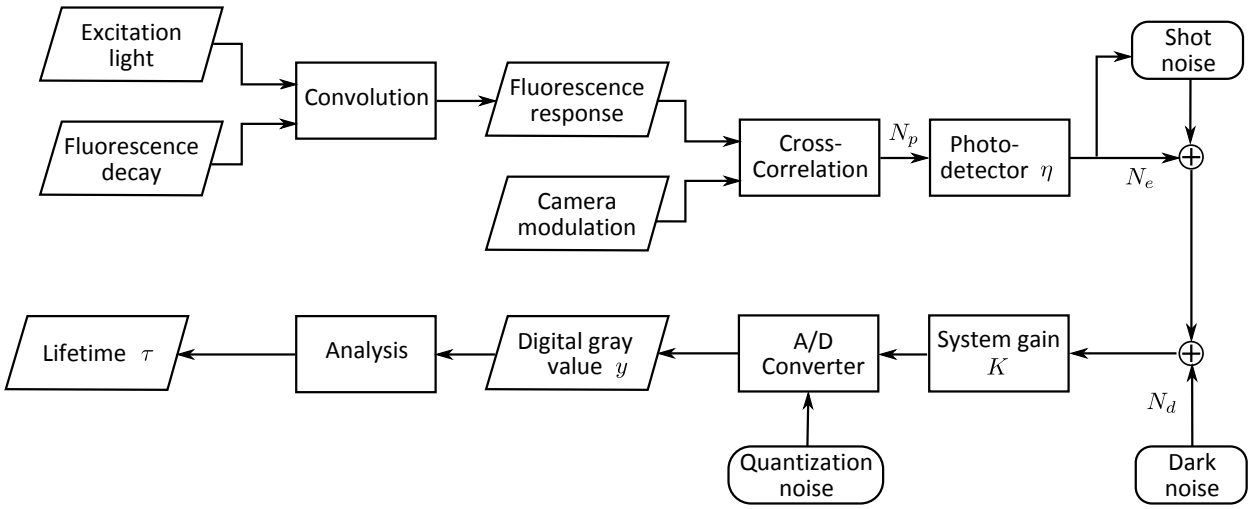

Figure 4.1: Block diagram showing the pipeline of FLIM simulation of a single pixel.

After sampling, the collected incident photons generate electrons with a quantum efficiency η. The number of accumulated electrons within a certain time range fluctuates statistically. According to the law of quantum mechanics, the probability is Poisson distribution. Therefore, the shot noise is added. Then, dark current electrons is also added which is also generated by the Poisson distribution.

The sum of all collected electrons in the quantum well is converted into voltage with a certain system gain K. The resulting voltage is digitized and output as a gray value y. In the end, the lifetime τ is calculated according to the gray value image (see Sect. 3.3.4).

4.4 Simulation Results

In this section, we simulated FLIM images to test the FLIM system simulations.

Fig. 4.2 shows the simulation result of two test patterns. The first test pattern contains 128×128 pixels. There were two lifetime components on the test pattern, one had a lifetime $\tau_1 = 5$ ns, the other one had a lifetime $\tau_2 = 15$ ns. The fraction amplitude α varied along the direction of the diagonal from 0 to 1. The distribution of the phasor plots is subject to the noise we synthesized. The phasor plots of the lifetime compound are distribution along the line segment connecting two single lifetime component in the mixture.

The second test pattern also contains 128×128 pixels. There were two species and a background on the test pattern, one has a compound lifetime of $\tau_1 = 5$ ns and $\tau_2 = 15$ ns, the other one has a compound lifetime of $\tau_3 = 2$ ns and $\tau_4 = 8$ ns. The fraction intensity $\alpha_1 = \alpha_2 = \alpha_3 = \alpha_4 = 0.5$. Two phasor plots clusters can be found on the phasor plane, each of which corresponds to one of the spices on the background. The means of the cluster appears on the mid-point of the line segment

connecting the phasor plots of single lifetime components. The variance of the data cluster results from the extent of the simulated noise.

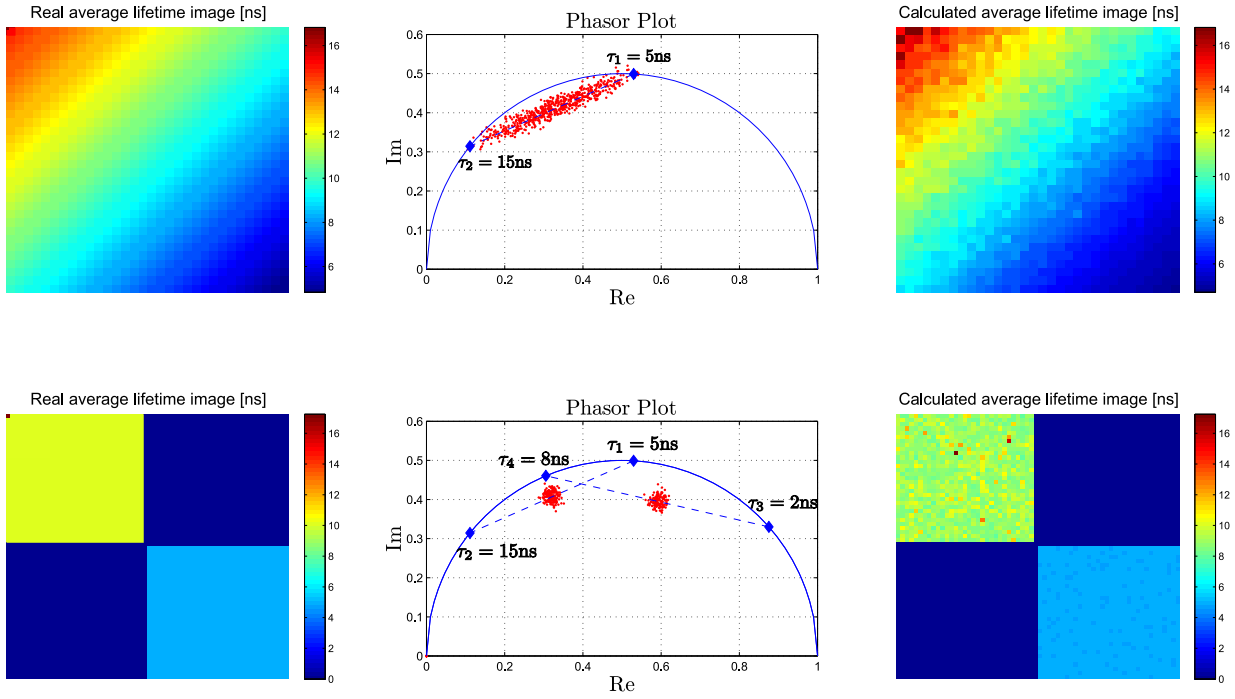

Figure 4.2: Phasor plots representation of simulated FLIM measurement data and the calculated average lifetime images by LiMA algorithm of 2 different test cases. 1st (top): uniform distribution of fraction intensity of two fluorescence components. 2nd (bottom): two objects with the combination of two fluorescence components, respectively.

Chapter 5

Statistical Analysis and Optimization

5.1 Overview

By the FLIM system, we have obtained the FLIM images, which are the measurement data. However, these intensity images from the camera system are not the information we are really interested. The quantities such as lifetimes, fraction amplitudes and phasor plots are the calculation results by combining those intensity images from FLIM measurement. In the imaging system, there are different noise sources which contributes to the uncertainty in the FLIM intensity images. Theses errors then propagate to the quantities of interest and increase the difficulties for data interpretation.

The aim of this chapter is to study how errors in acquired raw FLIM data affect the final calculated lifetimes and phasor plots. This analysis is performed using the Gaussian error propagation law. The other purpose of this chapter is to optimize the experimental parameters for the proposed FLIM schemes in order to bring the best performance for FLIM system.

In Sect. 5.2 we first analyze the mean and variance values of the raw data from the camera output. The variance of phasor plots and lifetimes are then derived. To evaluate and compare the FLIM performance, the analytical form of F-values, which provides an quantified measure for the photon economy, is calculated in Sect. 5.3. In Sect. 5.4 both data from Monte Carlo simulation and from real experiment are used to validate the theoretical results presented in this chapter. Both of them agree with our theoretical model. In Sect. 5.5 we optimize the system performance by several experimental parameters including shutter time of TriDiCam time-gated camera, excitation frequency, exposure time and waveform for HtM-FLIM.

5.2 Error Analysis

5.2.1 Mean and Variance

The camera raw values that are used to compute the fluorescence lifetime are subject to noise. Hence, both modulation lifetime τ_m and phase lifetime τ_ϕ as well as the coordinates of the phasor plots u_{Re} and u_{Im} (see Eq. 2.32 of Sect. 2.4.2) that one gets from the camera are noisy, as well. In this section, we give an analysis of this resulting variance.

Once an algorithm for calculating the values for τ_m, τ_ϕ, u_{Re} and u_{Im} or other quantities (such as individual component lifetimes for the mixture and their corresponding fraction intensities) is chosen, those quantities can be regarded as a function $\mathcal{F}$ of the random vector of camera outputs $Y = (y_0, y_1, \ldots, y_{N_s-1})$. The propagation of uncertainty through function $\mathcal{F}$ can be derived by the Gaussian error propagation law [Tay97].

Before we calculate the error propagation of the desired quantities, it is necessary to find the mean μ_{y_k} and variance $\sigma^2_{y_k}$ of the random variable of camera output in k-th frame $\mathbf{y}_k$. We first calculate the moment generating function of random variable $\mathbf{y}_k$. From Sect. 4.3, we assume a linear relation of camera output and number of collecting electrons resulting from incident photons. The photon number fluctuation follows the Poisson distribution.

For a Poisson distribution if the expected number of occurrences in a certain interval is υ, then the probability of getting exactly N_p number of photons (N_p being a non-negative integer, $N_p = 0, 1, 2, \ldots$) can be expressed as

$$P_{\mathbf{N}_p}(N_p) = \frac{\exp(-\upsilon)\upsilon^{N_p}}{N_p!} \tag{5.1}$$

where $\mathbf{N}_p$ is the random variable of photons. The moment generating function for the Poisson distribution can be computed as

$$\Phi_{\mathbf{N}_p}(s) = \mathbb{E}[\exp(s \cdot N_p)] = \sum_{N_p=0}^{\infty} \exp(s \cdot N_p) P_{\mathbf{N}_p}(N_p) = \exp\left(\upsilon \exp(s-1)\right) \tag{5.2}$$

where $\mathbb{E}$ is the mathematical expectation. According to Eq. 4.3, the camera output $\mathbf{y}_k$ is the linear combination of photon number and dark signal. Assuming $N_{p,k}$ is the number of photons collected at k-th frame, y_d is the gray value resulting from dark noise, we have $y_k = y_d + K\eta N_{p,k}$. Therefore, the moment generating function for $\mathbf{y}_k$ is

$$\Phi_{\mathbf{y}_k}(s) = \mathbb{E}[\exp(s \cdot y_k)] = \mathbb{E}[\exp(s \cdot y_d + s \cdot K N_{p,k})] = \exp(s \cdot y_d)\Phi_{\mathbf{N}_{p,k}}(Ks) \tag{5.3}$$

With the calculated moment generating function, the mean and the variance, μ_{y_k} and $\sigma^2_{y_k}$, of $\mathbf{y}_k$

can be computed as

$$\mu_{y_k} = \frac{\partial}{\partial s}\Phi_{\mathbf{y}_k}(s)\bigg|_{s=0} \qquad \sigma^2_{y_k} = \frac{\partial^2}{\partial s^2}\Phi_{\mathbf{y}_k}(s)\bigg|_{s=0} - \mu^2_{y_k} \tag{5.4}$$

After simplification we get

$$\mu_{y_k} = \mu_d + K\eta N_{p,k}c_k; \quad \sigma^2_{y_k} = K^2\sigma^2_d + K^2\eta N_{p,k}c_k; \tag{5.5}$$

where c_k is the kth frame of cross-correlation function of the camera.

5.2.2 Distribution of Phasor Plots

From the simulation result we know that pixels, which belong to species with same fluorescence lifetime in the image plane, appear in the same cluster on the phasor plane. They are statistically distributed. The center of the distribution depends on the lifetime values of fluorophores. But the variance of such distribution is still unknown. In this section efforts are made to analyze how errors resulting form imaging process affect the phasor plots distribution of the fluorescence signal.

According to Eq. 2.32, the coordinates of the phasor plot can be described by a vector $\mathbf{u} = (u_{\text{Re}}, u_{\text{Im}})^T$. It depends on two equations $\mathbf{f}_{u_{\text{Re}}}$ and $\mathbf{f}_{u_{\text{Im}}}$. Both coordinates are calculated from N_s number of inputs (sampling frames).

$$u_{\text{Re}} = \mathbf{f}_{u_{\text{Re}}}(y_0, y_1, \ldots, y_{N_s-1}) \tag{5.6}$$
$$u_{\text{Im}} = \mathbf{f}_{u_{\text{Im}}}(y_0, y_1, \ldots, y_{N_s-1}) \tag{5.7}$$

The $\mu_{u_{\text{Re}}}$ and $\sigma^2_{u_{\text{Re}}}$ can be exactly derived by single output error propagation law, where the variance $\sigma^2_{u_{\text{Re}}} = \mathbb{E}[(u_{\text{Re}} - \mu_{u_{\text{Re}}})^2]$. The additional aspect, which is introduced by u_{Im}, is the question of statistical dependence of u_{Re} and u_{Im}. It is expressed by their covariance $\text{cov}(u_{\text{Re}}, u_{\text{Im}}) = \mathbb{E}[(u_{\text{Re}} - \mu_{u_{\text{Re}}})(u_{\text{Im}} - \mu_{u_{\text{Im}}})]$.

Therefore, we are looking for a 2×2 output covariance matrix $\mathbf{C}_{u_{\text{Re}},u_{\text{Im}}}$

$$\mathbf{C}_{u_{\text{Re}},u_{\text{Im}}} = \begin{bmatrix} \sigma^2_{u_{\text{Re}}} & \text{COV}(u_{\text{Re}}, u_{\text{Im}}) \\ \text{COV}(u_{\text{Im}}, u_{\text{Re}}) & \sigma^2_{u_{\text{Im}}} \end{bmatrix} \tag{5.8}$$

which can be calculated by

$$\mathbf{C}_{u_{\text{Re}},u_{\text{Im}}} = \nabla\mathbf{F}^T_{u_{\text{Re}},u_{\text{Im}}}\mathbf{C}_y\nabla\mathbf{F}_{u_{\text{Re}},u_{\text{Im}}} \tag{5.9}$$

The matrix $\nabla\mathbf{F}_{u_{\text{Re}},u_{\text{Im}}}$ is defined as the transpose of gradient of u_{Re} and u_{Im}, whereas the gradient

is the outer product of ∇ and $\mathbf{F}_{u_{\mathrm{Re}},u_{\mathrm{Im}}}$. The $\mathbf{C}_y$ is a $N_s \times N_s$ input covariance matrix which contains all variances and covariances of the input variable y_0, y_1, ..., y_{N_s-1}.

The whole procedure of deriving $\mathbf{C}_{u_{\mathrm{Re}},u_{\mathrm{Im}}}$ can be found the appendix A.3. After derivation we get

$$\mathbf{C}_{u_{\mathrm{Re}},u_{\mathrm{Im}}} = \begin{bmatrix} \dfrac{\pi^2}{2m_{\mathrm{ex}}^2 N_s K^2} \displaystyle\sum_{k=1}^{N_s-1} \sigma_{y_k}^2 & 0 \\ 0 & \dfrac{\pi^2}{2m_{\mathrm{ex}}^2 N_s K^2} \displaystyle\sum_{k=1}^{N_s-1} \sigma_{y_k}^2 \end{bmatrix} \tag{5.10}$$

By assuming there is only shot noise, the covariance matrix can be further simplified to the following form.

$$\mathbf{C}_{u_{\mathrm{Re}},u_{\mathrm{Im}}} = \begin{bmatrix} \dfrac{\pi^2}{2m_{\mathrm{ex}}^2 N_p N_s} & 0 \\ 0 & \dfrac{\pi^2}{2m_{\mathrm{ex}}^2 N_p N_s} \end{bmatrix} \tag{5.11}$$

which yields very interesting result that the calculated covariance matrix is diagonal, and the standard deviations of real and imaginary direction of the phasor diagram are equal. That means the phasor distribution is always a full circle on the phasor plane.

The standard deviation only depends on three parameters, m_{ex}, N_s and N_p. The phasor plots get less noisier, i.e., variances get smaller, when the modulation depth of excitation function, number of sampling frames and photon number are increased. This is because increasing of the modulation depth is equivalent to raising the strength of the signal, increasing the sampling frames or number of photons also increases the SNR. All these behaviors reduce the noise level of camera output values.

According to the covariance matrix, we may describe the probability density function of the phasor plots by a bivariate normal distribution. The probability density function can be expressed as

$$P_{\mathbf{u}} = \frac{1}{2\pi\sigma_{u_{\mathrm{Re}}}\sigma_{u_{\mathrm{Im}}}} \exp\left(-\frac{(u_{\mathrm{Re}}-\mu_{u_{\mathrm{Re}}})^2}{2\sigma_{u_{\mathrm{Re}}}^2} - \frac{(u_{\mathrm{Im}}-\mu_{u_{\mathrm{Im}}})^2}{2\sigma_{u_{\mathrm{Im}}}^2}\right) \tag{5.12}$$

5.2.3 Distribution of Lifetimes

Mono-Exponential Lifetime Measured by TriDiCam

An example is demonstrated in this section to calculate the lifetime variance of scheme RLDO1 used for mono-exponential decay by TriDiCam image sensor. We use the standard error propagation techniques to calculate the uncertainties in the lifetime result in terms of the precisions of the measurement variables. We assume the two measurements after the pulse excitation are statistically independent. Let σ_{y_0} and σ_{y_1} represent the standard error that associate with these measurement variables. For τ given by a function, the error propagation expression for τ is:

$$\sigma_\tau^2 = \left(\frac{\partial \tau}{\partial y_0}\sigma_{y_0}\right)^2 + \left(\frac{\partial \tau}{\partial y_1}\sigma_{y_1}\right)^2 \tag{5.13}$$

The partial derivatives can be derived from a differentiation of the function of lifetime calculation from Eqs. 3.5 and 2.4.

$$\frac{\partial \tau}{\partial y_0} = \frac{\Delta t y_1}{\left[\ln\left(\frac{y_1}{y_0} - 1\right)\right]^2 y_0(y_0 - y_1)} \tag{5.14}$$

$$\frac{\partial \tau}{\partial y_1} = \frac{\Delta t}{\left[\ln\left(\frac{y_1}{y_0} - 1\right)\right]^2 (y_0 - y_1)} \tag{5.15}$$

The variance of lifetime can be derived by replacing the mean and variance of y_0 and y_1 into the above two partial derivatives.

$$\sigma_\tau^2 = \frac{\exp\left(\frac{\Delta t}{\tau}\right)\left(1 + \exp\left(\frac{\Delta t}{\tau}\right)\right)\left(1 + \exp\left(\frac{2\Delta t}{\tau}\right)\right)\Delta t}{\left(\exp\left(\frac{\Delta t}{\tau}\right) - 1\right) N_p \alpha \tau^2} \tag{5.16}$$

Phase and Modulation Lifetime Measured by HtM-FLIM Method

We denote the standard deviation associated with the phase lifetime as σ_{τ_ϕ}. The measurement output variables from the camera are assumed to be statistically independent or uncorrelated. Let $\sigma_{y_0}, \sigma_{y_1}, \ldots, \sigma_{y_{N-1}}$ represent the standard errors that associate with these measurement variables. The square of standard error in phase lifetime, which is propagated from the camera output variables, can be described as the sum of the squares of error of the camera output variables weighted

by a partial derivative of the Eq. 3.55 with respect to the corresponding camera output variable.

$$\sigma^2_{\tau_{\phi,h}} = \left(\frac{\partial \tau_\phi}{\partial y_0}\sigma_{y_0}\right)^2 + \left(\frac{\partial \tau_\phi}{\partial y_1}\sigma_{y_1}\right)^2 + ... + \left(\frac{\partial \tau_\phi}{\partial y_{N_s-1}}\sigma_{y_{N_s-1}}\right)^2 = \sum_{i=0}^{N_s-1}\left(\frac{\partial \tau_\phi}{\partial y_k}\sigma_{y_k}\right)^2 \tag{5.17}$$

The partial derivatives are determined from a differentiation of the function of phase lifetime calculation from the camera output data.

$$\frac{\partial \tau_{\phi,h}}{\partial y_{\hat{k}}} = \frac{\sin\left(2\hat{k}\pi\frac{n_h}{N_s}\right)\sum_{k=0}^{N_s-1} y_k \cos\left(2\pi k\frac{n_h}{N_s}\right) - \cos\left(2\hat{k}\pi\frac{n_h}{N_s}\right)\sum_{k=0}^{N_s-1} y_k \sin\left(2\pi k\frac{n_h}{N_s}\right)}{\omega\left(\sum_{k=0}^{N_s-1} y_k \cos\left(2\pi k\frac{n_h}{N_s}\right)\right)^2} \tag{5.18}$$

For simplicity, we replace the modulation frequency ω by a dimensionless quantity suggested by [PC03].

$$\tilde{\omega} = \omega\tau \tag{5.19}$$

By replacing the y_k and the $\sigma^2_{y_k}$ with the mean and variance calculated by Eq. 5.5 and assuming there is only shot noise, summing all terms up in Eq. 5.18, we get the variance of the phase lifetime

$$\sigma^2_{\tau_\phi,h} = \frac{2\tau^2\left(1+\tilde{\omega}^2h^2\right)^3}{\tilde{\omega}^2h^2m^2_{\text{ex},h}\cdot \operatorname{sinc}^2(\psi_h)N_sN_p} \tag{5.20}$$

The variance of the modulation lifetime can be also calculated using similar way.

$$\sigma^2_{\tau_m,h} = \frac{2\tau^2\left(1+\tilde{\omega}^2h^2\right)^3}{\tilde{\omega}^4h^4m^2_{\text{ex},h}\cdot \operatorname{sinc}^2(\psi_h)N_sN_p} \tag{5.21}$$

The variances of both phase lifetime and modulation lifetimes are increasing in each harmonic component because of the magnitude of sinc function is decreasing for higher harmonic terms (see Sect. 3.3.3), i.e., the lifetime measurement performance gets less precise for higher harmonic terms. The variances also depend on the photon number. Since the accumulated photons follow the Possion distribution, if we collect more photons, better SNR can be achieved. For difference FLIM methods and measuring modes, the number of collected photons varies from each other. Therefore, the form of lifetime variances can not be apply to evaluate of performance between these different methods. To fairly evaluate the performance of different FLIM methods, an F-value is generally used. Differ from the lifetime variance which evaluates how precisely lifetime can be measured, F-value evaluates how efficient the collected photons can be utilized.

5.3 Performance Evaluation by F-value

A number of different techniques and lifetime determination methods can be used in FLIM. In order to avoid the photonbleaching or drift caused by excessive recording time, in FLIM the number of collecting photons per pixel is relatively small, which leads to a poor SNR. Therefore, with the available recorded photons it is important to find a most efficient way to process the resulting signal. F-value was first introduced by Draaijer et al. [DSG95], it provides a way to evaluate the system performance between various lifetime determination techniques and the measurement parameters by measuring photon economy.

To define the F-value, we first assume the number of photons recorded during the a fixed measurement period is Poisson distributed, and it is denoted by N_p, which means the number of photons has mean N_p and standard deviation $\sqrt{N_p}$. The SNR of the process is $N_p/\sqrt{N_p} = \sqrt{N_p}$. This is the best achievable SNR that we can get with this number of detected photons. During fluorescence imaging process, the SNR is often reduced. F-value is defined to quantify the performance of these imaging techniques.

$$F = \frac{\sigma_\tau}{\tau}\sqrt{N_p} \tag{5.22}$$

where the σ_τ is the standard deviation of the fluorescence lifetime τ under repeated measurements. The F-value is also described as "normalized relative RMS noise". Theoretically the optimal achievable F-values is 1. The performance drops down when F-values get higher. It is worth to mention that F-values measures the photon economy and is independent of the number of photons. Therefore, one is able to compare performance of different FLIM techniques or different working modes using individual FLIM methods.

TriDiCam

F-value of the scheme RLDO1 can then be derived by summing up all terms of Eq. 5.13 and insertion of the calculated standard deviation into Eq. 5.22. After simplification we get

$$F_{\text{RLDo1}} = \sqrt{3}\sqrt{\frac{\exp\left(\frac{1}{\xi}\right) + 3\exp\left(\frac{2}{\xi}\right) + 2\exp\left(\frac{3}{\xi}\right)}{\frac{\alpha}{\xi}\left(\exp\left(\frac{1}{\xi}\right) - 1\right)}}; \quad \xi = \frac{\tau}{\Delta t} \tag{5.23}$$

Phase and Modulation Lifetimes

Using N_s number of camera frames to calculate the phase lifetime and modulation lifetime, the total amount of photons is $N_s \cdot N_p$. By combining the Eq. 5.20, 5.21 and Eq. 5.22 together, we get

the F-value for phase lifetime calculated in h-th harmonic.

$$F_{\tau_\phi,h} = \frac{\sigma_{\tau_\phi,h}}{\tau_{\phi,h}}\sqrt{N_s N_p} = \frac{\sqrt{2}\,(1+\tilde{\omega}^2h^2)^{\frac{3}{2}}}{\tilde{\omega}hm_{\text{ex},h}\cdot|\operatorname{sinc}\psi_h|} \tag{5.24}$$

And the F-value for modulation lifetime calculated in h-th harmonic.

$$F_{\tau_m,h} = \frac{\sigma_{\tau_m,h}}{\tau_{m,h}}\sqrt{N_s N_p} = \frac{\sqrt{2}\,(1+\tilde{\omega}^2h^2)^{\frac{3}{2}}}{\tilde{\omega}^2h^2m_{\text{ex},h}\cdot|\operatorname{sinc}\psi_h|} \tag{5.25}$$

5.4 Verification

5.4.1 FD-FLIM Data Distribution in Phasor Space

We have shown in Sect. 5.2.2 that the phasor plots of the fluorescence signals follows the Gaussian multivariate distribution.

The Gaussian mixture model is constructed parametrically. Those parameters can be encapsulated into a parameter vector. However, the data plots we simulated are discrete variables in the phasor space, they are incomplete for finding a fitting continuous Gaussian probability density function. Therefore, as shown in Fig. 5.1, the expectation-maximization (EM) algorithm [Bil98] is employed to determine approximately the parameters of the Gaussian mixture model from the phasor plots data we generated. The incomplete data are analyzed interactive by the EM algorithm, which is an interactive procedure for finding the maximum likelihood (ML) estimates with incomplete data.

Tab. 5.1 shows the standard deviation values of Re- and Im- direction of the phasor plane by theoretical calculation and EM algorithm estimation. The test pattern was made by 128×128 pixels to ensure enough amount of data points for a reliable EM algorithm parameter estimation. We found that the standard deviation of the phasor plots distribution would not change by different lifetimes and excitation frequencies. The estimated standard deviation only depend on three quantities as predicted by the theoretical results.

We simulated different measurement circumstances by varying the experimental parameters m_{ex}, N_s and N_s, and we added the Poisson noise to the collected photons. The estimated standard deviation affected by noise in both Re- and Im-direction of the phasor plane were nearly the same. They fitted well with the standard deviation calculated from Eq. 5.11. The EM estimated off-diagonal entries (covariance terms) were very small values, which can be totally ignored. So they are not listed on Tab. 5.1. The theoretical results agree with the estimated parameters.

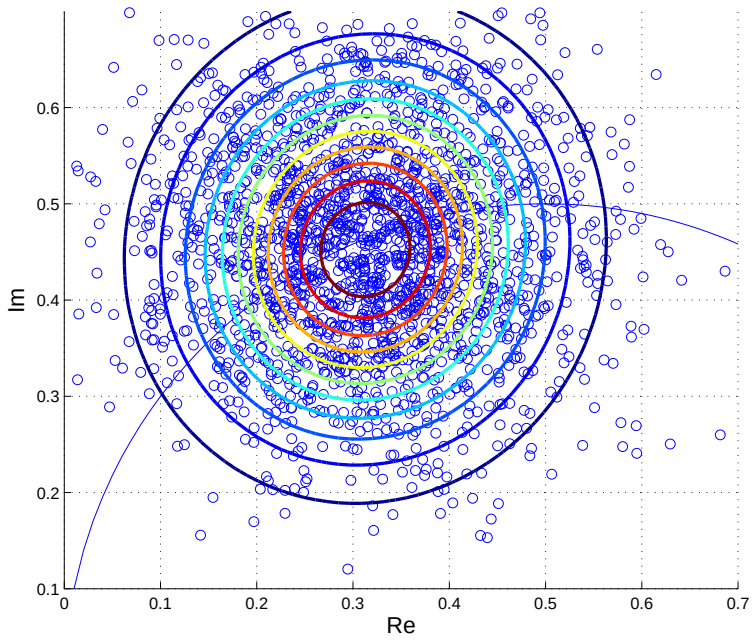

Figure 5.1: Data clouds of in Phasor space and the data fit contour by the EM algorithm which estimates the Gaussian mixture parameter.

Measurement parameters					
m_{ex}	N_s	N_p	$\sigma_{u_{\text{Re}}} = \sigma_{u_{\text{Im}}}$ (theoretical)	$\sigma_{u_{\text{Re}}}$ (Monte-Carlo)	$\sigma_{u_{\text{Im}}}$ (Monte-Carlo)
1	4	197	0.0794	0.0762	0.0768
0.85	4	197	0.0589	0.0574	0.0574
0.5	4	590	0.0911	0.0906	0.0922
0.5	8	590	0.0648	0.0640	0.0663

Table 5.1: The comparison of standard deviation values of the Re- and Im- direction of the phasor plane by theoretical calculation and EM algorithm estimation. Several Monte-Carlo simulations were made using different measurement parameters including modulation of excitation sinusoidal wave m_{ex}, number of sampling points N_s and the number of photons N_p.

5.4.2 F-value Verification using Monte-Carlo Simulation

Monte Carlo simulations of the FD-FLIM were carried out to validate the theoretical solution presented in this thesis. The average photon number within a certain exposure time can be determined by photon flux. The Poisson noise was simulated by the random process because of the discrete nature of the photons reception. The fluorescence response signal was produced by multiplying the photon counts in each sampling step by the gain. In the end the phase and modulation lifetimes were calculated by DFT. We synthesized image with 512 pixels, i.e. the standard deviation of the lifetime were computed by repeating the measurement 512 times to ensure the reliability of the statistics. In the simulation we took the 100% modulation depth of excitation, which F-values are considered as the best case. The results from the Monte Carlo simulation shows a good agreement with the theoretical calculations.

5.4.2.1 Time-Gated TD-FLIM by TriDiCam

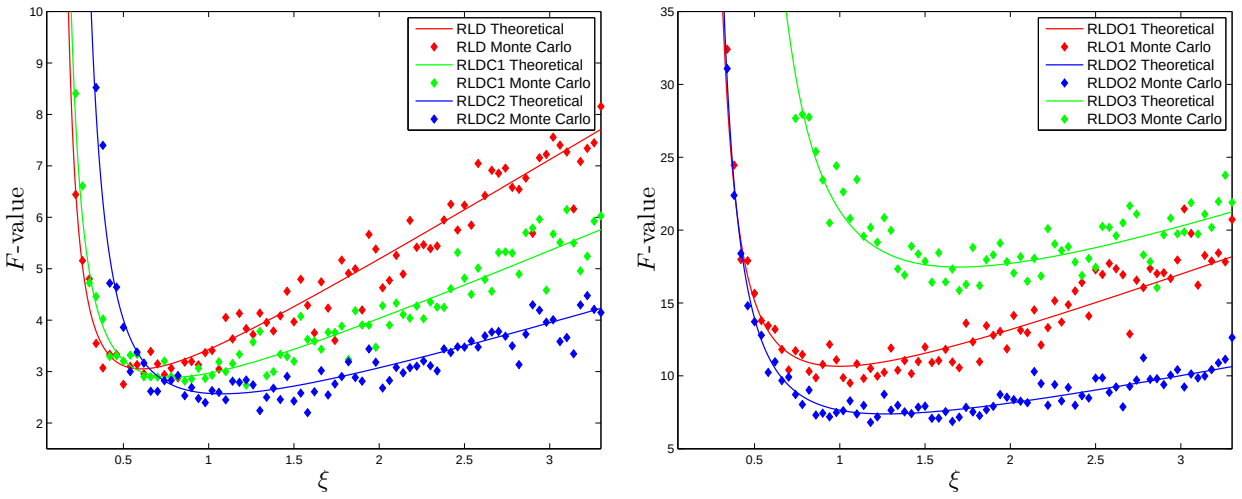

(a) Contiguous time gates

(b) Overlapping time gates

Figure 5.2: F-values as a function of ξ (relative length of lifetime τ to the unit length of exposure time Δt, $\xi = \tau/\Delta t$) for schemes using (a) Contiguous time gates and (b) Overlapping time gates. The ξ is increasing by keeping Δt as constant and increase τ. Both theoretical and Monte Carlo simulation data are shown, which are in good agreement.

Fig. 5.2 shows the F-values of different schemes. In order to find the optimal lifetime region for TriDiCam measurement using different schemes, we kept the unit shutter time Δt as constant and gradually increased the lifetime until the relative length ξ from 0.1 to 3.3.

It can be seen that for small ξ the performance drops rapidly, since the steep decay curves for short lifetimes yields small c_1 and c_2 values. The proportion of Poisson noise increases rapidly since it is the square root of the photon counts in an integral. At the other extreme, for too large ξ,

shutter time is relatively small compared to the decay time so that the photon counts within each unit shutter time Δt tend to be the same. The loss of precision comes from inadequate sample size.

Depending on the behaviors of the F-values, the results of the schemes are categorized into two groups: contiguous time gates and overlapping time gates. It can be seen from the result that the schemes using contiguous time gates (Fig. 5.2(a)) have a better performance than the schemes using overlapping gates (Fig. 5.2(b)). The reason can be explained by comparing of two very similar methods, scheme RLDO1 and the RLD. In scheme RLDO1 the total length of the integration areas of both shutters is $3\Delta t$, the extra amount of photons are collected in the overlapping area, which is unnecessary for the lifetime calculation and brings extra noise. Even through scheme RLDO1 and the RLD method have the same standard error, the scheme RLDO1 is less photon efficient than the RLD method.

For schemes using overlapping gates, it is quite obvious the performance ranking is RLDO2 $>$ RLDO1 $>$ RLDO3. By analysis of their time-gated settings, we found that the larger proportion of the overlapping region of both shutters possess, the worse performance it gets.

For schemes using contiguous time gates, the overall F-values are even smaller than the F-values using FD-FLIM techniques from the previous reported work [PC03, ESK08, LEJ10]. Among these three schemes, it is hard to say the performance of one of them is better than the other two. Scheme RLDC2 has the smallest F-value among all three methods. However, for the detection of lifetimes less than $0.65\Delta t$ the RLD method and scheme RLDC1 are better. It is wise to use them for their suitable region for measuring different lifetimes.

5.4.2.2 HtM-FLIM

For the simulation of the HtM-FLIM system, we used the camera sampling function as a square wave. Therefore, we have $t_{\text{exp}} = T_{\text{cam}}/2 = 1/2f_{\text{cam}}$. And $N_s = 32$ samples were taken. From the simulation we found that changing the number of sampling points does nearly no impact on the calculated F-values. We also tried to test different frequency ratios of sampling to modulation frequency and degrees of undersampling. They were also irrelevant to the calculated F-values. In the following we present some simulation scenarios according to different operation modes of the HtM-FLIM system, which affect the F-values significantly.

Varying Exposure Time

Fig. 5.3(a) shows the resulting F-values curve, the vertical axis is scaled logarithmically to present the shape of F-values curve more clearly. Direct connection between the F-values and sinc function behavior of modulation depth m_{cam} can be found in this plot. F-values curve contains three segments which correspond to first three half periods of sinc function in $0 < \nu < 2$, $2 < \nu < 4$ and $4 < \nu < 6$, respectively. The F-values are inverse proportional to the absolute amplitude of sinc function of m_{cam}. Every local optima of F-values appears when m_{cam} gets its local maximum. F-values are increasing rapidly when m_{cam} approaches 0, i.e. the length of exposure time getting

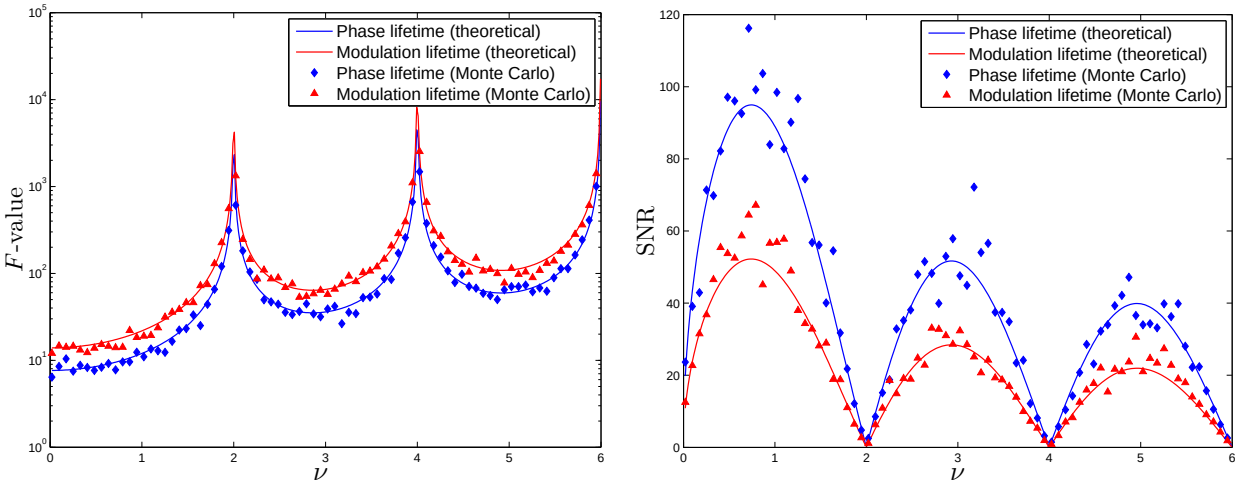

(a) (b)

Figure 5.3: (a) F-values as a function of relative length of exposure time $\nu = \omega t_{\text{exp}}/\pi$ to the modulation period for a sinusoidal excitation for phase lifetimes and modulation lifetimes. ν is increasing by keeping the modulation frequency ω constant and increase exposure time t_{exp}. Both theoretical and Monte Carlo simulation data are shown, which are in good agreement (b) SNR as a function of modulation frequencies of relative length ν with a sinusoidal excitation for phase lifetimes and modulation lifetimes. Both theoretical and Monte Carlo simulation results are shown.

close to the integer multiple of modulation periods, which brings very poor performance. These are the situations one should avoid in the real measurement. Despite of F-values taking place when ν gets close to $2n$, $n \in \mathbb{N}$, the overall performance of shorter than one modulation period exposure time $(\nu < 2)$ is better than the cases when $\nu > 2$. During the experiments, one should also pay attention to that by extending the exposure time to collect more photons or compensate errors leads to a reduction of modulation depth m_{cam} and poorer photon economy.

Interestingly, when t_{exp} approaches 0, F-values achieve its optimum ($F_{\tau_\phi} = 3.67$ and $F_{\tau_m} = 5.25$). But it just means the best photon economy and does not indicate the best SNR since too less photons are collected. Fig. 5.3(b) shows the SNR of lifetimes versus ν. Different from the F-values plot it shows poor SNR when t_{exp} gets close to 0. The best SNR appears at $\nu = 0.74$, where $F_{\tau_\phi} = 4.67$ and $F_{\tau_m} = 6.67$. Simulations under different constant modulation frequencies were also performed, we obtained the same ν positions where optimum SNRs appear. So that in HtM-FLIM $\nu = 0.74$ was found to be the best performance balance point to achieve the best SNR as a cost of losing a little photon economy.

In this simulation the fixed modulation was chosen in such a way that the F-values of phase lifetimes happen to show better performance than the ones of modulation lifetimes. It is not the general case, the relation with F-values and different modulation frequencies will be discussed in the next section.

Evaluations of F-values under different modulation frequencies were carried out the similar way as the previous works [PC03, ESK08, EGW07]. Differently, by using undersampling tech-

nique the modulation frequencies much higher than the Nyquist limit can be applied, which enables to explore the HtM-FLIM performance under a much wider region of modulation frequencies. We again used a pure sinusoidal signal as the excitation, the exposure time was firstly kept as constant and the modulation frequency is increased until $\nu = 6$. The frequency ratio of sampling and modulation was kept as constant by changing the sampling interval between two exposures for each different frequency. The second case of this simulation was performed by keeping the relative length ν as constant value 0.74, which the best SNR appeared. The length of exposure time was also changed when we increased the modulation frequency.

Varying Modulation Frequency

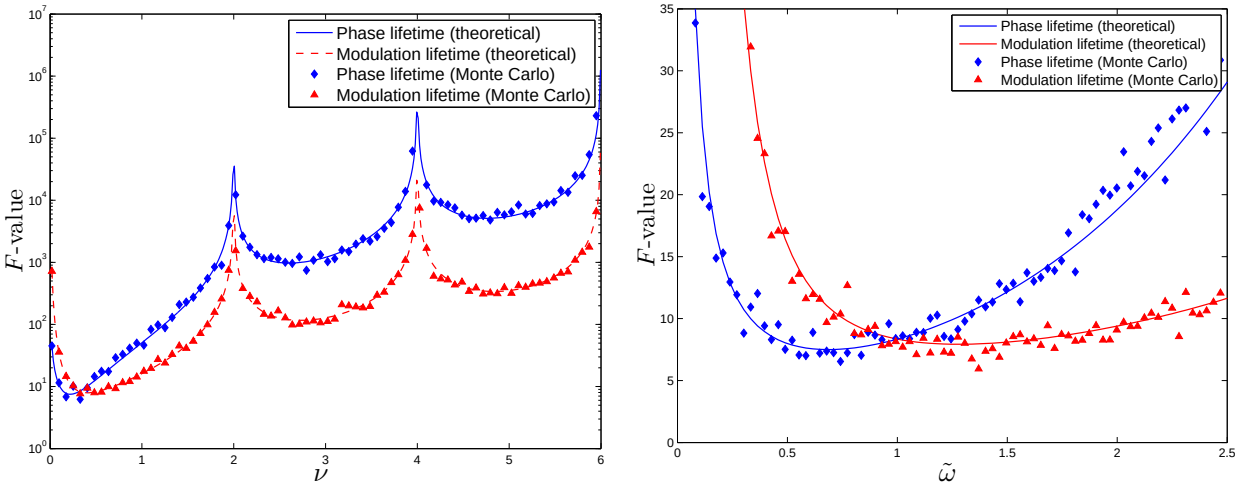

Figure 5.4: (a) F-values as a function of relative length of exposure time $\nu = \omega t_{\text{exp}}/\pi$ to the modulation period for a sinusoidal excitation for phase lifetimes and modulation lifetimes. ν is increasing by keeping the exposure time t_{exp} constant and increasing modulation frequency ω. The theoretical result agrees with the Monte Carlo simulation result nicely. (b) F-values as a function of dimensionless modulation frequencies $\tilde{\omega} = \omega\tau$ with a sinusoidal excitation for phase lifetimes and modulation lifetimes. Modulation frequency $\tilde{\omega}$ is increasing, in the same time the relative length ν is kept as constant by decreasing the exposure time. The theoretical result and the Monte Carlo simulation result are in good agreement.

Fig. 5.4(a) shows the curve of F-values calculated in different frequencies. Affected by the sinc function behavior, F-values curve contains also three segments which is similar to the curve of F-values in different exposure times. The optimum F-value of phase lifetime is 3.75, it happens when $\nu = 0.22$. The best F-value of modulation lifetime is 3.96, it happens when $\nu = 0.80$.

As shown in Fig. 5.4(b), the sinc effect can be eliminated by keeping the ν as constant. We achieved the similar result as the previous reported works [ESK08, PC03] . In addition we have discovered that since F-values of modulation lifetime equals to the F-values of phase lifetime multiplying $\tilde{\omega}$, the performance of calculating modulation lifetime are better than the performance

of calculating the phase lifetime when $\tilde{\omega} > 1$, vise visa. The intersection of both curves appears at $\tilde{\omega} = 1$, the proof will be given in the later sections. It is the balance point for both small F-values and achieving the same performance of phase and modulation lifetimes. This result also agrees with the best modulation frequency for obtaining the best lifetimes resolution in the graphical representation by phasor plane [RC05].

Multiple Harmonic Analysis

One of our important application for HtM-FLIM system is the measurement of multiple exponential lifetimes by using multiple frequencies. The lifetimes analysis by using DFT allows us to use the periodic excitation signal containing multiple harmonics and resolve the fluorescence response signal for each harmonic. In this simulation we took the analysis on several non-sinusoidal waveforms like square wave, sawtooth wave and pulse wave excitation. Since these periodic waves are composed of an infinite number of harmonics by Fourier representation, the frequency components of interest will get polluted by an aliased signal from another frequency by performing the DFT over limited number of sampling points. Therefore, we only take the first 10 terms of the waves by Fourier representation and calculate the fluorescence responses for the 1st, 3rd and 5th harmonic. To eliminate the dependency on ν in this experiment, we set ν equals 0.5, i.e., the camera modulation frequency is twice as high as the excitation frequency.

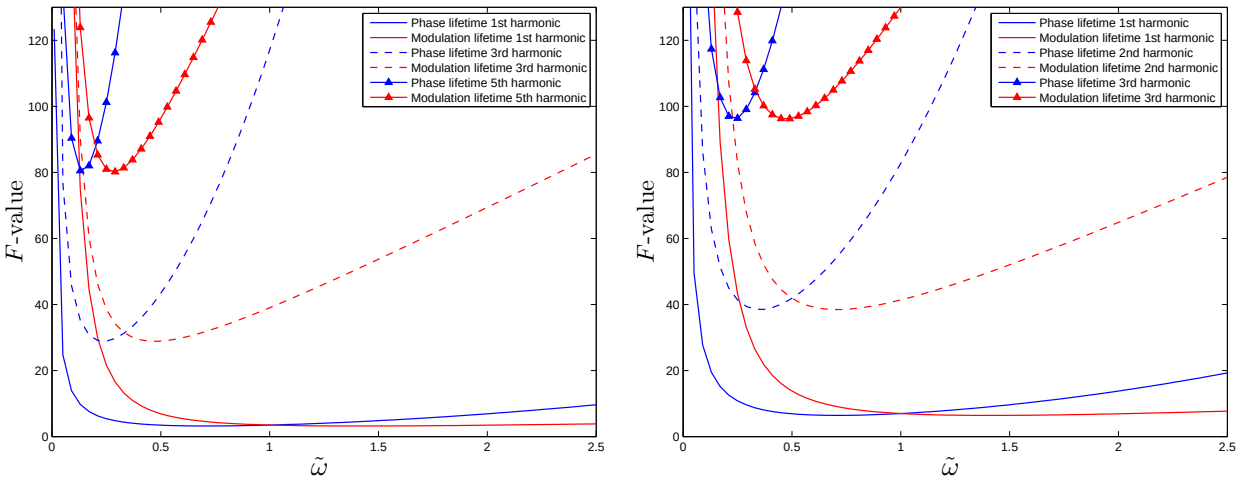

(a) (b)

Figure 5.5: (a) F-values of phase lifetime and modulation lifetime as a function of modulation frequency $\tilde{\omega}$ for the 1st, 3rd and 5th harmonic of square wave excitation. (b) F-value of phase lifetime and modulation lifetime as a function of modulation frequency $\tilde{\omega}$ for the 1st, 2nd and 3rd harmonic of sawtooth wave excitation.

The results show that F-values calculated from each harmonic are not affected by the other harmonic components contained in the excitation signal. The optimum F-values of phase lifetimes (see Fig. 5.5(a)) are 3.20, 28.91 and 80.50 for the 1st, 3rd and 5th harmonic respectively. The

optimum F-value of modulation lifetimes are 3.19, 28.87 and 80.16 for each harmonic. Both F-values of phase and modulation lifetimes are inverse proportional to the modulation depth of each harmonic, which again confirms the important factor that larger modulation depth shows better result. Furthermore, in HtM-FLIM the F-values of each harmonics are smaller than the previous reported work [ESK08]. Because in the homodyne detection method, the fluorescence signal is always mixing with the same frequency detection signal, which is not optimal to achieve smaller F-value. However, in HtM-FLIM the frequency of the camera modulation can be adjusted so that a better performance of the FLIM system can be achieved.

The position of where optimum F-value appears is related to the sinc function behavior. The sinc function of modulation depth m_{cam} for the higher harmonic has a higher frequency. The optimum F-values of higher harmonics where the corresponding optimum modulation depth appears sooner than the ones of lower harmonics. For the case of square wave modulation, if optimum F-value of 1st harmonic appears at $\hat{\nu}$, the optimum F-value of harmonic 3 and 5 are taken place at $\hat{\nu}/3$ and $\hat{\nu}/5$, respectively.

Fig. 5.5(b) shows the F-values of first three harmonics of sawtooth wave. The optimum F-values of phase lifetimes (see are 6.41, 38.51 and 96.38 for the 1st, 3rd and 5th harmonic respectively. The optimum F-value of modulation lifetimes are 6.40, 38.47 and 96.25 for each harmonic. It is obvious that the performance using square wave are much better since the excitation modulation values of each harmonic are smaller than the ones of sawtooth wave.

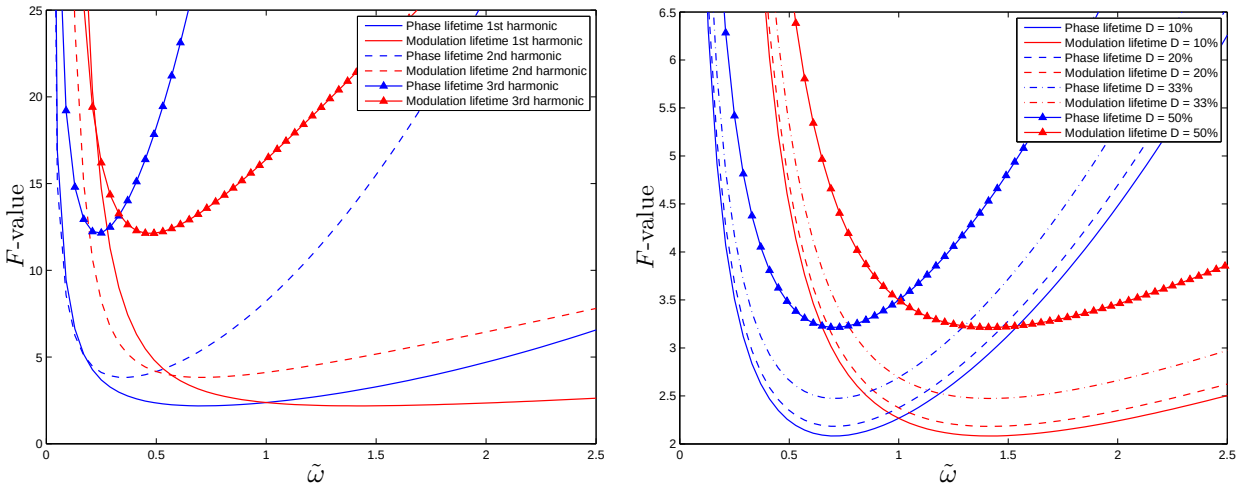

(a) (b)

Figure 5.6: (a) F-value of phase lifetime and modulation lifetime as a function of modulation frequency $\tilde{\omega}$ for the 1st, 2nd and 3rd harmonic of pulse train excitation with 20% duty cycle. (b) F-value of phase lifetime and modulation lifetime as a function of modulation frequency $\tilde{\omega}$ for different duty cycles of 10%, 20%, 33% and 50%, respectively.

Pulse Train Excitation

Previous work showed that excitation with a Dirac delta function provides optimal SNR for FD-FLIM measurement [PC03, ESK08]. Actually, the pulse train excitation can be considered as a special case of square wave as the duty cycle D gets very close to zero. Mathematically, it can also be described by a Fourier decomposition as a infinite number of Fourier series. In order to avoid the aliasing error, we took only the first 11 harmonics for analysis.

Fig. 5.6(a) shows the F-values of first three harmonics of pulse train excitation. The optimum F-values of phase lifetimes are 2.18, 3.82 and 12.15 for the 1st, 3rd and 5th harmonic respectively. The optimum F-value of modulation lifetimes are 2.18, 3.82 and 12.13 for the fist three harmonics. Although we were using different demodulation method as the homodyne detection method, the performance of using pulse wave excitation still are the best among all waveforms been tested. This is mainly because the modulation depth of first few harmonics in the pulse train waveform could even be larger than 1, which decrease the F-value. For instance, the lowest F-values of 1-st, 2nd and 3rd modulation depth of $D = 20\%$ duty cycle pulse train are 1.86, 1.51 and 1.01, respectively.

Fig. 5.6(b) shows the F-values of pulse train excitation of different duty cycles. As can be seen, as the duty cycle decreases, lowest F-value also decreases. Theoretically, an unity of F-value is achieved when the duty cycle approaches zero. The optimum F-values of phase lifetime and modulation lifetimes of pulse train excitation with a 10% duty cycle are 2.082 and 2.083, respectively. They are better than the F-values using the Dirac pulse, which were given by the work of [PC03, ESK08]. This is because we optimized the frequency of camera modulation in this experiment, which showed a better performance than the performance of using homodyne detection method.

5.4.3 Experimental Verification by Line-Scan Camera

The experimental measurements to support the theoretical result in this thesis were carried out in the work of Erz [Erz11]. The variance of the measured phase shift can be described by the variance of gray values σ_y^2 and AC part C_{AC} of the cross-correlation function [FPR$^+$09].

$$\sigma_\phi^2 = \frac{\sigma_y^2}{2C_{\mathrm{AC}}^2} \tag{5.26}$$

According to the derivation based on the error propagation law and the camera model described in Sect. 4.2, under certain circumstance the standard deviation of the phase lifetime can be represented by the following formula [Erz11].

$$\sigma_{\tau_\phi} = \frac{1}{\sqrt{2}}\left(\frac{1}{\omega} + \omega\tau_\phi^2\right) \cdot \frac{\sqrt{K \cdot (\mu_y - \mu_{y_d})}}{C_{\mathrm{AC}}}; \quad \text{for} \quad \nu = \omega t_{\mathrm{exp}}/\pi = 1. \tag{5.27}$$

where μ_y is the mean gray value, μ_{y_d} is the mean dark gray value.

5.4.3.1 Overview of Experimental Setup

The system is configured for fluorescence lifetime measurements in a cuvette. The system consists of a diode laser (RGB Nova^{pro}-445) for fluorescence excitation and a line-scan CMOS camera (BASLER SPL2048-70KM) for detection. The laser wavelength is 445 nm with a full width at half maximum (FWHM) of 10 nm and the maximum possible modulation frequency without a fall off in the modulation contrast is about 250 kHz. A computer-controlled function generator of Tektronix AFG 3102 is used to generate periodic signals for the laser and camera modulation. The diameter of the laser beam was decreased with two lenses to 100 μm.

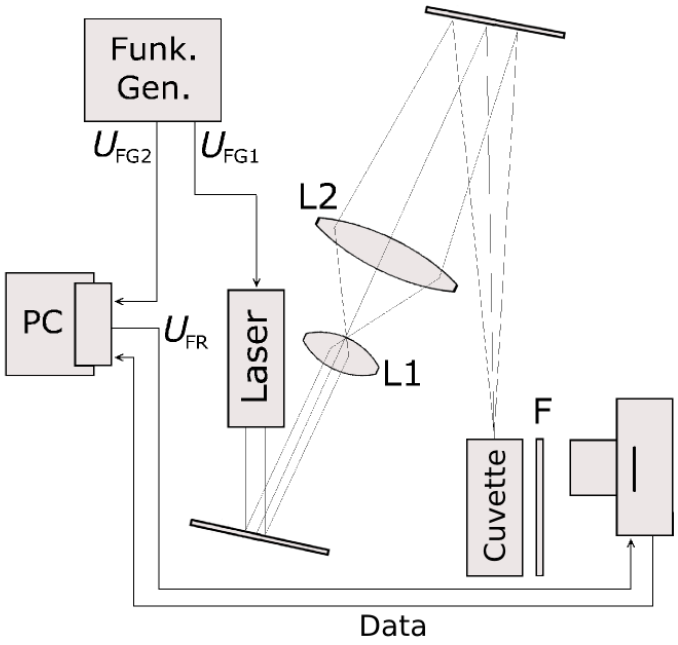

Figure 5.7: Experimental configuration for the measurement of the luminescence lifetime in the cuvette: diode laser, two lenses (L1 and L2), function generator (FunGen), trigger signals U_{FG1} and U_{FG2} for the frame grabber, and the CMOS line-scan camera BASLER SPL2048-70KM .

Fluorescence emission of the specimen, $[Ru(dpp(SO_3Na)_2)_3]Cl_2$, is imaged onto the CMOS line-scan camera. The function generator and the oscilloscope are synchronized to the trigger signal coming from the frame grabber. For details of the experimental setup can be found in [Erz11].

5.4.3.2 Results

The measurement was carried out in two modes. The first one was designed to analyze the effect of different excitation frequencies affecting the system performance by a constant ν value. The

second one was designed to investigate the relation of camera modulation frequency and the system performance by setting a constant excitation frequency value. The detailed experimental protocol can be found in [Erz11].

Fig. 5.8(a) shows the σ_{τ_ϕ} as a function of $\tilde{\omega}$ for $\nu = \omega t_{\text{exp}}/\pi = 0.92$. In this experiment, there were only 3 of them (black cross) lying outside the error bar predicted by the theoretical result (Eq. 5.27) under all 12 measurements. The shape of the curve agrees with the theoretical curves of F-values. we found the minimum deviation of this measured data happened at $\tilde{\omega} \approx 0.6$, which is near to our theoretical prediction that the optimum frequency for phase lifetime is $\tilde{\omega} = 0.701$. The deviation is due to the fact that the $\nu = \omega t_{\text{exp}}/\pi$ is not exactly 1.

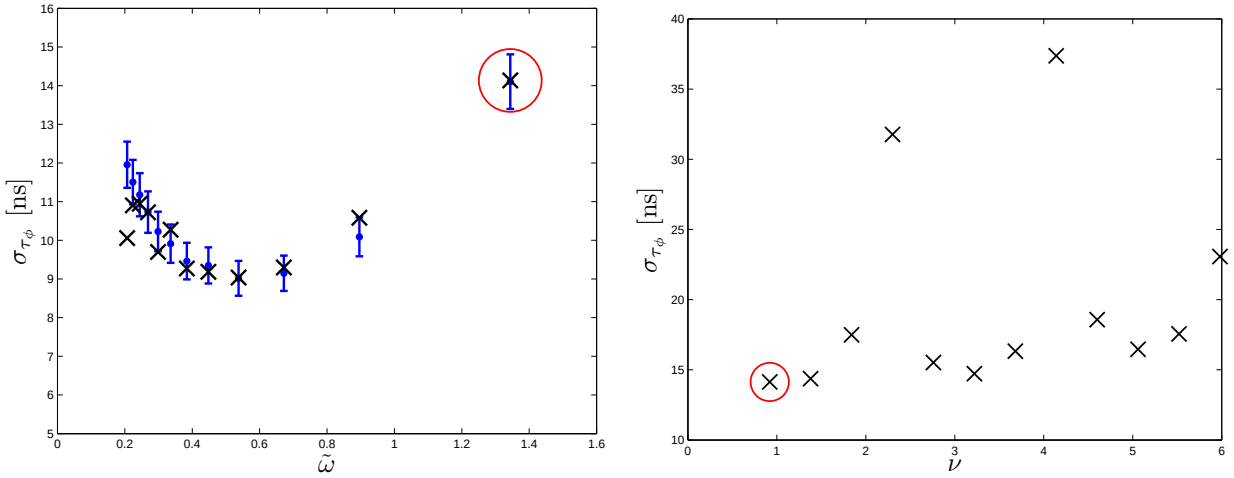

(a) (b)

Figure 5.8: The measured (black cross) and the theoretical (blue dots) noise of the standard deviation of the phase lifetime σ_{τ_ϕ}. (a) σ_{τ_ϕ} values as a function of dimensionless modulation frequency $\tilde{\omega}$, which is obtained by $\tilde{\omega} = \omega\bar{\tau_\phi}$, with a constant $\nu = 0.92$. (b) σ_{τ_ϕ} values as a function of excitation and camera frequency ratio ν with a constant modulation frequency $f_{\text{ex}} = 230$ kHz.

Fig. 5.8(b) shows the σ_{τ_ϕ} as a function of ν with a constant modulation frequency $f_{\text{ex}} = 230$ kHz. The point surrounding by a red circle is the same one shown in Fig. 5.8(a). The shape of the curve fits the theoretical predicted sinc function shape of the system performance. When ν gets close to the even integer numbers, the whole period of the signal is sampled which results in bad performance of measurement. By repeating the experiment under the range of $0.24 < \nu < 1$, we found that different ν does very little affect on the variance of τ_ϕ. It confirms the fact that the performance depends on the sinc behavior. Inside the region of $\nu < 1$, the amplitude of sinc function does not vary too much, which results in a relatively constant performance range when $\nu < 1$.

5.5 Optimization

In this section, efforts are made to find the optimum experimental parameters for the lifetime measurement according to the close form of F-value derived.

5.5.1 Optimum Shutter Time for TriDiCam

From Eq. 5.23, we found that the form of F-values of ends up with a function of ξ, i.e. the relative length of lifetime to the shutter time. It means the FLIM performance can be changed by varying either lifetime or unit shutter time. The analytical form of the F-value is attractive for finding the appropriate parameters in order to achieve the optimal system performance, which corresponds to the minimum F-value. The optimal parameter $\hat{\xi}$, which minimizes F, can be found by optimization of the Eq. 5.23 for ξ,

$$\frac{\partial F}{\partial \xi} = 0 = \frac{\exp\left(\frac{1}{\xi}\right)\left(1-\xi+\exp\left(\frac{1}{\xi}\right)\left(6-2\xi\exp\left(\frac{1}{\xi}\right)\left(3+2\exp\left(\frac{1}{\xi}\right)(\xi-2)+\xi\right)\right)\right)}{\left(\exp\left(\frac{1}{\xi}\right)-1\right)^2 \alpha\xi} \tag{5.28}$$

To satisfy the Eq. 5.28, the numerator should be equal to zero. So that the optimal $\hat{\xi}$ can be found as $\hat{\xi} = 0.997$. For TriDiCam imaging system, the minimum adjustable shutter time is $15\,\text{ns}$. Therefore, using scheme A the optimal lifetime for detection is $\hat{\xi}/15\,\text{ns} = 15\,\text{ns}$.

The F-values function of all the schemes are convex within the tested interval, i.e. there is only one optimum lifetime for measurement relative to a fixed Δt. The optimum lifetime and corresponding minimum of the F-values can be calculated for each schemes. They are listed and compared in Tab. 5.2

Time-gated setting	Scheme	C_1 interval $[\Delta t]$	C_2 interval $[\Delta t]$	$\min(F)$ $[-]$	Optimal lifetime $[\xi]$
Contiguous	RLD	[0, 1]	[1, 2]	3.05	1.66
	RLDC1	[0, 1]	[1, 3]	2.89	1.27
	RLDC2	[0, 1]	[2, 3]	2.56	0.93
Overlapping	RLDO1	[0, 1]	[0, 2]	10.65	1.00
	RLDO2	[0, 1]	[0, 3]	7.39	0.79
	RLDO3	[0, 2]	[0, 3]	17.47	0.59

Table 5.2: Performance comparison of all RLD related schemes

According to the previous researches of the fluorescence standard [BQB$^+$07, ISS], we conclude some luminescent dyes with lifetimes below 35 ns, which are appropriate for detection, using current TriDiCam imaging system in Tab. 5.3 [1].

Fluorophore	Solvent	Lifetime [ns]	Recommended schemes	Refs.
2-Aminopurine	water	11.34	RLDC2	[ISS]
Anthranilic Acid	water	8.9	RLDC1	[ISS]
anthracecne	CyH	5.32	RLD	[BQB$^+$07]
9-cyanoanthracene	MeOH	16.27	RLDC2, RLDO2	[BQB$^+$07]
	CyH	13.47	RLDC2, RLDO2	[BQB$^+$07]
DPA	MeOH	8.77	RLDC1	[BQB$^+$07]
	CyH	7.76	RLDC1	[BQB$^+$07]
N-methylcarbazole	CyH	14.06	RLDC2, RLCO2	[BQB$^+$07]
rubrene	MeOH	9.79	RLDC1	[BQB$^+$07]
SPA	water	30.90	RLDC2, RLCO2	[BQB$^+$07]

Table 5.3: Suitable luminescent dyes in fluid solution with nanoseconds range lifetime for TriDiCam lifetime measurement with unit shutter length as 15 ns. Abbreviations used, MeHO = methanol, CyH = cyclohexane, SPA = N-(3-sulfopropyl)acridinium, DPA = 9,10-diphenylanthracene.

5.5.2 Optimum Modulation Frequency

Phase lifetime

To optimize performance of phase lifetime measurement with respect to the dimensionless modulation frequency $\tilde{\omega}$, we may find a $\tilde{\omega}$ value which minimizes the F-value of phase lifetime. It is not necessary to take the harmonic number h into account, since the optimum performance is given for each individual frequency. Here we only consider the fundamental frequency, i.e., $h = 1$. The optimum modulation frequency can be found, when the partial derivative of F-value of phase lifetime with respect to the $\tilde{\omega}$ equals zero.

$$\frac{\partial F_{\tau_\phi}}{\partial \tilde{\omega}} = 0 = \frac{\partial}{\partial \tilde{\omega}} \frac{\sqrt{2}\,(1+\tilde{\omega}^2)^{\frac{3}{2}}}{m_{\text{ex}} \cdot \tilde{\omega} \cdot |\operatorname{sinc}\psi|} = \frac{(2\tilde{\omega}^2 - 1)\sqrt{2(1+\tilde{\omega}^2)}}{m_{\text{ex}} \cdot \tilde{\omega}^2 \cdot |\operatorname{sinc}\psi|} \tag{5.29}$$

By solving the above equation, the optimal $\tilde{\omega}$ for phase lifetime measurement is obtained.

[1] The recommender schemes in the table are determined by taking the Δt of each scheme equal to the minimum adjustable length of 15 ns. By increasing the Δt, the TriDiCam system is also suitable for detection of fluorescent dyes with a longer lifetime in serval hundred nanoseconds.

$$\tilde{\omega} = \frac{1}{\sqrt{2}} \tag{5.30}$$

This result is also known from [LG10].

Modulation lifetime

Similarly, the optimal $\tilde{\omega}$ of obtaining best performance of modulation lifetime measurement can be found by solving the equation that the partial derivative of F-value of modulation lifetime with respect to $\tilde{\omega}$ equals zero.

$$\frac{\partial F_{\tau_m}}{\partial \tilde{\omega}} = 0 = \frac{\partial}{\partial \tilde{\omega}} \frac{\sqrt{2}\,(1+\tilde{\omega}^2)^{\frac{3}{2}}}{m_{\text{ex}} \cdot \tilde{\omega}^2 \cdot |\operatorname{sinc}\psi|} = \frac{(\tilde{\omega}^2 - 2)\sqrt{2(1+\tilde{\omega}^2)}}{m_{\text{ex}} \cdot \tilde{\omega}^3 \cdot |\operatorname{sinc}\psi|} \tag{5.31}$$

So that the optimal $\tilde{\omega}$ for modulation lifetime can be found as

$$\tilde{\omega} = \sqrt{2} \tag{5.32}$$

According to the optimization results of 5.30 and 5.32, the modulation frequency for achieving optimum performance of modulation lifetime is always two times larger than the optimum modulation frequency for phase lifetime measurement.

Phase and modulation lifetimes

If we solve the equation of $F_{\tau_\phi} = F_{\tau_m}$, we will end up with the solution of $\tilde{\omega} = 1$. The same modulation lifetime and phase lifetime performance are found in this specific frequency. Then we find the $\tilde{\omega}$ that optimizes the sum of F_{τ_ϕ} and F_{τ_m} with

$$\frac{\partial}{\partial \tilde{\omega}}(F_{\tau_m} + F_{\tau_\phi}) = 0 = \frac{(2\tilde{\omega}^2 + \tilde{\omega}^2 - \tilde{\omega} - 2)\sqrt{2(1+\tilde{\omega}^2)}}{m_{\text{ex}} \cdot \tilde{\omega}^3 \cdot |\operatorname{sinc}\psi|} \tag{5.33}$$

By solving the above equation, we get the optimal modulation frequency for both phase and modulation lifetimes.

$$\tilde{\omega} = 1 \tag{5.34}$$

It is coincident with the modulation frequency of obtaining the same F_{τ_ϕ} and F_{τ_m}. If we use a sinusoidal excitation for the measurement of mono-exponential lifetime, the modulation frequency $\tilde{\omega} = 1$ is the best choice for achieving equally good performance of modulation lifetime and phase lifetime.

Two components system

To find the optimum performance of two lifetime components system, with distinct lifetimes τ_1 and τ_2, it is impossible to find a $\tilde{\omega}$ value, since $\tilde{\omega}$ is defined as dimensionless quantity and bounded together to only one lifetime. Therefore, it is necessary to switch back to the absolute modulation frequency ω, and find optimum ω which minimizes with the sum of F-values of all lifetime values of two fluorophores.

$$\frac{\partial}{\partial \omega}(F_{\tau_{m,1}} + F_{\tau_{\phi,1}} + F_{\tau_{m,2}} + F_{\tau_{\phi,2}}) = 0 \tag{5.35}$$

By solving the above equation, the only non-complex and positive root is

$$\omega = \frac{1}{\sqrt{\tau_1 \tau_2}} \tag{5.36}$$

which is the optimum modulation frequency of two lifetime components system. It yields equivalent result found by ensuring the best resolution of two lifetime signal plots in the phasor plane, the detail derivation is given in the section A.2.

5.5.3 Optimum Exposure Time

As found in the simulation (Fig. 5.3), best F-values can be obtained when the exposure time approaches zero, which is the case of ideal sampling. It means all collected photons can be very efficiently used even through the total amount of them is very less. However, it is not practical for the real FLIM measurement since very poor SNR results from very low intensity images.

The length of exposure time depends on the camera modulation frequency. By combining the Eq. 3.48 and 3.49, we may derive the relation $t_{\text{exp}} = \nu\pi/\omega$. Once the ω is fixed, the length

of exposure time is proportional to ν. Therefore, to analyze the optimum exposure time for HtM-FLIM, it is equivalent of finding a best ν that maximize the SNR of the lifetimes. For phase lifetime we have

$$\frac{\partial \mathrm{SNR}_{\tau_\phi}}{\partial \nu} = \partial_\nu \frac{\sigma_{\tau_\phi}}{\tau_\phi} = 0 = \frac{m_{\mathrm{ex}} \cdot \tilde{\omega} \cdot \left(\pi\nu \cos\left(\frac{\pi\nu}{2}\right) - 2\sin\left(\frac{\pi\nu}{2}\right)\right)}{\sqrt{2}\left(1+\tilde{\omega}^2\right)^{\frac{3}{2}}} \tag{5.37}$$

For modulation lifetime we have

$$\frac{\partial \mathrm{SNR}_{\tau_m}}{\partial \nu} = \partial_\nu \frac{\sigma_{\tau_m}}{\tau_m} = 0 = \frac{m_{\mathrm{ex}} \cdot \tilde{\omega}^2 \cdot \left(\pi\nu \cos\left(\frac{\pi\nu}{2}\right) - 2\sin\left(\frac{\pi\nu}{2}\right)\right)}{\sqrt{2}\left(1+\tilde{\omega}^2\right)^{\frac{3}{2}}} \tag{5.38}$$

By solving the above the equations, we found the same optimum exposure times for both phase lifetime and modulation lifetime. It is equivalent to the position of the extreme of sinc function. The optimum ν are

$$\hat{\nu} = 0.74 \qquad \text{for} \qquad 0 < \nu < 2 \tag{5.39}$$
$$\hat{\nu} = 2.92 \qquad \text{for} \qquad 2 \leqslant \nu < 4 \tag{5.40}$$
$$\hat{\nu} = 4.94 \qquad \text{for} \qquad 4 \leqslant \nu < 6 \tag{5.41}$$
$$\hat{\nu} = 6.96 \qquad \text{for} \qquad 6 \leqslant \nu < 8 \tag{5.42}$$

Except for the range of $0 < \nu < 2$, the optimum ν appears the same position where the absolute amplitude of sinc function gets its maximum (Fig. 3.5). Since the absolute amplitude of sinc decreases as the ν increases. The performance of bigger ν range is worse than the ν in a smaller range. If the frequency of camera modulation allows, it is wise to choose the optimum ν in the range of $0 < \nu < 2$.

5.5.4 Waveform Optimization

The previous sections in this chapter shows the main error source in the FLIM system caused by shot noise if too low excitation intensity is applied. In the contrary, the problems such as photonbleaching, unexpected cell responses, sample damages and shortened lifetime by exciton-exciton annihilation could happen when excessive high excitation intensity is used [MDDW95, BJL+97, KBF+99]. Therefore, in order to avoid these unpleasant results, excitation lights are always set with a highest amplitude limit, or peak amplitude constraint.

It is difficult to find an appropriate excitation waveform for the FLIM-measurement. Firstly, as shown in the Sect. 5.4, some waveforms containing higher harmonics have better performance than a sinusoidal waveform. However, due to the problem of aliasing error, these waveforms, such like square wave, are approximated by truncated number of terms in the Fourier series. This approximation can exhibit overshoot of the peak amplitude. Secondly, we found that the performance of lifetime measurement from higher harmonic is much worse than base frequency for the well-known waveforms like square wave or sawtooth wave. It is not practical to perform a multiple frequency measurement by using waveforms with very unbalanced responses for different harmonics. Therefore, there is need to design the optimum waveforms for difference purposes.

Within a certain peak amplitude constraint, finding a waveform which provides the best performance for FLIM measurement can be described as an optimization problem with the analytical form of F-value as the objective function. However, the optimization of nonlinearity under the peak amplitude constraint has not been studied extensively. As suggested in [HB96, Hor00] a close-form solution of the peak amplitude problem does not exist. There were approaches [Sch70, VdB87] trying to derive a formula for the phase angles that yields a low peak amplitude. However, we found that the peak amplitude after minimization would not fulfill the constraint in many cases.

Instead of using such approaches, we use the "Semi-Infinite Programming" (SIP) [HK93, RR98, RG98, LS07] to solve this optimization problem.

Problem Formulation

At first, we formalize the problem. Since finding the exact form of peak amplitude of periodic excitation is not possible, we formalize this constraint by covering the full period of the base frequency, which also includes the periods of higher harmonic terms. To simplify the form of excitation wave for the optimization problem, we use a dimensionless time variable $\tilde{t}$, where

$$\tilde{t} = \omega t \tag{5.43}$$

The dimensionless time period will be 2π. Therefore, the excitation signal of Eq. 5.44 will be

$$I_{\text{ex}}(\tilde{t}) = 1 + \sum_{h=1}^{N_h} m_{\text{ex},h} \sin(h\tilde{t} + \phi_{\text{ex},h}) \tag{5.44}$$

which is a multi-harmonic wave with period 2π.

The form of F-values contains a part which does no impact to the optimization result. It can be calculated in each harmonic term by choosing a constant ν. We use a κ_h term to replace this part to simplify the objective function for optimization.

$$\kappa_h = \frac{\sqrt{2}}{h \cdot |\operatorname{sinc} \psi_h|} \tag{5.45}$$

The optimization problem for finding the best performance for phase lifetime measurement of using N_s harmonics excitation wave can then be formalized as follows.

$$\begin{aligned} \text{minimize} \quad & \sum_{h=1}^{N_h} \frac{\kappa_h \left(1 + \tilde{\omega}^2 h^2\right)^{\frac{3}{2}}}{\tilde{\omega} m_{\text{ex},h}} \\ \text{subject to} \quad & I_{\text{ex}}(\tilde{t}) \leqslant PA, \ \ \forall\, \tilde{t} \in [0,\ 2\pi]; \\ & m_{\text{ex},h} > 0; \quad h = 1, 2, \ldots, N_h; \\ & 0 < \tilde{\omega} \leqslant \frac{1}{\sqrt{2}} \end{aligned} \tag{5.46}$$

The objective function uses the F-value function of phase lifetime, it can be tailored for optimization of the modulation lifetime by changing the objective function. Where PA is the peak amplitude constraint, it can be infinity number because $\tilde{t} \in [0,\ 2\pi]$ can be infinity. The modulation depth $m_{\text{ex},h}$ should be constrained to a positive value to avoid a negative F-value. Since the best modulation frequency of phase lifetime of base frequency term is $1/\sqrt{2}$ derived by Eq. 5.32, according the behavior of F-values, the best modulation frequencies for phase lifetime of higher harmonic terms are smaller than $1/\sqrt{2}$. Therefore, the modulation frequency $\tilde{\omega}$ is constrained in a small range between 0 and $1/\sqrt{2}$ to reduce the complexity of optimization.

Semi-Infinite Programming

The SIP is a mathematical optimization method dealing with a finite number of variables , but an infinite many constraints. For the SIP algorithm We uses the `fseminf` solver in the optimization toolbox in MATLAB [GW90]. The `fseminf` consists of a quasi-Newton sequential quadratic programming algorithm that uses line search with a merit function applied to a finite problem that results from the SIP problem with infinite constraints discretized in certain points. This approach can be classified as a discretization method, since the search space is sampled by an interval which generates a grid of points where constraints can be computed.

Results

The results of optimization of excitation are shown in this section with different scenarios.

Scenarios 1

Lots of FLIM applications are concerned about resolving biexponential fluorescence decays using wide field FLIM [WBS+08, LRR+09, SEE+09]. In such cases, a rapid imaging approach can be realized using a supercontinuum excitation source with multiple harmonics, and Weber's method to calculate the lifetime from the phase and modulation information contained in the two harmonic components. In Sect. 5.4.2.2 we have shown that lifetime calculated from higher harmonic component always suffers from much worse SNR than the one from the base frequency component. Therefore, it is necessary to design a optimum waveform which provide the best performance of two (or more) of its harmonic component.

Fig. 5.9 shows the waveforms after the SIP optimization. We set the $PA = 2$ as the peak amplitude constraint. We present the optimized waveform for 5 harmonics case and 11 harmonics case. The best F-values of using 5 harmonics waveform were 20.1 and 10.1 for the 1st and 2nd harmonic, the overall performance of 30.2 F-value can be achieved. The best F-values of using 11 harmonics waveform were 10.5 and 11.3 for the 1st and 2nd harmonic, the F-value of using these two harmonics together was 21.8. The better performance was obtained by using the waveform including higher harmonics.

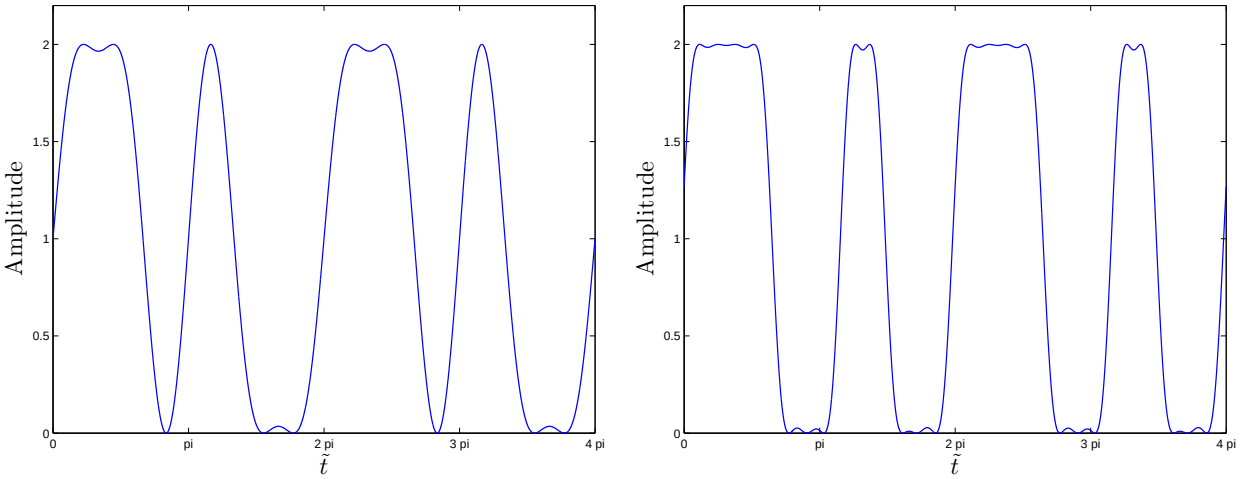

(a) Optimized waveform containing 5 harmonics

(b) Optimized waveform containing 11 harmonics

Figure 5.9: Optimized waveforms for achieving best performance of lifetime measurement for the first two harmonics.

Scenarios 2

In Sect. 5.4.2.2 and 5.4.2.2, we have shown that the better performance in lifetime measurement using the base frequency can be obtained by the pulse train excitation with smaller duty cycle. However, in order to avoid aliasing error, the tested pulse train are Fourier series approximation using the finite number of harmonics, which causes the overshoot of the peak amplitude limit. Such phenomena can be eliminated by waveform optimization using SIP.

Fig. 5.10 shows the optimized waveform of using just the base frequency for lifetime measurement. Both 5 harmonics case and 11 harmonics case are presented. The best F-values were 6.02 and 5.23, respectively. Even better performance can be achieved by including higher harmonics. In both cases, we have achieved a larger than 1 modulation depth in the base frequency component without overshooting the peak amplitude limit.

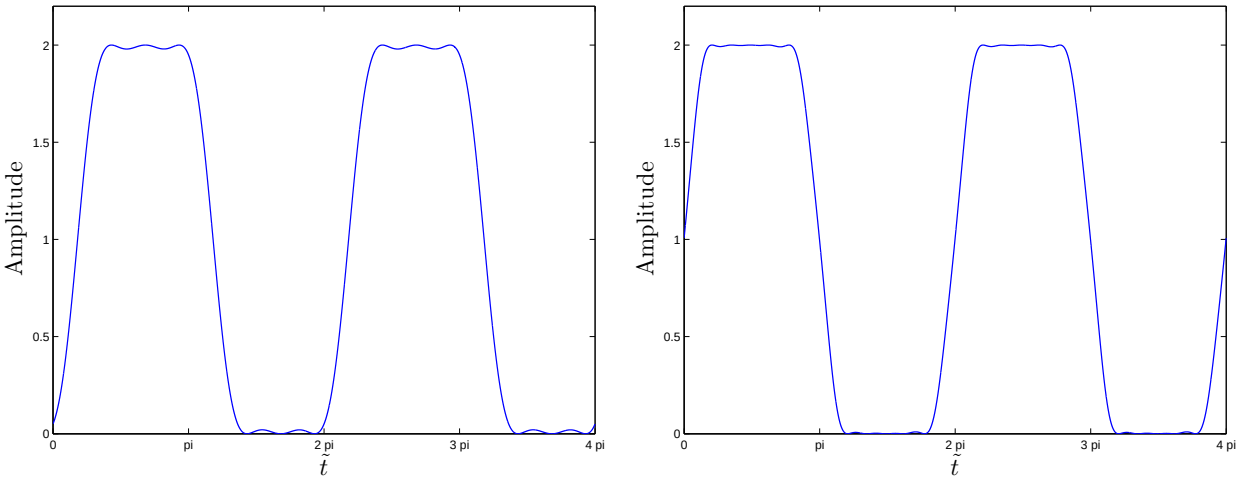

(a) Optimized waveform containing 5 harmonics (b) Optimized waveform containing 11 harmonics

Figure 5.10: Optimized waveforms for achieving best performance of lifetime measurement by the base frequency.

5.6 Summary

In this section we perform a thorough statistics analysis of the two types of lifetime measurement system we applied and optimized the measurement parameters.

In order to compare and optimize the performance of the RLD method and all proposed schemes for FLIM by TriDiCam time-gated camera, we quantified the photon economy by F-values. By calculation of the F-values, we found that although the overlapping time-gated setting used in TriDiCam imaging system is not designed for FLIM, by choosing appropriate schemes the performance is comparable to the performance of FD-FLIM from previous reported work [PC03, ESK08, LEJ10]. For the performance of measuring the optimal lifetimes, the schemes using contiguous

time-gates are $5 \sim 6$ times better than the performance of schemes using overlapping time-gates. Therefore, the contiguous time-gates settings are highly recommended.

Current TriDiCam imaging system has a minimum of shutter time of $\Delta t = 15\,\text{ns}$. It can be also extended in $15\,\text{ns}$ steps. If we assume $1.2 \times \min(F)$ as the criterium of F-value for getting a reasonable performance, the shortest resolvable lifetime in TriDiCam is $5.4\,\text{ns}$ for contiguous time-gates and $11.3\,\text{ns}$ for overlapping time-gates. For the detection of longer lifetimes, same reasonable performance can be also achieved by extending the shutter times to several integer multiples.

We also quantified the photon economy by F-values to optimize the performance of the HtM-FLIM system. Different from previous FD-FLIM researches, we proposed a more convenient approach to calculate the F-values using the error propagation theory and validated the results by Monte-Carlo simulations. The derivation of F-values was based on the lifetimes calculation using the Fourier analysis. By calculating F-values under different scenarios we found that if exposure time is independent of the modulation period, in small scale of relative length $\nu(\nu < 1)$, the degree of F-values affected by sinc function is not very obvious because inside this region the amplitude of sinc function does not vary too much. The optimum exposure time can be found inside this region that equals to $\nu = 0.74$ times the length of modulation period. The same performance of phase lifetimes and modulation lifetimes can be achieved by choosing the modulation frequency as $\tilde{\omega} = 1$. In large scale of $\nu(\nu \gg 1)$, the performance of the system is proportional to the absolute amplitude of the sinc function. For multiharmonic sinusoidal excitation, smaller F-values of higher harmonics were found than the previous reported work [ESK08], because sampling by heterodyne scheme provides the possibility of choosing an optimum camera modulation frequency. Using the multi-harmonic excitation, the oscillation frequency of sinc function of higher harmonic components is even several times larger than the one of base frequency component, i.e., the poor performance ($m_{\text{cam}} \to 0$) happens several times more frequent, which brings more unstable system performance compared to the one of base frequency. This instability of the system performance caused by sinc effect can be eliminated if a constant ν is chosen.

Chapter 6

FLIM Denoising by Total Variation

6.1 Overview

In FD-FLIM system, poor SNR phase intensity images, which are mainly caused by shot noise and instrument noise, generate poor quality and unreliable lifetime images. This can be misleading for a correct interpretation of fluorescence lifetime data and will affect the careful quantification applications such like FRET for the detection of subnanometer conformational changes, protein-protein interactions and protein biochemical status [WE08].

In this chapter, we focuse on the lifetime precision improvements for the noise contaminated FLIM images by image analysis techniques. For denoising the FD-FLIM images we propose a vector-valued total variational (TV) based approach. Instead of denoising the FLIM intensity images, the filtering is performed for calculated lifetime data in a way that both phase angle and modulation depth are transfer to phasor coordinates vector and taken into account as vector-valued data for TV denoising.

In the beginning of this chapter (Sect. 6.2), an introduction of TV based image denoising is given. In Sect. 6.3 a vector-valued TV model for the FLIM images denoising is shown. The impact of the denoising algorithm on the FLIM data is evaluated and its applications are also given in Sect. 6.4,

6.2 Introduction to Total Variation Denoising

Image denoising, restoration and enhancement are important techniques in image processing, computer vision and artificial intelligence. A review article by Buades et al. [BCM$^+$06] summarizes a classification of currently used image denoising algorithms, as well as provides a detail comparison among them.

During the last decade a new branch in image processing techniques has emerged from the mathematical community. These methods can be categorized as PDE- (Partial Differential Equation) or variational-based [SGG+09] image processing. Variational and PDE based methods are different from conventional image processing in that the processing is formulated as a diffusion process or an optimization problem that both can be solved with PDE techniques.

Total variation (TV) denoising [CS05, CCC+10], also known as TV regularization, is often used for the noise removal for intensity (gray value) images. The TV based image model were first introduced by Rudin-Osher-Fatemi (ROF) on their pioneering work [ROF92] on edge preserving denoising. The TV denoising model is constructed with the definition of their "energy", or energy function $\mathcal{E}(u)$. Usually the objective *energy function* $\mathcal{E}(u)$ is composed of two parts

$$\mathcal{E}(u) = H(u) + J(u) \tag{6.1}$$

where $H(u)$ indicates the *data term*, also referred as fidelity, which forces the denoised image to be close with the input data. $J(u)$ stands for the *regularizer term*, which enforces a smooth constraint on the output denoised image. The regularizer works by minimizing the total variation, which is defined as the integral of the norm of image gradient. An ideal TV model for denoising balances the fidelity to the observation and the prior expectation of smoothness.

6.3 Vector-Valued TV Model for FLIM Data Denoising

Recent development has shown that the TV denoising model can be also extended to multichannel images, or vector-valued images for denoising the color images [BC02, GC10] or multi-labeling problem [LS11].

From the FD-FLIM techniques, both phase lifetime and modulation lifetime are obtained. To resolve each individual lifetimes from multiple lifetime components system, both measured phase and modulation lifetime are important. They can connected by a nonlinear relation described in [Web81]. Performing the denoising filter on one of them and totally ignoring the other one (independent filtering) creates large bias to the ground truth. Therefore, we treat them as dependent vector-valued data in our TV model.

Because of the complex relation between the phase and modulation lifetime, we transfer them to a vector of phasor plane coordinates $\mathbf{u} = (u_{\mathrm{Re}}, u_{\mathrm{Im}})^T$ by Eq. 2.32 for the TV model. This transfer provides a intuitive way of data interpretation and does not alter the data. The phase and modulation lifetime information can be calculated back from $\mathbf{u}$ without losing information.

6.3.1 TV Model

Let Ω denote a 2-D bounded image region takes vectorial values on which the phasor vector $\mathbf{u}$ is defined. That is

$$\mathbf{u} : \Omega \to \mathbb{R}^2, \quad x = (x_1, x_2) \to \mathbf{u}(x) = (u_1(x), u_2(x)) = (u_{\text{Re}}, u_{\text{Im}}) \in \mathbb{R}^2 \tag{6.2}$$

The standard model for noisy image is given by

$$\mathbf{z} = \mathbf{u} + \epsilon \tag{6.3}$$

where $\mathbf{u} = (u_{\text{Re}}, u_{\text{Im}})^T$ is the ideal underlying vector-valued image, $\mathbf{z} = (z_{\text{Re}}, z_{\text{Im}})^T$ is the input vector-valued data. ϵ is the additive Gaussian noise, the variance of it follows the relation given in Eq. 5.11. Our approach for the vector-valued FLIM data denoising can be formalized in the following variational problem.

$$\mathcal{E}(\mathbf{u}) = \int_\Omega |z_{\text{Re}} - u_{\text{Re}}| dx + \int_\Omega |z_{\text{Im}} - u_{\text{Im}}| dx + \lambda \int_\Omega \sqrt{||\nabla u_{\text{Re}}||^2 + ||\nabla u_{\text{Im}}||^2} dx \tag{6.4}$$

where λ is a weighting parameter with $\lambda > 0$, it controls the tradeoff between the goodness of fit to the data. The data term consists of the first two terms of the energy function, the last term of the energy function is the regularizer term.

Data term

The ROF TV model began to use L^2 norm of the data term since it is differentiable and can be solved using the steepest decent approach. However, the L^1 functional of the data term has attracted attention due to a number of advantages, including its robustness against outliers and superior performance with impulse noise [CE05].

In the realistic FLIM data, we found that it suffers from outliers where few or more pixels do not obey the Gaussian noise model. The L^2 norm is sensitive to this kind of noise and would not provide a good result. Therefore, we choose the L^1 norm data term for its tolerance to noise.

Regularizer term

The gradient of one of the image channel in regularizer term is given by $\nabla \mathbf{u}$. In practice, it is based on the first-order discrete derivatives using finite differences on the pixel grid. The TV part of the energy function

$$\text{TV}(\mathbf{u}) = \int_\Omega \sqrt{||\nabla u_{\text{Re}}||^2 + ||\nabla u_{\text{Im}}||^2} dx \tag{6.5}$$

uses the Euclidean norm. By using the phasor vector instead of phase and modulation vector for denoising, the meaning of Euclidean norm of the regularizer term is more straightforward. It means the sum of spatial distances of phasor plot $\mathbf{u}$ to the its adjacent pixels's phasor plots.

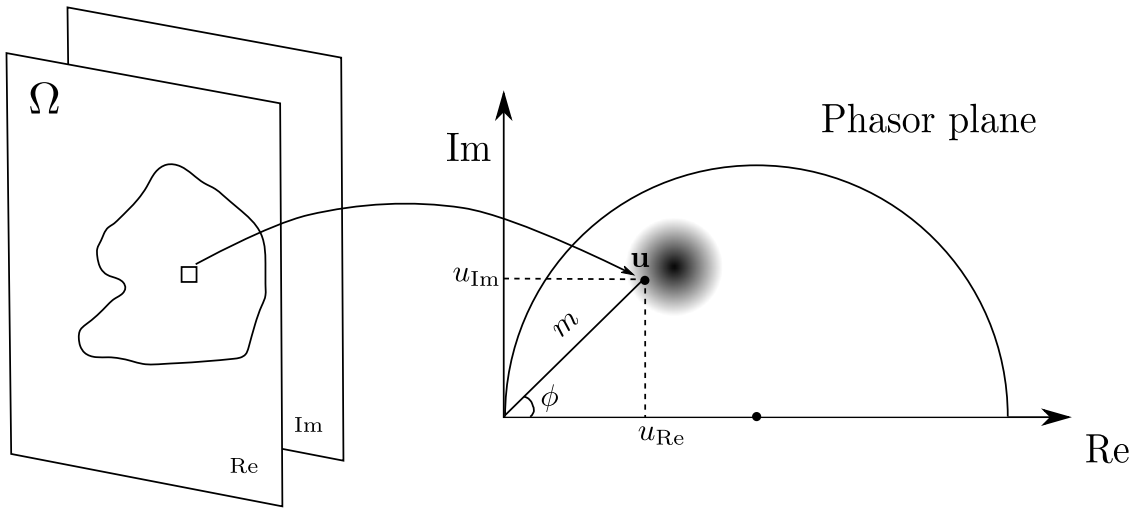

Figure 6.1: The vector-valued image plane Ω and its phasor plane representation.

As illustrated in Fig. 6.1, a vector $\mathbf{u}$ can be graphically represented on the phasor plane. The idea behind is that we assume the smooth lifetime change on the FLIM image, neighboring pixels belonging to same species exhibit similar lifetimes, i.e., their corresponding phasor plots should be close to each other on the phasor plane, the pixels in Ω having similar lifetimes should appear in the same cluster of the phasor plane. The regularizer takes the advantage of the spatial information on Ω and penalizes the phasor plots appearing at positions having a long distance from its neighboring pixels' phasor plots. By minimizing the energy function iteratively, the phasor plots with the larger variance to the mean "move" to the center of the phasor plots distribution which appears to be the real lifetime position on the phasor plane.

6.3.2 Algorithm

The implementation of vector-value TV denoising used for this thesis is adapted by a method so called "generalized vector-value total variation algorithm" proposed by Rodriguez and Wohlberg [RW09, RW]. This algorithm extends the iterative methods for TV denoising on scalar data [VO96] to the vector-valued data.

6.4 Results

6.4.1 Noise Reduction of FD-FLIM Data

The FLIM data of this experiment are from the Laboratory for Molecular and Cellular system of University of Göttingen, which participates in the FLICam project. In their application, the fluorescence lifetime were used as an indicator to analyze the FRET between the proteins. GFP (Green Fluorescence Protein) and mCherry were used as a FRET fluorophore pair, which are so called as donor and acceptor. If only GFP (donor) is expressed in neurons, there is no FRET happening, the lifetime of the donor do not change. When GFP and mCherry (donor + acceptor) are both expressed in the same cell, the FRET happens between them which led to the decrease of donor's lifetime.

Fig. 6.2 shows the modulation lifetime and phase lifetime images used for this FRET analysis. Both raw images and denoised images are shown to compare the result of image analysis. As can be seen, the removal of the noise is apparent. Instead of blurring the image's detail, the vector-valued TV model appears to preserve the fine structure contained in the image. More insight can be found by making the use of the phasor plane representation of denoised data.

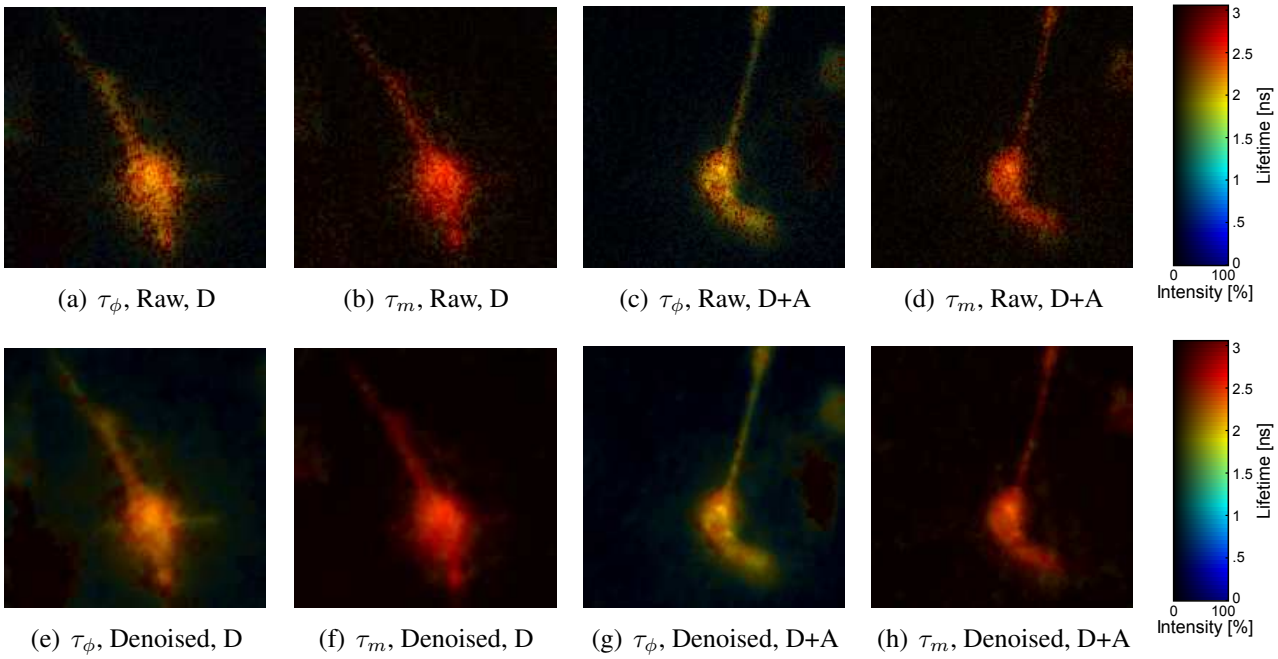

(a) τ_ϕ, Raw, D (b) τ_m, Raw, D (c) τ_ϕ, Raw, D+A (d) τ_m, Raw, D+A

(e) τ_ϕ, Denoised, D (f) τ_m, Denoised, D (g) τ_ϕ, Denoised, D+A (h) τ_m, Denoised, D+A

Figure 6.2: Comparison of FLIM images of phase lifetime τ_ϕ and τ_m before and after denoising. The donor reduces its lifetime after FRET taken place between donor and acceptor. Therefore, the donor and accepter FLIM image exhibits a slightly shorter lifetime than donor's FLIM image. This lifetime decreasing phenomena can be much more easier observed in the denoised image. Abbreviations used, D = Donor, D + A = Donor + Acceptor.

In Fig. 6.3, a significant reduction in the data plots distribution in the phasor plane histograms is accomplished by the vector-valued TV denoising algorithm. The plots on the phasor plane tends to cluster together to the mean of phasor plots distribution. This result shows the effect of our regularizer term which tends to minimize the distance of the phasor plots of adjacent pixels in the image domain.

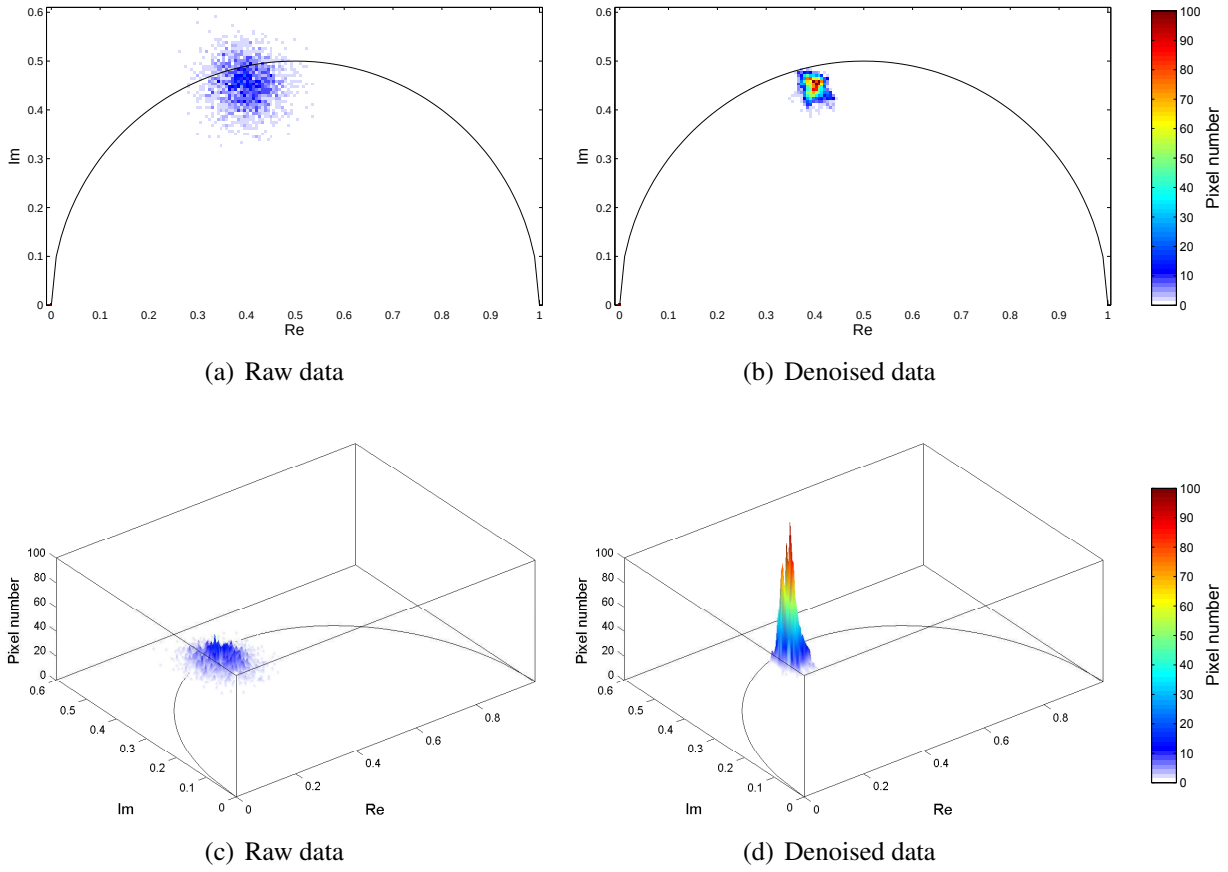

(a) Raw data (b) Denoised data

(c) Raw data (d) Denoised data

Figure 6.3: Improvement of the quality of the FLIM image is apparent after denoising image analysis (vector-valued TV). 2D and 3D phasor plot histograms are shown for reducing the variance of the data on the phasor plane.

Table 6.1 presents the mean value of the standard deviation of the Re- and Im-coordinates of the data plots of the phasor space and the modulation and phase lifetime before and after denoising. The center of the standard deviation of the data plots was estimated by the EM algorithm. However, we only took the pixels of foreground object into account since the background pixels are nothing but pure noises and do not belong to our region of interest. In this statistical analysis, we only took the foreground object into account, the low intensity background pixels were removed by taking a intensity thresholding technique. By using the thresholding, the disadvantages of the TV regularizer, such as introducing a loss of contrast, can be circumvented.

The analysis shows that the denoising algorithm makes an obvious improvement in the SNR of the FLIM data. According to the standard deviations presented in Tab. 6.1, the fluorescence

Sample	Data	$u_{\text{Re}} \pm \sigma_{u_{\text{Re}}}$	$u_{\text{Im}} \pm \sigma_{u_{\text{Im}}}$	$\tau_m \pm \sigma_{\tau_m}$ [ns]	$\tau_\phi \pm \sigma_{\tau_\phi}$ [ns]
Raw	D	0.402 ± 0.046	0.454 ± 0.048	2.615 ± 0.329	2.275 ± 0.362
TV denoised	D	0.402 ± 0.012	0.452 ± 0.014	2.620 ± 0.100	2.244 ± 0.092
Raw	D + A	0.443 ± 0.046	0.440 ± 0.045	2.48 ± 0.305	2.001 ± 0.309
TV denoised	D + A	0.443 ± 0.019	0.439 ± 0.018	2.49 ± 0.125	1.973 ± 0.123

Table 6.1: Re- and Im- coordinate values of data plots on the phasor plane and their corresponding modulation lifetime and phase lifetime values before and after vector-valued TV denoising. The modulation frequency is 80MHz. Abbreviations used, D = Donor, D + A = Donor + Acceptor.

lifetime resolution is improved from about ± 320 ps to ± 100 ps (more than 3 times reduction) than the image analysis presented by Spring and Clegg [SC09b], which uses the "TI-Haar + VST" algorithm and improves the lifetime resolution from ± 200 ps to ± 100 ps (about 2 times reduction).

6.4.2 Comparison of Vector-Valued TV Model to Scalar-Valued TV Model

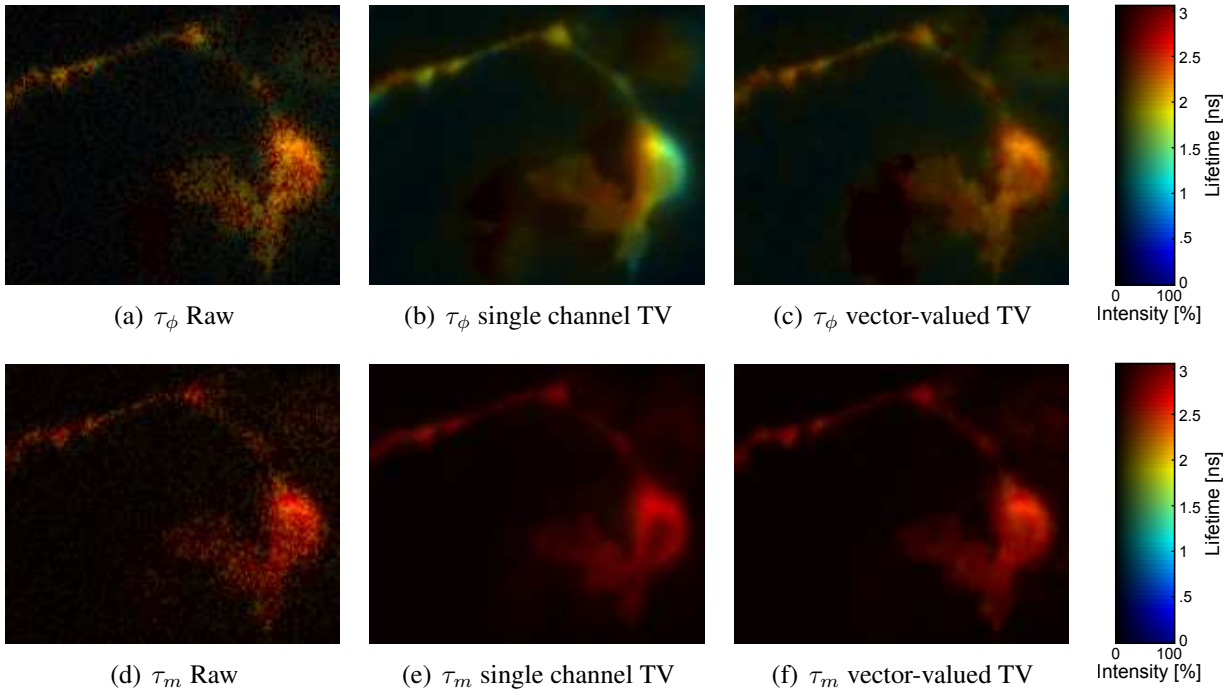

(a) τ_ϕ Raw (b) τ_ϕ single channel TV (c) τ_ϕ vector-valued TV

(d) τ_m Raw (e) τ_m single channel TV (f) τ_m vector-valued TV

Figure 6.4: Comparison of the independent filtering of the lifetime image of phase τ_ϕ and the lifetime image of modulation τ_m by TV, and the vector-valued TV filtering.

Fig. 6.4 shows the comparison of denoising results of using vector-valued TV model and using

single channel TV filtering to the τ_ϕ and τ_m lifetime image. Thresholding technique was also used here to avoid the influences by the low intensity background pixels. It is obvious that the results of vector-valued TV model has a better performance. Using the single channel TV filtering, the result of lifetime image of τ_ϕ failed in the correct lifetime restoration. Some areas of the foreground object, which is adjacent to the background, are affected by the lifetime of the background during TV regularization. This phenomena can be eliminated by using vector-valued TV model, since it takes both channels into account. Deviation from the truth value in one channel is compensated by the other channel.

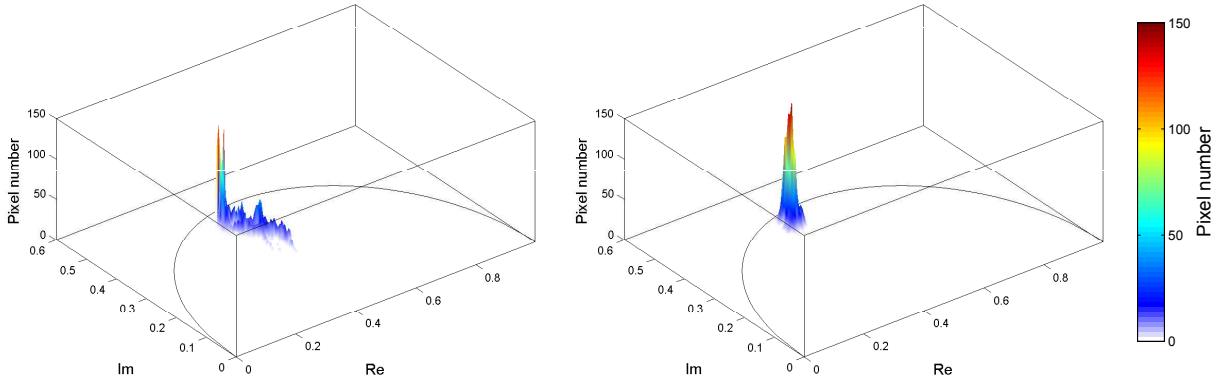

(a) Denoised by single channel TV

(b) Denoised by vector-valued TV

Figure 6.5: 3D phasor plot histogram comparison for the denoised result of independent filtering of the lifetime images by TV and vector-valued TV filtering. (a) The phasor plots distribution after single channel TV fails to shrink to one cluster. (b) The phasor plots distribution after vector-valued TV reduces the variance of the phasor plots distribution and keeps the original mean of the data cluster.

Fig. 6.5 represents the corresponding 3D phasor plot histogram for both single channel TV and vector-valued TV denoising result shown in Fig. 6.4. The single channel TV ignores the changes of the phasor plot's position during independent filtering. Phasor plots, which belong to the foreground object, were dragged to the background. However, they are clustered together by using the vector-valued TV.

6.4.3 Application of Denoising to FLIM-FRET Analysis

FRET can happen between two fluorophores when they are close enough and have overlapped emission and excitation spectrum. The most popular FRET pair for biological use is a cyan fluorescent protein (CFP) yellow fluorescent protein (YFP) pair. This can be used to analyze protein-protein interaction, molecule binding, conformational change and so on. When CFP and YFP are tandemly fused together, which leads to FRET, lifetime of this CFP-YFP fusion protein is different from (or shorter than) the donor CFP itself [WE08].

Fig. 6.6 shows two 3D phasor plot histograms before and after denoising the simulated FLIM data of compound of CFP-YFP and CFP along. We simulated the lifetime of CFP as 1.7 ns, lifetime of YFP as 2.3 ns and the CFP-YFP compound expressed a lifetime as 2.3 ns. Before the denoising, the two distributions are strongly overlapped on the phasor plane, which results from the added poisson noise of the low intensity image. On the phasor plane, the denoised FLIM data shows two clearly separated clusters of CFP-YFP compound and CFP along.

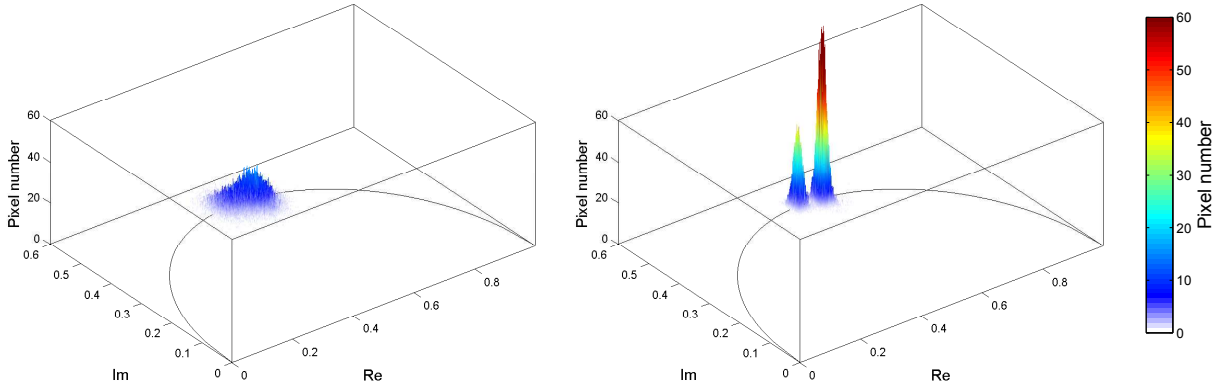

(a) Raw data (b) Denoised data

Figure 6.6: 3D phasor plot histogram comparison for a distribution of CFP along and a distribution of CFP with YFP that exhibits FRET. The color indicates pixel number at each position of the phasor plane (see scale bar). (a) The raw FLIM data on the phasor plane are a smear of two distributions, corresponding to the compound of CFP-YFP and CFP along. (b) The denoised data show two distinct distribution. The small CFP lifetime can be located on the semicircle (lower core) as a single lifetime (1.7 ns) compared to the higher core, which expresses a reduced lifetime of compound of CFP and YFP because of FRET.

As shown in [WE08], the phasor approach can be applied as a useful tool to analyze the FRET efficiency. However, a poor SNR FLIM data results in large variance of the phasor plots distribution which increases the difficulty for FLIM interpretation. By means of the efficient denoising algorithm we presented, the real meaning of the data hidden by noise can be unveiled.

6.4.4 Improvement of the Lifetime Calculation

As shown in the early chapter, the Weber's algorithm resolve the analytical lifetime calculation method is a very effective way. However, it is quite vulnerable to the noise. The proposed denoising algorithm can be also applied to increase the precision of lifetime calculation using Weber's method or any other lifetime calculation scheme.

The FLIM data of this experiment were from PCO AG, which is one of the collaboration member in the FLI-Cam project. In this experiment two fluorescent plates were stacked together to synthesize a mixture of two fluorescence components system. Each of these two fluorescent plates presents a different lifetime, with 4 ns and 60 ns, respectively. The stack of the plates should exhibit

a 32 ns lifetime. Six frequencies in the range from 1MHz to 20MHz were used as the sinusoidal excitation source. The measurement were undertaken by SwissRanger SR3000 camera.

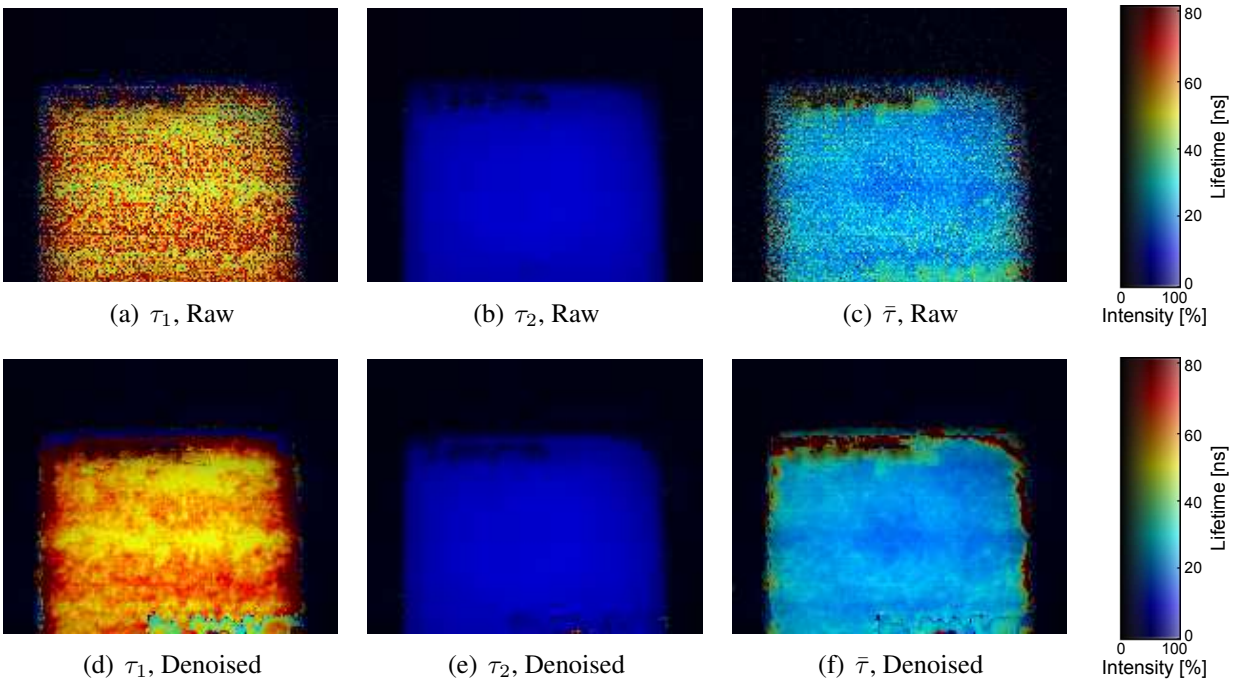

(a) τ_1, Raw (b) τ_2, Raw (c) $\bar{\tau}$, Raw

(d) τ_1, Denoised (e) τ_2, Denoised (f) $\bar{\tau}$, Denoised

Figure 6.7: Comparison of FLIM images of single lifetime component of τ_1 and τ_2 and average lifetime $\bar{\tau}$ in a bi-exponential lifetime mixture by Weber's lifetime calculation method before and after vector-valued TV denoising. The performance of the Weber's method increased after denoising.

Fig. 6.7 shows the Weber's lifetime calculation result applied on the FLIM images before and after denoising. We found that much less singularities were happening by applying the calculation on the FLIM images of the denoised version. The error of the calculated lifetime were drastically reduced by using the denoised FLIM image as input. Such a denoising algorithm could be applied as a preprocessing step before the lifetime calculation step (not only the Weber's method but also global analysis or LiMA method) in order to improve the precision.

6.5 Summary

We apply the vector-valued TV for the first time for the denoising of the FLIM image. It can be used to improve the precision of the phase and modulation lifetime acquired for noise contaminated FD-FLIM data. Instead of independent filtering of phase or modulation lifetime image channel, we considered the relation of phase angle and modulation depth and transferred them to a coordinates vector on the phasor plane and applied the vector-valued TV regularization on the phasor vector image.

According to the presented denoising results, the proposed denoising scheme shows a better performance in the improvement of lifetime resolution compared to other state-of-the-art FD-FLIM image denoising schemes [SC09a, BKC$^+$08]. Our proposed algorithm increases the lifetime contrast by reducing the variance in the input data, which leads to easier data interpretation. Such a denoising algorithm has broad applications such as improving the quantification FRET analysis, separating the noisy phasor plots distributions for different species and increasing the robustness of lifetime calculation. Moreover, for rapid FLIM imaging system, high frame rate results in less exposure and poorer SNR contained in the image. Combing with the proposed denoising algorithm, the increasing of the imaging speed with reasonable lifetime accuracy can be realized.

Chapter 7

Conclusion and Outlook

7.1 Summary

This dissertation provides a comprehensive and in-depth analysis of fluorescence lifetime imaging using the two types of ToF cameras. Such cameras enable the possibility of direct sensing of fluorescence signals by time-gated approach (pulse-based excitation) or by photon mixing technology (continuous-wave-based excitation). Due to the short length of exposure time and limited excitation intensity required by FLIM measurement, the SNR of the FLIM data is poor. Bringing FLIM schemes using such cameras with reasonable accuracy is not an easy task. So that we proposed several novel schemes especially tailored for the FLIM solution using each type of the current ToF cameras.

By analyzing the pulse-based ToF camera, we found the FLIM performance were dependent to the ratio of sample's lifetime and the length of the shutter, i.e., there is an optimal shutter time for a certain lifetime that we wanted to measure. Generally, the optimum shutter time is proportional to the lifetime. The optimum lifetime to the shutter time ratios of all proposed schemes were listed, which were within the range of 0.9 to 1.66. That means to detect a certain lifetime, the shutter time of the camera should be better designed as 60% to 110% of the lifetime. The current available pulsed-based ToF camera utilizes the overlapping time-gates for the depth scene measurement. However, we found the performance of FLIM by using continuous time-gates were 5 to 6 times better.

For the continuous-wave-based ToF camera, we proposed a generalized heterodyne modulation scheme which allows a different camera modulation frequency to the excitation signal. Such technique enlarges the measured range of fluorescence lifetimes for a frequency-limited ToF camera. According to the generalized formula of heterodyne modulation scheme we derived, the performance follows a sinc function behavior. The optimum excitation frequency to camera modulation frequency ratios were derived. By using the best ratio, the performance is 25% increased compared to the commonly used homodyne detection method.

The heterodyne modulation scheme we proposed is suitable for multiple frequency measurement by using a supercontinuous multi-harmonics excitation. Because of the weak fluorescence response to the high harmonic component, we also optimized the waveform of the multi-harmonics excitation with peak amplitude constraint to compensate the modulation depth of the high harmonic component. So that the best combined performance of multiple frequencies' measurement can be achieved. The waveform optimization can be applied to increase the modulation depth of base frequency term as to improve performance of base frequency measurement by including multi-harmonic components without overshooting the peak amplitude limit.

Previous work [PC03, ESK08] used the homodyne detection technique and derived the standard deviation of the lifetime the same way via accuracy estimation by the Taylor expansion of the expectation of the lifetime. Different from their approach, we dedicated to derive the standard deviation by the Gaussian error propagation theory. The theoretical results have been successfully validated by both Monte-Carlo simulation and the real experiments.

From the statistical analysis, we found the phasor plots follows bivariate normal distribution with equal and independent variance on the both coordinate direction of the phasor plane. The image denoising algorithm we proposed took the advantage of this property of the phasor plots distribution. It effectively reduces the variance of both phase lifetime and modulation lifetime as a result of shrinking the variance of the phasor plots distribution by vector-valued total variational approach. The denoising scheme could play an important role for high-frame rate FLIM using ToF camera while preserving the accuracy of the fluorescence lifetime data.

7.2 Outlook

In the future, following aspects can be consider as the extension or improvement of this thesis.

- To avoid the aliasing error, in our demodulation scheme, we utilized enough phase samples to resolve all significant harmonic component. However, this scheme requires long recording time. A modified demodulation scheme using ToF camera can be designed to suppress the higher harmonics as suggested by [VMGJ04, EKF09].
- The FLIM technique can be applied for vivo measurement. In such cases, we should take the moving object into account. A specially designed algorithm is necessary for FLIM image stabilization and motion compensation.
- The phasor plots distribution model and the lifetime distribution model we proposed only took the shot noise into account. It would be interesting to introduce the systematic error into this model and validate by real experiments.
- With the noise model of phasor plot we presented in Eq. 5.12, the noise at each pixel is independent Gaussian distributed. The variance depends on the modulation depth, number of sampling points and average photon number of each camera exposure time. The coordinate

of the phasor plot is then given by a linear combination of the noise-free data and the error. Therefore, we may assign a weight term to each pixel of the data term according to the multiplicative inverse variance of its phasor plot. So that pixel with large variance on the phasor plane will have a small weight in the data term, and be corrected by the regularizer of the TV approach.

Appendix A

Proof of Theorem

A.1 Mono Exponential Distribution

To show that the distribution of the single fluorescence phasor plot along the arc of the semi-circle, the central angle φ is used to represent the lifetime.

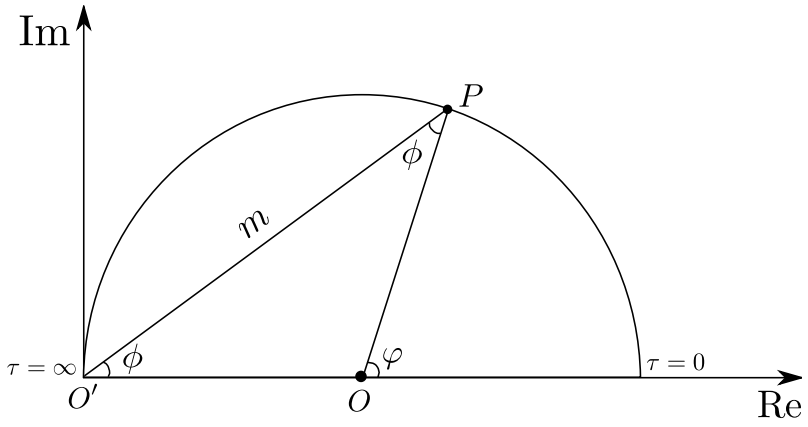

Figure A.1: Mono-exponential lifetime distribution along the semi-circle of the phasor plane

As shown in Fig. A.1, because $OO' = OP = R$(Radius), the angle $\angle OO'P = \angle OPO' = \phi$. The angle φ is an exterior angle of $\triangle OO'P$, so that

$$\varphi = 2\phi \tag{A.1}$$

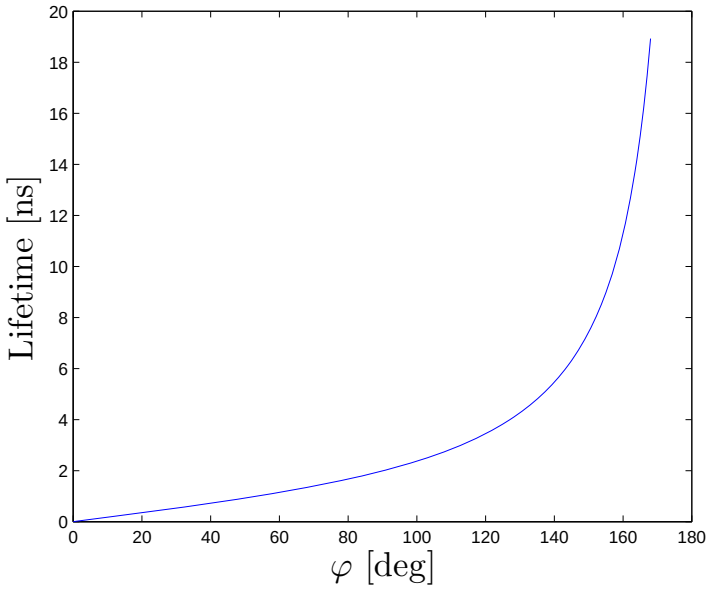

Figure A.2: Mono-exponential lifetime distribution along the semi-circle of the phasor plot depending on the central angle φ

The single lifetime τ_P in P can then be represented by φ:

$$\tau_P = \frac{1}{\omega} \tan \frac{\varphi}{2} \tag{A.2}$$

With a given frequency, the phasor plot distribution of single fluorescence lifetime along the semi-circle follows the relation of tangent.

A.2 Optimal Modulation Frequency of a Mixture of Two Fluorophores System

The optimal modulation frequency of the given lifetimes is chosen to ensure the best resolution in the phasor plane. In other words, best modulation frequency should keep the phasor plots of distinct fluorescence samples in a maximum distance in the phasor diagram.

In the case of two single fluorescence sample with distinct lifetimes, as illustrated in Fig. **??** the phasor plots of both sample u_1 and u_2 are located in the semi-circle. The maximum distance of u_1 and u_2 is equivalent to the longest arc between u_1 and u_2. The length of the arc depends on the central angle, so that the optimal modulation frequency ω are selected when the difference of two central angle gets maximum, which is

$$\omega = \arg\max \left(\varphi_2 - \varphi_1\right) \tag{A.3}$$

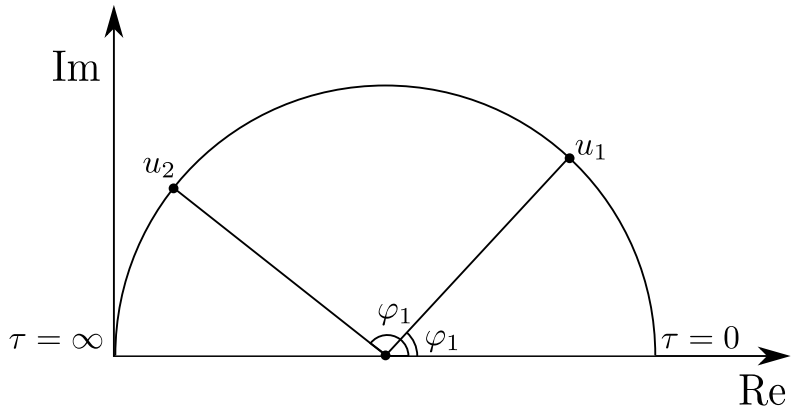

Figure A.3: The proof of best frequency of two single fluorescence lifetime sample

From Eq. A.2 we get

$$\varphi_2 - \varphi_1 = 2\arctan\omega\tau_2 - 2\arctan\omega\tau_1 \tag{A.4}$$

then we can optimize it for ω,

$$\frac{\partial(\varphi_2 - \varphi_1)}{\partial\omega} = 0 = 2\left(\frac{\tau_2}{1+\omega^2\tau_2^2} - \frac{\tau_1}{1+\omega^2\tau_1^2}\right) \tag{A.5}$$

$$\frac{\partial(\varphi_2 - \varphi_1)}{\partial\omega} = 0 = \frac{2(\tau_2 - \tau_1)(1-\omega^2\tau_2\tau_1)}{(1+\omega^2\tau_2^2)(1+\omega^2\tau_1^2)} \tag{A.6}$$

therefore, the best modulation frequency can be calculated as

$$\omega = \frac{1}{\sqrt{\tau_1\tau_2}} \tag{A.7}$$

A.3 Derivation of Covariance Matrix of Phasor Plot

By Eqs. 3.55, 3.57 we know that the phasor and modulation can be calculate by N_s cross-correlation frames. By using the well known trigonometry relation

$$\sec^2 x = 1 + \tan^2 x \tag{A.8}$$

we get

$$\cos\phi = \frac{1}{\sqrt{\tan^2\phi + 1}} \tag{A.9}$$

$$= \frac{1}{\sqrt{\left(\sum_{k=0}^{N_s-1} y_k \sin\left(2\pi k\frac{n}{N_s}\right) \Big/ \sum_{k=0}^{N_s-1} y_k \cos\left(2\pi k\frac{n}{N_s}\right)\right)^2 + 1}} \tag{A.10}$$

$$= \frac{\sum_{k=0}^{N_s-1} y_k \cos\left(2\pi k\frac{n}{N_s}\right)}{\sqrt{\left(\sum_{k=0}^{N_s-1} y_k \sin\left(2\pi k\frac{n}{N_s}\right)\right)^2 + \left(\sum_{k=0}^{N_s-1} y_k \cos\left(2\pi k\frac{n}{N_s}\right)\right)^2}} \tag{A.11}$$

similarly we obtain

$$\sin\phi = \frac{\sum_{k=0}^{N_s-1} y_k \sin\left(2\pi k\frac{n}{N_s}\right)}{\sqrt{\left(\sum_{k=0}^{N_s-1} y_k \cos\left(2\pi k\frac{n}{N_s}\right)\right)^2 + \left(\sum_{k=0}^{N_s-1} y_k \cos\left(2\pi k\frac{n}{N_s}\right)\right)^2}} \tag{A.12}$$

The coordinates of an individual point u in phasor space are given by Eq. 2.32. By combining the Eq. 3.55 and 3.57 together, we get

$$\begin{aligned} u_{\text{Re}} &= m\cos\phi = \frac{\pi}{m_{\text{ex}}} \cdot \sum_{k=0}^{N_s-1} y_k \cos\left(2\pi k\frac{n}{N_s}\right) \Big/ \sum_{k=0}^{N_s-1} y_k \\ u_{\text{Im}} &= m\sin\phi = \frac{\pi}{m_{\text{ex}}} \cdot \sum_{k=0}^{N_s-1} y_k \sin\left(2\pi k\frac{n}{N_s}\right) \Big/ \sum_{k=0}^{N_s-1} y_k \end{aligned} \tag{A.13}$$

It is well-known that the covariance matrix of the random vector $(u_{\text{Re}}, u_{\text{Im}})$ can be computed approximately by

$$\mathbf{C}_{u_{\text{Re}},u_{\text{Im}}} = \nabla\mathbf{F}^T_{u_{\text{Re}},u_{\text{Im}}} \mathbf{C}_y \nabla\mathbf{F}_{u_{\text{Re}},u_{\text{Im}}} \tag{A.14}$$

where $\mathbf{C}_{u_{\text{Re}},u_{\text{Im}}}$ is a symmetric 2×2 output covariance matrix. The diagonal elements contain the variances for each variable, while the off-diagonal elements contain the covariances between variables.

$$\mathbf{C}_{u_{\text{Re}},u_{\text{Im}}} = \begin{bmatrix} \sigma^2_{u_{\text{Re}}} & \text{COV}(u_{\text{Re}}, u_{\text{Im}}) \\ \text{COV}(u_{\text{Im}}, u_{\text{Re}}) & \sigma^2_{u_{\text{Im}}} \end{bmatrix} \tag{A.15}$$

the matrix $\nabla\mathbf{F}_{u_{\text{Re}},u_{\text{Im}}}$ is defined as the transpose of gradient of u_{Re} and u_{Im}, whereas the gradient

is the outer product of ∇ and $\mathbf{F}_{u_{\mathrm{Re}},u_{\mathrm{Im}}}$

$$\nabla \mathbf{F}^{T}_{u_{\mathrm{Re}},u_{\mathrm{Im}}} = \begin{bmatrix} \dfrac{\partial u_{\mathrm{Re}}}{\partial y_0} & \dfrac{\partial u_{\mathrm{Re}}}{\partial y_1} & \cdots & \dfrac{\partial u_{\mathrm{Re}}}{\partial y_{N_s-1}} \\ \dfrac{\partial u_{\mathrm{Im}}}{\partial y_0} & \dfrac{\partial u_{\mathrm{Im}}}{\partial y_1} & \cdots & \dfrac{\partial u_{\mathrm{Im}}}{\partial y_{N_s-1}} \end{bmatrix} \tag{A.16}$$

By Eq. A.13 each terms in the jacobian matrix can be calculated. We have

$$\begin{aligned} \frac{\partial u_{\mathrm{Re}}}{\partial y_k} &= \frac{\pi}{m_{\mathrm{ex}}} \cdot \cos\left(2\pi k \frac{n}{N_s}\right) \Bigg/ \left(\sum_{k=0}^{N_s-1} y_k\right)^2 \\ \frac{\partial u_{\mathrm{Im}}}{\partial y_k} &= \frac{\pi}{m_{\mathrm{ex}}} \cdot \sin\left(2\pi k \frac{n}{N_s}\right) \Bigg/ \left(\sum_{k=0}^{N_s-1} y_k\right)^2 \end{aligned} \tag{A.17}$$

$\mathbf{C}_y$ is a $N_s \times N_s$ input covariance matrix which contains all variances and covariances of the input variable $y_0, y_1, \cdots, y_{N_s-1}$.

$$\mathbf{C}_y = \begin{bmatrix} \sigma^2_{y_0} & \mathrm{cov}(y_0, y_1) & \dots & \mathrm{cov}(y_0, y_{N_s-1}) \\ \mathrm{cov}(y_1, y_0) & \sigma^2_{y_1} & \dots & \mathrm{cov}(y_1, y_{N_s-1}) \\ \vdots & \vdots & \ddots & \vdots \\ \mathrm{cov}(y_{N_s-1}, y_0) & \mathrm{cov}(y_{N_s-1}, y_1) & \dots & \sigma^2_{y_{N_s-1}} \end{bmatrix} \tag{A.18}$$

We assume y_ks are independent, all $\mathrm{cov}(y_k, y_l)$ terms with $k \neq l$ disappear. So that $\mathbf{C}_c$ turns out to be a diagonal matrix.

$$\mathbf{C}_{u_{\mathrm{Re}},u_{\mathrm{Im}}} = \begin{bmatrix} \dfrac{\partial u_{\mathrm{Re}}}{\partial y_0} & \dfrac{\partial u_{\mathrm{Re}}}{\partial y_1} & \cdots & \dfrac{\partial u_{\mathrm{Re}}}{\partial y_{N_s-1}} \\ \dfrac{\partial u_{\mathrm{Im}}}{\partial y_0} & \dfrac{\partial u_{\mathrm{Im}}}{\partial y_1} & \cdots & \dfrac{\partial u_{\mathrm{Im}}}{\partial y_{N_s-1}} \end{bmatrix} \cdot \begin{bmatrix} \sigma^2_{y_0} & & & \\ & \sigma^2_{y_1} & & \\ & & \ddots & \\ & & & \sigma^2_{y_{N_s-1}} \end{bmatrix} \cdot \begin{bmatrix} \dfrac{\partial u_{\mathrm{Re}}}{\partial y_0} & \dfrac{\partial u_{\mathrm{Im}}}{\partial y_0} \\ \dfrac{\partial u_{\mathrm{Re}}}{\partial y_1} & \dfrac{\partial u_{\mathrm{Im}}}{\partial y_1} \\ \vdots & \vdots \\ \dfrac{\partial u_{\mathrm{Re}}}{\partial y_{N_s-1}} & \dfrac{\partial u_{\mathrm{Im}}}{\partial y_{N_s-1}} \end{bmatrix} \tag{A.19}$$

By calculating the multiplication of the matrix,

$$\mathrm{cov}(u_{\mathrm{Re}}, u_{\mathrm{Im}}) = \mathrm{cov}(u_{\mathrm{Im}}, u_{\mathrm{Re}}) = \sum_{k=0}^{N_s-1} \left(\frac{\partial u_{\mathrm{Re}}}{\partial y_k}\right) \left(\frac{\partial u_{\mathrm{Im}}}{\partial y_k}\right) \sigma_{y_k}^2 \tag{A.20}$$

By introducing Eq. A.17, we get

$$\mathrm{cov}(u_{\mathrm{Re}}, u_{\mathrm{Im}}) = \mathrm{cov}(u_{\mathrm{Im}}, u_{\mathrm{Re}}) = \frac{\pi^2}{m_{\mathrm{ex}}^2} \cdot \sum_{k=1}^{N_s-1} \sigma_{y_k}^2 \cos\left(2\pi k \frac{n}{N_s}\right) \sin\left(2\pi k \frac{n}{N_s}\right) = 0 \tag{A.21}$$

All the covariance terms end up with zero $\mathrm{cov}(u_{\mathrm{Re}}, u_{\mathrm{Im}}) = \mathrm{cov}(u_{\mathrm{Im}}, u_{\mathrm{Re}}) = 0$. Only the variance terms remain

$$\begin{aligned} \sigma_{u_{\mathrm{Re}}}^2 &= \sum_{k=0}^{N_s-1} \left(\frac{\partial u_{\mathrm{Re}}}{\partial y_k}\right)^2 \sigma_{y_k}^2 \\ \sigma_{u_{\mathrm{Im}}}^2 &= \sum_{k=0}^{N_s-1} \left(\frac{\partial u_{\mathrm{Im}}}{\partial y_k}\right)^2 \sigma_{y_k}^2 \end{aligned} \tag{A.22}$$

By introducing Eq. A.17, we get

$$\sigma_{u_{\mathrm{Re}}}^2 = \frac{\pi^2}{m_{\mathrm{ex}}^2} \cdot \sum_{k=1}^{N_s-1} \sigma_{y_k}^2 \cos^2\left(2\pi k \frac{n}{N_s}\right) \Bigg/ \left(\sum_{k=0}^{N_s-1} \mu_{y_k}\right)^2 \tag{A.23}$$

By using the relation of Eq. 5.5 we get

$$\sigma_{u_{\mathrm{Re}}}^2 = \frac{\pi^2}{m_{\mathrm{ex}}^2} \cdot \frac{N_s}{2} \cdot \frac{1}{N_s^2 K^2 N_p^2} \cdot \sum_{k=1}^{N_s-1} \sigma_{y_k}^2 \tag{A.24}$$

$$= \frac{\pi^2}{2 m_{\mathrm{ex}}^2 N_s K^2} \sum_{k=1}^{N_s-1} \sigma_{y_k}^2 \tag{A.25}$$

Assuming there are only Poisson noise, we get

$$\sigma_{u_{\mathrm{Re}}}^2 = \frac{\pi^2}{2 m_{\mathrm{ex}}^2 N_s N_p} \tag{A.26}$$

Similarly we may obtain

$$\sigma_{u_{\text{Im}}}^2 = \frac{\pi^2}{2m_{\text{ex}}^2 N_s N_p} \tag{A.27}$$

We have the covariance matrix as

$$\mathbf{C}_{u_{\text{Re}},u_{\text{Im}}} = \begin{bmatrix} \dfrac{\pi^2}{2m_{\text{ex}}^2 N_p N_s} & 0 \\ 0 & \dfrac{\pi^2}{2m_{\text{ex}}^2 N_p N_s} \end{bmatrix} \tag{A.28}$$

Bibliography

[BBB+03] W. Becker, A. Bergmann, C. Biskup, L. Kelbauskas, T. Zimmer, N. Klöcker, and K. Benndorf. High resolution tcspc lifetime imaging. In *Proc. SPIE*, volume 4963, pages 175–184, 2003.

[BBH+04] W. Becker, A. Bergmann, MA Hink, K. König, K. Benndorf, and C. Biskup. Fluorescence lifetime imaging by time-correlated single-photon counting. *Microscopy research and technique*, 63(1):58–66, 2004.

[BC02] P. Blomgren and T.F. Chan. Color TV: total variation methods for restoration of vector-valued images. *Image Processing, IEEE Transactions on*, 7(3):304–309, 2002.

[BCM+06] A. Buades, B. Coll, J.M. Morel, et al. A review of image denoising algorithms, with a new one. *Multiscale Modeling and Simulation*, 4(2):490–530, 2006.

[BD89] R.M. Ballew and JN Demas. An error analysis of the rapid lifetime determination method for the evaluation of single exponential decays. *Analytical Chemistry*, 61(1):30–33, 1989.

[BD91] RM Ballew and JN Demas. Error analysis of the rapid lifetime determination method for single exponential decays with a non-zero baseline. *Analytica chimica acta*, 245:121–127, 1991.

[Bee92] J.M. Beechem. [2] Global analysis of biochemical and biophysical data. *Methods in enzymology*, 210:37–54, 1992.

[Bil98] J.A. Bilmes. A gentle tutorial of the em algorithm and its application to parameter estimation for gaussian mixture and hidden markov models. *International Computer Science Institute*, 4:126, 1998.

[BJL+97] M.A. Bopp, Y. Jia, L. Li, R.J. Cogdell, and R.M. Hochstrasser. Fluorescence and photobleaching dynamics of single light-harvesting complexes. *Proceedings of the National Academy of Sciences*, 94(20):10630, 1997.

[BKC+08] C. Buranachai, D. Kamiyama, A. Chiba, B.D. Williams, and R.M. Clegg. Rapid frequency-domain flim spinning disk confocal microscope: lifetime resolution, image improvement and wavelet analysis. *Journal of fluorescence*, 18(5):929–942, 2008.

[BQB+07] N. Boens, W. Qin, N. Basarić, J. Hofkens, M. Ameloot, J. Pouget, J.P. Lefevre, B. Valeur, E. Gratton, N.D. Silva Jr, et al. Fluorescence lifetime standards for time and frequency domain fluorescence spectroscopy. *Anal. Chem*, 79(5):2137–2149, 2007.

[BW04] MJ Booth and T. Wilson. Low-cost, frequency-domain, fluorescence lifetime confocal microscopy. *Journal of microscopy*, 214(1):36–42, 2004.

[CC09] Haley J Carlson and Robert E Campbell. Genetically encoded fret-based biosensors for multiparameter fluorescence imaging. *Current Opinion in Biotechnology*, 20(1):19–27, 2009.

[CCC+10] A. Chambolle, V. Caselles, D. Cremers, M. Novaga, and T. Pock. An introduction to total variation for image analysis. In *Theoretical Foundations and Numerical Methods for Sparse Recovery*. De Gruyter, 2010.

[CCG+98] B. Chance, M. Cope, E. Gratton, N. Ramanujam, and B. Tromberg. Phase measurement of light absorption and scatter in human tissue. *Review of scientific instruments*, 69:3457, 1998.

[CE05] T.F. Chan and S. Esedolu. Aspects of total variation regularized l1 function approximation. *SIAM Journal on Applied Mathematics*, pages 1817–1837, 2005.

[Cha09] C.W. Chang. *Improving accuracy and precision in biological applications of fluorescence lifetime imaging microscopy*. PhD thesis, 2009.

[CHV04] AHA Clayton, QS Hanley, and PJ Verveer. Graphical representation and multicomponent analysis of single-frequency fluorescence lifetime imaging microscopy data. *Journal of microscopy*, 213(1):1–5, 2004.

[CL97] K. Carlsson and A. Liljeborg. Confocal fluorescence microscopy using spectral and lifetime information to simultaneously record four fluorophores with high channel separation. *Journal of Microscopy*, 185(1):37–46, 1997.

[CL98] K. Carlsson and A. Liljeborg. Simultaneous confocal lifetime imaging of multiple fluorophores using the intensity-modulated multiple-wavelength scanning (ims) technique. *Journal of microscopy*, 191(2):119–127, 1998.

[CLAB00] K. Carlsson, A. Liljeborg, RM Andersson, and H. Brismar. Confocal pH imaging of microscopic specimens using fluorescence lifetimes and phase fluorometry: influence of parameter choice on system performance. *Journal of Microscopy*, 199(2):106–114, 2000.

[Cle95] R.M. Clegg. Fluorescence resonance energy transfer. *Current opinion in biotechnology*, 6(1):103–110, 1995.

[CM10] C.W. Chang and M.A. Mycek. Enhancing precision in time-domain fluorescence lifetime imaging. *Journal of Biomedical Optics*, 15:056013, 2010.

[CS05] T.F. Chan and J. Shen. *Image processing and analysis: variational, PDE, wavelet, and stochastic methods*. Society for Industrial Mathematics, 2005.

[DCZG08] M.A. Digman, V.R. Caiolfa, M. Zamai, and E. Gratton. The phasor approach to fluorescence lifetime imaging analysis. *Biophysical journal*, 94(2):L14–L16, 2008.

[DSG95] A. Draaijer, R. Sanders, and HC Gerritsen. Fluorescence lifetime imaging, a new tool in confocal microscopy. *Handbook of biological confocal microscopy*, pages 491–505, 1995.

[EGW05] A. Esposito, H.C. Gerritsen, and F.S. Wouters. Fluorescence lifetime heterogeneity resolution in the frequency domain by lifetime moments analysis. *Biophysical journal*, 89(6):4286–4299, 2005.

[EGW07] A. Esposito, H.C. Gerritsen, and F.S. Wouters. Optimizing frequency-domain fluorescence lifetime sensing for high-throughput applications: photon economy and acquisition speed. *Journal of the Optical Society of America A*, 24(10):3261–3273, 2007.

[EKF09] A.D. Elder, C.F. Kaminski, and J.H. Frank. ϕ^2 FLIM: a technique for alias-free frequency domain fluorescence lifetime imaging. *Optics Express*, 17(25):23181–23203, 2009.

[EMV10] EMVA. EMVA Standard 1288: Standard for characterization and presentation of specification data for image sensors and cameras. *European Machine Vision Association*, Release 3.0, 2010.

[EOG+05] A. Esposito, T. Oggier, H. Gerritsen, F. Lustenberger, and F. Wouters. All-solid-state lock-in imaging for wide-field fluorescence lifetime sensing. *Optics Express*, 13(24):9812–9821, 2005.

[Erz11] M. Erz. *Charakterisierung von Laufzeitkamerasystemen für Lumineszenzlebensdauermessungen*. PhD thesis, University of Heidelberg, 2011.

[ESK08] AD Elder, S. Schlachter, and CF Kaminski. Theoretical investigation of the photon efficiency in Frequency-domain FLIM. *Journal of the Optical Society of America A: Optics Image Science and Vision*, 25:452–62, 2008.

[FAT11] S. Foix, G. Alenya, and C. Torras. Lock-in time-of-flight (tof) cameras: A survey. *Sensors Journal, IEEE*, (99):1–1, 2011.

[FPR+09] Mario Frank, Matthias Plaue, Holger Rapp, Ullrich Kthe, Bernd Jhne, and Fred A. Hamprecht. Theoretical and experimental error analysis of continuous-wave time-of-flight range cameras. *Optical Eng.*, 48:013602, 2009.

[GAAVS02] HC Gerritsen, MAH Asselbergs, AV Agronskaia, and W. Van Sark. Fluorescence lifetime imaging in scanning microscopes: acquisition speed, photon economy and lifetime resolution. *Journal of microscopy*, 206(3):218–224, 2002.

[Gad08] T.W.J. Gadella. *FRET and FLIM techniques*, volume 33. Elsevier Science, 2008.

[GC10] B. Goldluecke and D. Cremers. An approach to vectorial total variation based on geometric measure theory. In *Computer Vision and Pattern Recognition (CVPR), 2010 IEEE Conference on*, pages 327–333. IEEE, 2010.

[GJJC93] T.W.J. Gadella Jr, T.M. Jovin, and R.M. Clegg. Fluorescence lifetime imaging microscopy (flim): spatial resolution of microstructures on the nanosecond time scale. *Biophysical chemistry*, 48(2):221–239, 1993.

[Gol09] E.M. Goldys. *Fluorescence applications in biotechnology and life sciences*. Blackwell Pub, 2009.

[GSD+97] H.C. Gerritsen, R. Sanders, A. Draaijer, C. Ince, and YK Levine. Fluorescence lifetime imaging of oxygen in living cells. *Journal of Fluorescence*, 7(1):11–15, 1997.

[GW90] A. Grace and M. Works. *Optimization Toolbox: For Use with MATLAB: User's Guide*. The Math Works, 1990.

[GZM+08] D.M. Grant, W. Zhang, E.J. McGhee, T.D. Bunney, C.B. Talbot, S. Kumar, I. Munro, C. Dunsby, M.A.A. Neil, M. Katan, et al. Multiplexed fret to image multiple signaling events in live cells. *Biophysical journal*, 95(10):L69–L71, 2008.

[HB96] A. Horner and J. Beauchamp. A genetic algorithm-based method for synthesis of low peak amplitude signals. *Journal of the Acoustical Society of America*, 99(1):433–443, 1996.

[HC05] QS Hanley and AHA Clayton. AB-plot assisted determination of fluorophore mixtures in a fluorescence lifetime microscope using spectra or quenchers. *Journal of microscopy*, 218(1):62–67, 2005.

[HK93] R. Hettich and K.O. Kortanek. Semi-infinite programming: theory, methods, and applications. *SIAM review*, pages 380–429, 1993.

[Hor00] A. Horner. Low peak amplitudes for wavetable synthesis. *Speech and Audio Processing, IEEE Transactions on*, 8(4):467–470, 2000.

[ISS] ISS. Iss fluorescence and biomedical instrumentation. `http://www.iss.com`.

[JGH84] D.M. Jameson, E. Gratton, and R.D. Hall. The measurement and analysis of heterogeneous emissions by multifrequency phase and modulation fluorometry. *Applied Spectroscopy Reviews*, 20(1):55–106, 1984.

[KBB83] J.R. Knutson, J.M. Beechem, and L. Brand. Simultaneous analysis of multiple fluorescence decay curves: A global approach* 1. *Chemical physics letters*, 102(6):501–507, 1983.

[KBF+99] K. König, TW Becker, P. Fischer, I. Riemann, and K.J. Halbhuber. Pulse-length dependence of cellular response to intense near-infrared laser pulses in multiphoton microscopes. *Optics letters*, 24(2):113–115, 1999.

[Lak06] J.R. Lakowicz. *Principles of Fluorescence Spectroscopy*. Springer, 2006.

[Lan00] R. Lange. *3D Time-of-Flight Distance Measurement with Custom Solid-State Image Sensors in CMOS/CCD-Technology*. PhD thesis, University of Siegen, 2000.

[LEJ10] Zhuang Lin, Michael Erz, and Bernd Jähne. Multi-frequency multi-sampling fluorescence lifetime imaging using a high-speed line-scan camera. In *Optics, Photonics, and Digital Technologies for Multimedia Apllications, 12–15 April 2010, Brussels*, volume 7723 of *SPIE Proc.*, page 77231S, 2010.

[LG10] Y. Lin and A.F. Gmitro. Statistical analysis and optimization of frequency-domain fluorescence lifetime imaging microscopy using homodyne lock-in detection. *Journal of the Optical Society of America A*, 27(5):1145–1155, 2010.

[LLC+84] J.R. Lakowicz, G. Laczko, H. Cherek, E. Gratton, and M. Limkeman. Analysis of fluorescence decay kinetics from variable-frequency phase shift and modulation data. *Biophysical journal*, 46(4):463–477, 1984.

[LRR+09] A. Leray, F.B. Riquet, E. Richard, C. Spriet, D. Trinel, and L. Héliot. Optimized protocol of a frequency domain fluorescence lifetime imaging microscope for fret measurements. *Microscopy research and technique*, 72(5):371–379, 2009.

[LS07] M. López and G. Still. Semi-infinite programming. *European journal of operational research*, 180(2):491–518, 2007.

[LS11] J. Lellmann and C. Schnörr. Regularizers for vector-valued data and labeling problems in image processing. *Control Systems and Computers*, 2:43–54, 2011.

[LST+11] A. Leray, C. Spriet, D. Trinel, R. Blossey, Y. Usson, and L. Héliot. Quantitative comparison of polar approach versus fitting method in time domain flim image analysis. *Cytometry Part A*, 2011.

[LW73] J.R. Lakowicz and G. Weber. Quenching of fluorescence by oxygen. Probe for structural fluctuations in macromolecules. *Biochemistry*, 12(21):4161–4170, 1973.

[Lyo04] R.G. Lyons. *Understanding digital signal processing*. Prentice Hall PTR Upper Saddle River, NJ, USA, 2004.

[McC04] P. McCormack. Effects and benefits of undersampling in high-speed adc applications. *Design & Elektronik (Germany)*, 2004.

[MCR07] G.C. MALACHOWSKI, R.M. CLEGG, and G.I. REDFORD. Analytic solutions to modelling exponential and harmonic functions using chebyshev polynomials: fitting frequency-domain lifetime images with photobleaching. *Journal of Microscopy*, 228(3):282–295, 2007.

[MDDW95] J. Moll, S. Daehne, J.R. Durrant, and D.A. Wiersma. Optical dynamics of excitons in j aggregates of a carbocyanine dye. *Journal of Chemical Physics*, 102(16):6362–6370, 1995.

[mes] Mesa Imaging AG. http://www.mesa-imaging.ch/index.php.

[MWMM02a] AC Mitchell, JE Wall, JG Murray, and CG Morgan. Direct modulation of the effective sensitivity of a ccd detector: a new approach to time-resolved fluorescence imaging. *Journal of microscopy*, 206(3):225–232, 2002.

[MWMM02b] AC Mitchell, JE Wall, JG Murray, and CG Morgan. Measurement of nanosecond time-resolved fluorescence with a directly gated interline ccd camera. *Journal of microscopy*, 206(3):233–238, 2002.

[OP86] D.V. O'Connor and D. Phillips. Time-correlated single photon counting. *Applied Optics*, 25:460–463, 1986.

[PC03] J. Philip and K. Carlsson. Theoretical investigation of the signal-to-noise ratio in fluorescence lifetime imaging. *Journal of the Optical Society of America A*, 20(2):368–379, 2003.

[RC05] G.I. Redford and R.M. Clegg. Polar plot representation for frequency-domain analysis of fluorescence lifetimes. *Journal of fluorescence*, 15(5):805–815, 2005.

[Red05] G.I. Redford. *Fast Fluorescence Lifetime Imaging Using a Full-field Homodyne System with Applications in Biology*. PhD thesis, University of Illinois at Urbana-Champaign, 2005.

[RFHJ08] H. Rapp, M. Frank, F.A. Hamprecht, and Bernd Jhne. A theoretical and experimental investigation of the systematic errors and statistical uncertainties of time-of-flight cameras. *Int. J. Intelligent Systems Technologies and Applications*, 5:402–413, 2008.

[RG98] R. Reemtsen and S. Görner. Numerical methods for semi-infinite programming: a survey. *Semi-infinite programming*, 25:195–275, 1998.

[RMH07] T. Ringbeck, T. Möller, and B. Hagebeuker. Multidimensional measurement by using 3-d pmd sensors. *Advances in Radio Science*, 5:135–146, 2007.

[ROF92] L.I. Rudin, S. Osher, and E. Fatemi. Nonlinear total variation based noise removal algorithms. *Physica D: Nonlinear Phenomena*, 60(1-4):259–268, 1992.

[RR98] R. Reemtsen and J.J. Rückmann. *Semi-infinite programming*, volume 25. Kluwer Academic Publishers, 1998.

[RW] P. Rodríguez and B. Wohlberg. A generalized vector-valued total variation algorithm. In *Image Processing (ICIP), 2009 16th IEEE International Conference on*, pages 1309–1312. IEEE.

[RW09] P. Rodríguez and B. Wohlberg. Efficient minimization method for a generalized total variation functional. *Image Processing, IEEE Transactions on*, 18(2):322–332, 2009.

[SC09a] B.Q. Spring and R.M. Clegg. Frequency-domain flim. *FLIM microscopy in biology and medicine*, page 115, 2009.

[SC09b] BQ Spring and RM Clegg. Image analysis for denoising full-field frequency-domain fluorescence lifetime images. *Journal of Microscopy*, 235(2):221–237, 2009.

[Sch70] M. Schroeder. Synthesis of low-peak-factor signals and binary sequences with low autocorrelation (corresp.). *Information Theory, IEEE Transactions on*, 16(1):85–89, 1970.

[Sch08] Martin Schmidt. *Spatiotemporal Analysis of Range Imagery*. Dissertation, IWR, Fakultt fr Physik und Astronomie, Univ. Heidelberg, 2008.

[SEE+09] S. Schlachter, AD Elder, A. Esposito, GS Kaminski, JH Frank, LK van Geest, and CF Kaminski. mhFLIM: Resolution of heterogeneous fluorescence decays in widefield lifetime microscopy. *Optics Express*, 17(3):1557–1570, 2009.

[SFY+95] PTC So, T. French, WM Yu, KM Berland, CY Dong, and E. Gratton. Time-resolved fluorescence microscopy using two-photon excitation. *Bioimaging*, 3(2):49–63, 1995.

[SGG+09] O. Scherzer, M. Grasmair, H. Grossauer, M. Haltmeier, and F. Lenzen. *Variational methods in imaging*, volume 167. Springer Verlag, 2009.

[SPA+99] K.K. Sharman, A. Periasamy, H. Ashworth, JN Demas, and NH Snow. Error analysis of the rapid lifetime determination method for double-exponential decays and new windowing schemes. *Anal. Chem*, 71(5):947–952, 1999.

[SSVH95] T. Spirig, P. Seitz, O. Vietze, and F. Heitger. The lock-in ccd-two-dimensional synchronous detection of light. *Quantum Electronics, IEEE Journal of*, 31(9):1705–1708, 1995.

[Sun01] D. Sundararajan. *The discrete Fourier transform: theory, algorithms and applications*. World Scientific Pub Co Inc, 2001.

[SVDGG98] J. Sytsma, JM Vroom, CJ De Grauw, and HC Gerritsen. Time-gated fluorescence lifetime imaging and microvolume spectroscopy using two-photon excitation. *Journal of Microscopy*, 191:39–51, 1998.

[Tay97] J.R. Taylor. *An introduction to error analysis: the study of uncertainties in physical measurements*. Univ Science Books, 1997.

[Tri] TriDiCam®GmbH. http://www.tridicam.de/.

[Tri09] TriDiCam GmbH. *3D Sensor Application Kit — Building up a 3D Sensor System*, preliminary document, version 1.02 edition, 11 2009.

[VdB87] A. Van den Bos. A new method for synthesis of low-peak-factor signals. *Acoustics, Speech and Signal Processing, IEEE Transactions on*, 35(1):120–122, 1987.

[VMGJ04] EB Van Munster and TWJ Gadella Jr. ϕflim: a new method to avoid aliasing in frequency-domain fluorescence lifetime imaging microscopy. *Journal of microscopy*, 213(1):29–38, 2004.

[VO96] C.R. Vogel and M.E. Oman. Iterative methods for total variation denoising. *SIAM Journal on Scientific Computing*, 17(1):227–238, 1996.

[VSB00] P.J. Verveer, A. Squire, and P.I.H. Bastiaens. Global analysis of fluorescence lifetime imaging microscopy data. *Biophysical journal*, 78(4):2127–2137, 2000.

[WBS+08] C. Wu, B. Bull, C. Szymanski, K. Christensen, and J. McNeill. Multicolor conjugated polymer dots for biological fluorescence imaging. *ACS nano*, 2(11):2415–2423, 2008.

[WE08] F.S. Wouters and A. Esposito. Quantitative analysis of fluorescence lifetime imaging made easy. *HFSP journal*, 2(1):7, 2008.

[Web81] G. Weber. Resolution of the fluorescence lifetimes in a heterogeneous system by phase and modulation measurements. *The Journal of Physical Chemistry*, 85(8):949–953, 1981.

[WN04] R.M. Willett and R.D. Nowak. Fast multiresolution photon-limited image reconstruction. In *Biomedical Imaging: Nano to Macro, 2004. IEEE International Symposium on*, pages 1192–1195. IEEE, 2004.

[WP05] H. Wallrabe and A. Periasamy. Imaging protein molecules using fret and flim microscopy. *Current opinion in biotechnology*, 16(1):19–27, 2005.

[Zim04] H. Zimmermann. *Silicon optoelectronic integrated circuits*, volume 13. Springer Verlag, 2004.